DEPARTMENT OF PHYSICS, UNIVERSITY OF JYVÄSKYLÄ
RESEARCH REPORT No. 3/2000

MULTI-CONFIGURATION MIXING APPROACH DESIGNED FOR LARGE SCALE NUCLEAR STRUCTURE CALCULATIONS

BY
TUOMAS HJELT

Academic Dissertation
for the Degree of
Doctor of Philosophy

Jyväskylä, Finland
May 2000

URN:ISBN:978-951-39-9480-8
ISBN 978-951-39-9480-8 (PDF)
ISSN 0075-465X

Jyväskylän yliopisto, 2023

ISBN 951-39-0666-3
ISSN 0075-465X

DEPARTMENT OF PHYSICS, UNIVERSITY OF JYVÄSKYLÄ
RESEARCH REPORT No. 3/2000

MULTI-CONFIGURATION MIXING APPROACH DESIGNED FOR LARGE SCALE NUCLEAR STRUCTURE CALCULATIONS

BY
TUOMAS HJELT

Academic Dissertation
for the Degree of
Doctor of Philosophy

To be presented, by permission of the
Faculty of Mathematics and Natural Sciences
of the University of Jyväskylä,
for public examination in Auditorium FYS 1 of the
University of Jyväskylä on May 5, 2000,
at 12 o'clock noon

Jyväskylä, Finland
May 2000

Preface

I would like to express my gratitude to the "father" of the VAMPIR-MONSTER model family, Prof. Karl Wilhelm Schmid for encouraging and inspiring guidance and also his warm and friendly hospitality during my several visits in Tübingen.

I would like to thank Dos. Esko Hammarén for introducing me this field of theoretical nuclear physics and guiding as well as supporting my studies, Prof. Jouni Suhonen who have also guided me during my studies and Emeritus Prof. Pertti Lipas for valuable teaching and advises. Special thanks go to Mr. Markus Kortelainen for performing the SCM calculations.

It has been a privilege to work in a research centre of excellence like our department of physics, which has a friendly and fine atmosphere thanks to all our staff. The presence of a wide variety of different fields of physics is our speciality and advantage.

The financial support from the University of Jyväskylä, the Academy of Finland and the Deutscher Akademischer Austauschdienst (DAAD) are gratefully acknowledged.

Finally, I wish to thank my family and especially my wife Riitta and my son Elias for their love, encouragement and patience.

Jyväskylä, February 2000
Tuomas Hjelt

Abstract

A new program, which is an advanced stage in the numerical implementation of a specific family of nuclear structure models, is developed. In this approach a many-body Hamiltonian is diagonalized in the configuration space of general fully symmetry projected Hartree-Fock-Bogoliubov type quasiparticle determinants. The configurations are build on top of a mean-field solution of the Hartree-Fock-Bogoliubov problem with restoration of broken symmetries by projection before the variation of the wavefunction using the most general symmetry unrestricted quasi-particle transformation. In the approach, named GENERAL COMPLEX MONSTER the configuration space of the symmetry projected Hartree-Fock-Bogoliubov determinant is supplemented by all the symmetry projected 2-quasiparticle states build on top of this determinant. With this method a wide range of doubly-even, doubly-odd and odd nuclei can be treated on the same footing in comparatively large model spaces and a huge amount of states can be obtained. The involved mathematical tools and the solutions found to construct the code are presented. The implemented method was tested for the even ^{28}Si and the odd ^{27}Al nuclei from the middle of the $1s0d$-shell. The new results are discussed and compared with the results of complete shell model diagonalizations.

Table of Contents

Introduction

Being a complex composite system of many constituents, the atomic nucleus represents one of the most challenging many-body systems. The nucleus displays a multitude of various excitations, which can be classified by their constants of motion: energy, total angular momentum, parity, proton and neutron numbers and in light systems also the total isospin. In this work we consider regions of discrete levels lying below the emission threshold of hadronic particles and the nuclear continuum. The decay between these levels can happen by photon emission, electron conversion into the energetically lower state of the same or, for example, by β-decay of a neighboring nucleus.
To explore these excitations and trying to explain the complex interplay of collective and single particle degrees of freedom causing the measurable properties of nuclei is the central aim of theoretical nuclear shell structure physics.

The shell model configuration mixing model SCM is one of the most fundamental models of nuclear structure. In this model nucleons occupy chosen valence quantum orbitals in a mean-field one-body potential. This is analogous to the atomic shell model, but the nuclear case is complicated by a strong two-body residual interaction that moves nucleons among the orbitals and is a major determinant of nuclear properties. The original model was introduced over 50 years ago by Mayer [May49] and by Haxel, Jensen and Suess [Hax49]. It yields in general a very good description of at least the low energy phenomena in nuclear structure physics [Whi77, Bru77, Mcg80, Tal93] like, energy levels, magnetic

and quadrupole moments, electromagnetic transition probabilities, β-decay rates and reaction cross-sections. The SCM is considered as a standard model for describing the $0p$- [Coh65], $1s0d$- [Wil88, Bro88a] and lower $1p0f$- [Fre69, Cau95, Mar97] shell nuclei. Since the size of the configuration spaces grow combinatorially with both the number of orbitals and the number of nucleons occupying them the full major shell SCM calculations employing highly sophisticated algorithms are recently limited for $1p0f$-shell up to $A \sim 57$ [Cau99]. Thus, moderately sized nuclei such as zink require matrices of the order of 10^8, for which direct diagonalization is not currently possible. One could argue, that as the rapid development of computer technology continues this milestone will be soon passed by. This is true, but sort of short-sighted. The fact is that the complete shell model diagonalization calculations will always be restricted to relatively small basis systems. For the description of many nuclear structure problems one needs much larger basis systems consisting not only one but several major shells. Examples are the investigation of giant resonances, medium-heavy and heavy nuclei, superdeformations and even comparatively simple tasks like the study of negative parity states in light even-even nuclei. Recently a wide range of new approximate methods has been proposed for solving the large scale shell model problems, like shell model diagonalization including stochastic approaches [Var94, Hor94], a generalized pair mean-field method [Che92], various quantum Monte Carlo methods (QMC) [Koo97], which still suffer from the minus-sign problem absent from quantum Monte Carlo diagonalization method (QMCD) [Hon96]. In all these cases one is trying to reduce the basis-dimension problem of the diagonalization of the shell model.

An alternative way to approach this problem is to apply variational techniques. One should note that in the complete basis constructed from all Slater determinants this is equivalent to an exact SCM diagonalization. In the method described here the selection

of the relevant many nucleon configurations is left entirely to the dynamics of the system. In practice the truncation of the shell model expansion is done by extracting an optimal average mean-field, each of the nucleon feels due to its interaction with the others, directly from the many-nucleon Hamiltonian using a variational procedure. The resulting mean-field is represented by a so called "quasi-particle reference determinant" which accounts for many more correlations than some *ad hoc* chosen basis creating mean-field customary to the SCM. In this way the residual interaction between the resulting A-nucleon configurations and the corresponding reference determinant (i.e. the quasi-particle vacuum) is minimized without explicitly diagonalizing the Hamiltonian. In the most simple case the many body nuclear wave functions are expanded around a single generalized quasi-particle determinant represented by a manageable number of variational parameters.

The famous models of this type are the well known Hartree-Fock [Har28, Foc30] and the more general Hartree-Fock-Bogoliubov (HFB) [Bog58, Bog59a, Bog59b, Rin80] approaches. Though the nuclear ground state is approximated here by one single generalized Slater determinant only, this configuration usually accounts for a large part of the SCM expansion of the nuclear ground state. The price we have to pay when trying to account for as many degrees of freedom as possible by as few quasi-particle configurations as possible is that in general this state does not contain the symmetries required by the many-body Hamiltonian and hence cannot represent its physical eigenstate. The physical states are obtained from these intrinsic structures by restoring the broken symmetries, which can be done with the help of projection techniques. Moreover, in order to obtain really optimal solutions for each set of simultaneously conserved quantum numbers separately it is essential that the restoration of the broken symmetries is done before the mean-field variation.

Along these lines several symmetry conserving mean-field methods were developed during the last decade [Sch84a, Sch84b, Sch87a, Sch87b]. They have become known as the VAMPIR (**V**ariation **A**fter **M**ean field **P**rojection **I**n **R**ealistic model spaces) and the MONSTER (**MO**del for handling many **N**umber- and **S**pin-projected **T**wo-quasiparticle **E**xcitations with **R**ealistic interactions and model spaces) approaches.

In the VAMPIR [Sch84a, Sch84c, Sch87a, Sch87b, Sch89, Sch92] approach each of the yrast states of a given nucleus is approximated by a single symmetry-projected Hartree-Fock-Bogoliubov (HFB) determinant, with the underlying mean-fields being determined by independent variational calculations. The excited states with the same quantum numbers can be obtained with the EXCITED VAMPIR [Sch86, Sch87b, Sch89] model by repeating this procedure with a new HFB test determinant which is constrained to be orthogonal to all the solutions already obtained. A straightforward extension of these approaches are the **Few** **D**eterminant (FED) VAMPIR and the EXCITED FED VAMPIR models [Sch87b, Sch89, Pet91], which approximate each state not by a single, but by a linear combination of several non-orthogonal symmetry-projected HFB configurations, which are now determined by independent, successive variations. Finally then, in these EXCITED VAMPIR and EXCITED FED VAMPIR models the residual interaction between all the obtained solutions is diagonalized. By such chains of variational calculations the lowest few states of a given symmetry representation can be obtained, irrespective of their particular structure. Because the excited states come with increasing energy and the numerical burden increases rapidly if the additional determinants are included it is unrealistic to continue such chains of variational calculations to high excited states.

In case the complete excitation spectrum of the nucleus with respect to some particular (e.g. electromagnetic) transition operator is to be described some other method

has to be used. If the transition operator is of one-body nature, it is desired to consider only excited states which have similar structure like the ground (final) state, and thus are reached by applying with that operator. In this thesis the nuclear wave functions are expanded around the VAMPIR reference state solution using the MONSTER approach [Sch84a, Sch84b, Sch87a, Ben95a, Ben95b, Ben96], which diagonalizes the chosen Hamiltonian in the space of the symmetry-projected reference vacuum and all the symmetry-projected 2-quasiparticle excitations with respect to it.

Within the last fifteen years all these methods have been applied rather successfully to many nuclear structure problems (see, e.g., the reviews [Sch87a, Sch92, Pet99c]). For example, they have been used rather extensively for the theoretical investigation of shape coexistence, shape transitions [Pet00, Pet99a, Pet97, Pan96, Pet96, Pet94, Pet92] and proton-neutron pairing correlations [Pet99b] in the $A \sim (70 - 80)$ mass-region nuclei.
In the past many symmetry restrictions had to be imposed on the underlying HFB transformations in order to simplify the numerics. Consequently, the corresponding HFB vacua do not contain all principally possible correlations, but only a particular part of them, which becomes more and more restricted as more symmetry requirements are imposed.

The history of VAMPIR-MONSTER model family involves mainly three steps regarding the symmetry restrictions. In the first VAMPIR calculations only real, time-reversal invariant and axially symmetric HFB transformations, which neither mix proton and neutron states nor states of different parity, were admitted [Sch84a, Sch84c]. With this so called *Real* VAMPIR approach only even spin and positive parity states in doubly even nuclei could be described. If a MONSTER calculation is based on such a *Real* VAMPIR transformation the missing couplings are avoided in a sense that also the other possible negative parity and odd spin states in the particular nucleus are introduced by

the configuration mixing. For applications of such *Real* MONSTER e.g. a rather nice description of nuclear structure phenomena in the mass $A \sim 130$ region, see [Ham85, Ham86a].

The second step in releasing the symmetry restrictions was the introduction of *Complex* VAMPIR [Sch87b, Zhe89] approach, where essentially complex HFB transformations as well as parity- and proton-neutron-mixing were allowed. But still time-reversal and axial symmetry were kept. Now already many more correlations were considered and states of all possible spin-parity in even mass nuclei could be described. In fact the use of essentially complex HFB-transformation matrix *with* the requirement of time reversal invariance and axial symmetry is sufficient to incorporate all the two-particle couplings into the HFB vacuum. The MONSTER calculation on top of *Complex* VAMPIR solution [Ben95a, Ben95b, Ben96] enables also the description of doubly odd nuclei on the basis on HFB transformations particularly derived for such systems, but for the description of odd systems one is forced to use mean-fields obtained for neighboring nuclei as in the *Real* MONSTER approach.

It is important to notice, that first of all, although the MONSTER approach overcomes the problem of "missing couplings" of *Real* VAMPIR and *Complex* VAMPIR approaches it does not necessarily introduce all the appropriate correlations for a particular state. Secondly, if the structure of a particular state differs considerably from the structure of the VAMPIR reference state it cannot necessarily be described well (if at all) with the MONSTER on VAMPIR approach. These two considerations hold even for the MONSTER on top of symmetry unrestricted VAMPIR presented in this thesis.

All the above mentioned symmetry restrictions are released in the third, and final stage

of the development of the VAMPIR-MONSTER model family, when the symmetry unrestricted GENERAL COMPLEX VAMPIR (GCV) [Sch84a] and the corresponding GENERAL COMPLEX MONSTER (GCM) [Sch84b, Sch87a] approaches are introduced. They employ the most general linear underlying transformations. Consequently, the configuration spaces are much larger than those of earlier approaches and thus more correlations can be described and also a better description of many states is expected. The most sophisticated VAMPIR and MONSTER models utilize most general, symmetry unrestricted linear HFB transformations and realistic effective interactions. Although the mathematical formalism of such GCV and GCM approaches has been known for over 15 years [Sch84a] the dream of accomplishing such calculations has become true only recently. The GCV was first applied to selected nuclei in the full $1s0d$-shell [Ham98] and after that in the full $1p0f$-shell [Hje00]. Until then all the VAMPIR calculations ever published have been established with at least time reversal invariant and axially symmetric mean-fields [Sch92].

In this thesis I will, after first providing a short theoretical background of the GCM approach, introduce the mathematical machinery and the numerical methods which I found essential in constructing the highly non-trivial numerical implementation of the GCM code. Furthermore, the applications of the approach in this thesis represent the first ever published GCM calculations.

In the next chapter I will review the general features of the VAMPIR-MONSTER model family by first outlining the GCV method in section 1.3 and then proceeding with the description of the GCM method on the basis of the corresponding GCV solutions in section 1.4. Some essential, explicit formulations are derived in appendixes. Chapter 2 represents the "heart" of this thesis, since the numerical implementation and the technical solutions found to construct the GCM code are discussed there. As a first

test this method is applied to two nuclei in chapter 3, namely the even mass ^{28}Si and the odd mass ^{27}Al, in the $1s0d$-shell single particle basis. The resulting wide spectra is compared with complete shell model diagonalizations. Finally, in chapter 4 this thesis work is summarized and an outline for the future is given.

Chapter 1

The VAMPIR-MONSTER Model Family

The VAMPIR-MONSTER model family offers a theoretical tool for solving a general nuclear many-body problem in principle as exactly as desired. The exactness of the solution depends on the problem itself and on the computational resources available. The power of the method lurks in its applicability to describe all kinds (and type) of nuclei in relatively large model spaces, where the resulting dimensions exceed the reach of the direct SCM diagonalizations. I begin this chapter by outlining the underlying quantum mechanical nuclear many-body problem, which serves then as a starting point for the VAMPIR and MONSTER models. After that I will concentrate on explaining the theoretical basics of a GENERAL COMPLEX VAMPIR model and extend the prescription to a GENERAL COMPLEX MONSTER model in the subsequent section. I will consider neither the numerical implementation of the GENERAL COMPLEX VAMPIR nor its extensions, mentioned in chapter 1.3.5.

1.1 General Considerations

The following fundamental assumptions outline the characteristics of the present VAMPIR-MONSTER model family as a microscopic nuclear (shell-)structure method

1. Treat protons and neutrons as structureless, non-relativistic elementary constituents of the atomic nucleus

2. For the description of the desired (low lying) discrete states the use of a finite subspace i.e. the one-body basis of the complete Hilbert space is sufficient

3. The effective Hamiltonian for this model space does exist and can be sufficiently well approximated by only one- and two-body terms

These postulates define the attempt to facilitate the problem of extremely complicated, complete many-body Schrödinger equation of atomic nucleus, which cannot be solved with the present knowledge in full beauty. As a defect, nevertheless, something is "swept under the carpet" along these limitations. How drastically the original problem is then reduced and what are we left with?

To give an answer I will first shortly consider those limitations. First of all, nucleons are not regarded as elementary particles in modern physics. It is commonly accepted that they consist of strongly interacting quarks, with gluons as force carriers. The quantum chromodynamics (QCD) represents a branch of nuclear physics, where the nuclear forces and then nuclear structures are described relativistically starting from the quark and gluon degrees of freedom. However, due to the complexity of QCD, it is still not capable of solving basic equations in a form that is actually useful for nuclear structure. On the other hand, more than 50 years of nuclear physics has shown that at the low energies the nucleonic substructure can be successfully omitted. Nowadays it is commonly accepted that at the low energies the nucleon-nucleon interaction is a residual interaction of the underlying quark-gluon dynamics of QCD. Today we know several such successful prescriptions of nucleon-nucleon "effective" interaction in terms of a meson exchange potentials, which has been fit directly to the experimental nucleon-nucleon scattering

data (and deuteron properties) in their parametrization [Nijmdb]. The most famous modern effective high-quality nucleon-nucleon potentials of this kind are the Nijmegen [Sto94], Argonne [Wir95] and CD-Bonn [Mac96] potentials. Another main issue in this context is how to obtain the force interacting between nucleons *inside* the nucleus. There the states already occupied by other nucleons must be excluded from the nucleon-nucleon scattering process by the so called Pauli-operator. This brings up a fundamental problem. The Pauli-operator depends on the structure of the considered system, which we wish to know after having appropriate interaction. But now we need this operator to obtain that interaction. We must continue assuming some kind of average Pauli-operator. The interaction is then given approximatively by a non-relativistic reaction "G-matrix", being the solution of a Bethe-Goldstone equation for some effective nucleon-nucleon potential within the Brückner-Hartree-Fock approximation for a finite system, like the nucleus. Furthermore, in order to obtain an effective nuclear interaction in a finite model space the G-matrix, which still acts in a full Hilbert space had to be renormalized. Summarizing these approximation carried out here, first we assumed an effective bare nucleon-nucleon interaction, which is used as an input to the Bethe-Goldstone equation were no relativistic effects are considered and the Pauli-principle is fulfilled only approximatively. We end up with an effective two-body type interaction inside the nucleus for a chosen model space. In the above discussion all the three- four- and higher many-body interactions are treated as a minor "residual" part of the effective nuclear interaction, which can be ignored. This was justified mainly, by considering only low energy nuclear structure phenomena. Recent nuclear matter calculation has pointed out the importance of three nucleon forces in obtaining the appropriate nuclear saturation [Son98]. On the other hand, it has been shown by studying light $A \leq 8$ nuclei [Wir97] that the inclusion of 3-body potential might be crucial in some cases, otherwise

a considerable underbinding is detected.

However, in practice we shall restrict ourselves to some effective two-body interaction for any particular model space like, e.g. a G-matrix or even a more phenomenological interaction like the Chung-Wildenthal force [Wil84], which is used for the $1s0d$-shell example calculations in the present thesis.

1.1.1 A Realistic Example

Although the goal of the above discussion was to define only the "minimal" restrictions in a way to achieve a hopefully solvable nuclear many-body problem, we are actually left with a rather drastically reduced problem. Obviously the next step further would be the attempt to solve it. It is well known, that the conventional shell model configuration (SCM) method yields an exact solution in a complete model space of all possible nucleon configurations in this framework. So why to bother even consider other alternative approaches?

To shed light on the existing problem let us consider an example. If our chosen spherical single particle basis consists of $0s$-,$0p$-,$1s0d$-,$1p0f$-shells plus the $0g_{9/2}$- orbit the total number of possible 0^+ configurations for the ^{28}Si nucleus is [Sch87b]

$$n(^{28}\mathrm{Si}, I^\pi = 0^+) = 136\,124\,437\,576\,139\,270\,616 \approx 1.36 \times 10^{20}.$$

The dimensions of this magnitude are clearly out of the reach of today's PCs or workstations still for a long time and represent an impossible task even for the next generations high performance supercomputers. Today's best supercomputers with parallel processing can perform the order of TFlops. Assuming a 1 TFlops speed, a single floating point operation involving each of those configurations would take over 4 *years* to accomplish. Furthermore, to store 100 bit's of information for each configuration would require over 1.5×10^{12} *gigabytes* of diskspace. On the other hand, the corresponding "first order"

GCV variational calculation being composed with "only" 10 000 [see section 1.3] variables would be a piece of cake for such a supercomputer. In principle, the GCV results could be even improved by additional correlations, until the complete model space with exact solution in attained.

This is just one example to illustrate the impossibility to obtain exact solutions by diagonalizations in large, but still realistic, model spaces due to monstrous dimensions. I mean "realistic" in a sense that if you desire to obtain say, negative parity states, or even a comprehensive multi-shell description of positive parity states for light $1s0d$-shell nuclei one should include at least the neighboring $0p$- and $1p0f$-shells in the single particle basis. For heavier nuclei the dimensions become generally even larger. In some cases the use of such large model spaces is inevitable, and the utilization of GCV, GCM or some other alternative approach, like recently developed various quantum Monte-Carlo methods [Koo97, Hon96], becomes compulsory.

1.2 The Restricted Many-body Problem

The starting point for the nuclear shell structure calculations is the restricted nuclear many-body problem, which can be solved exactly, at least in principle. The model space for the problem is defined as a finite M_b-dimensional set of orthonormal, spherical single nucleon states $\{|i\rangle, |k\rangle, \dots\}_{M_b}$, which span the chosen sub-space of the infinite Hilbert space. Each of the states are characterized by quantum numbers n = radial excitation, l = orbital angular momentum, which coupled with the nucleon spin $s = 1/2$ gives $(l \otimes s) = j$ = total angular momentum, m = 3-projection of the j, τ = isospin-projection. I apply a shorthand notation i for the triplet $\{n_i l_i j_i\}$ containing implicitly the $2j_i + 1$ degeneracy of the states with different magnetic m_i quantum number. The τ quantum number distinguishes a neutron $\tau = 1/2$ and proton $\tau = -1/2$. Adapting the second

quantization formalism, the corresponding nucleon creation and annihilation operators are denoted by $\{c_i^\dagger, c_k^\dagger, \dots\}_{M_b}$ and $\{c_i, c_k, \dots\}_{M_b}$, respectively. They fulfill the usual anticommutation relations for fermion operators. The particle (nucleon) vacuum $|0\rangle$ is defined by $c_i|0\rangle \equiv 0 \quad \forall \quad i = 1, \dots M_b$. Furthermore the conjugate states are defined as

$$|\bar{i}\rangle \equiv (-)^{j_i+l_i-m_i}|i; -m_i\tau_i\rangle. \tag{1.1}$$

The chosen effective Hamiltonian can be written in this nucleon basis as (see the arguments of the previous section)

$$\hat{H} \equiv \hat{T} + \hat{V} = \sum_{ik} t(ik)c_i^\dagger c_k + \frac{1}{4}\sum_{ikrs} v(ikrs)c_i^\dagger c_k^\dagger c_s c_r, \tag{1.2}$$

where $t(ik) = \langle i|\hat{T}|k\rangle$ are the one-body matrix elements of the kinetic energy (or, if an inert core is used some single particle energies) while $v(ikrs) = \langle ik|\hat{V}|rs - sr\rangle$ denote the anti-symmetrized two-body matrix elements of the effective interaction. The hermicity of the Hamiltonian guarantees the real eigenenergies.

One can see immediately from equation (1.2) that $\hat{H}$ conserves the total nucleon number A and it is required to conserve the total charge of the system. Consequently the energy eigenstates must have good A and good proton number Z. Therefore the 3-component of the total isospin $T_z = \frac{1}{2}A - Z$ must be conserved, too. In the coordinate space the $\hat{H}$ is a sum of the kinetic and interaction generated potential energy, so it is a scalar and therefore commutes with the square J^2 of the total angular momentum operator and its 3-component. This means good total angular momentum J and its 3-component, which is usually denoted as M quantum number in the laboratory frame of reference and it corresponds to a K quantum number with respect to the intrinsic quantization axis of the nucleus. If the phases of the single particle basis states are properly chosen the matrix elements of $\hat{T}$ and $\hat{V}$ are real [Boh69]. Furthermore, this means that the one-body matrix elements are symmetric. If the weak interactions are neglected, as

will be done in this thesis, $\hat{H}$ conserves the total parity. Obviously the Coulomb force distinguishes between protons and neutrons and introduces isovector as well as isoscalar components into $\hat{H}$ [Hey94]. Even if the Coulomb interaction was neglected the isospin is not, in general, conserved. It means that the Hamiltonian does not always commute with the square $\hat{T}^2$ of the total isospin operator and is hence not a scalar in isospin space. For an excellent discussion of isospin, see Ref. [Law80].

The Galilei invariance i.e. equivalence of all inertial systems, requires that the total effective Hamiltonian, however complicated it may be, cannot depend on the center of mass coordinate of the system $\mathbf{R} = (1/A)\sum_{i=1}^{A} \mathbf{r}_i$ and only on the trivial way on the total linear momentum $\mathbf{P} = \sum_{i=1}^{A} \mathbf{p}_i$. We can always split the Hamiltonian into an internal part depending (besides on spin and isospin degrees of freedom) only on the relative coordinates and linear momenta of the nucleons and a trivial $(1/A)\mathbf{P}^2/2m$ describing the motion of the system as a whole. In the last part the m is the nucleon mass. Obviously we are only interested in the internal part, which we shall call simply H in the following. The symmetries of this Hamiltonian (1.2) can be hence summarized as

$$[\hat{H}, \hat{A}] = [\hat{H}, \hat{T}_z] = [\hat{H}, J^2] = [\hat{H}, \hat{J}_z] = [\hat{H}, \hat{\Pi}] = [\hat{H}, \hat{\mathbf{P}}] = [\hat{H}, \hat{\mathbf{R}}] = 0, \qquad (1.3)$$

where $\hat{\Pi}$ is the parity operator. The calculations presented in chapter 3 are performed in full $1s0d$-shell using the mass-dependent version of Chung-Wildenthal [Wil84] effective interaction. The chosen interaction is determined by taking the three single particle energies and all possible 63 two-body interaction matrix elements as parameters. These parameters are fitted to experimental binding energies for 447 ground and excited states of $1s0d$-shell nuclei. For the particular interaction all the resulting states have good isospin T. Furthermore the Hamiltonian is confined to a single major shell and consequently the center of mass will always be in its groundstate. Therefore, no spurious

center of mass admixtures exist. In the chosen single particle basis the one-body spectrum is diagonal

$$t(ik) \equiv \langle i|\hat{T}|k\rangle = \delta(l_i, l_k)\delta(j_i, j_k)\delta(m_i, m_k)\delta(\tau_i, \tau_k)t(ik), \tag{1.4}$$

and the two-body term reads

$$\begin{aligned} v(ikrs) \equiv \langle ik|\hat{V}|rs - sr\rangle &= \delta(\tau_i + \tau_k, \tau_r + \tau_s) \cdot \\ &\cdot \delta((-)^{l_i+l_k}(-)^{l_r+l_s})\delta(m_i + m_k, m_r + m_s) \cdot \\ &\cdot \delta(min\{j_i + j_k, j_r + j_s\} \geq max\{|j_i - j_k|, |j_r - j_s|\})v(ikrs). \end{aligned} \tag{1.5}$$

In fact, any other Hamiltonian of type (1.2) could have been chosen, since our purpose is not to judge the interaction, but rather provide a first test for GENERAL COMPLEX MONSTER (GCM) and compare its quality to the exact SCM calculation. The freedom of choosing the interaction exhibits the diversity of the VAMPIR-MONSTER model family.

1.3 The General Complex Vampir

1.3.1 The Location in the Family Tree

The GENERAL COMPLEX VAMPIR (GCV) method represents a sub-group of a General Coordinate Method [Rin80], with a particular choice of complex generator coordinates.

The general variation equation

$$\delta E = \delta \frac{\langle \Phi|\hat{H}|\Phi\rangle}{\langle \Phi|\Phi\rangle} = 0 \tag{1.6}$$

is equivalent to the exact Schrödinger equation for the restricted nuclear many-body problem

$$\hat{H}|\Phi\rangle = E|\Phi\rangle. \tag{1.7}$$

In the conventional SCM method the solution is found by a direct diagonalization of the Hamiltonian in the complete basis of orthonormal wave functions $|\sigma; SK\rangle$, which are linear superpositions of all Slater determinants $|[SD]_i\rangle$ i.e.

$$\left\{ |\sigma; SK\rangle = \sum_{i=1}^{n} \langle [SD]_i | \sigma; SK\rangle |[SD]_i\rangle; \sigma = 1, \ldots, n(S) \leq n = \binom{M_b}{A} \right\}, \tag{1.8}$$

where the M_b is the basis dimension, A is the valence space nucleon number, K is the angular momentum 3-component, and the letter $S \equiv AT_zI\pi$ denotes the symmetries (1.3) required by the many-body Hamiltonian. On the other hand, the GCV wave functions, being solutions of a variation equation of the form (1.6), can also be written as linear combinations of states (1.8). How well this wave function fulfills the equation (1.7) depends on the variational parameters, i.e. the generating coordinates, which determine the generating wave function. In the GCV approach we choose a single symmetry projected Hartree-Fock-Bogoliubov (HFB) quasiparticle reference determinant as a product type generating wave function. Therefore the exactness of the GCV solution depends actually on the completeness of the particular quasiparticle basis, i.e. the underlying mean-field. In other words, if the number of variational parameters is large enough, the GCV approach can yield an exact solution to the many-body problem. Otherwise it gives always somewhat less bound state. In that case the extension to EXCITED GCV or EXCITED FED GCV method increases the number of variational parameters and obviously a better description for a particular state is expected. The GCM method represent an alternative extension of the GCV calculation, where all symmetry projected 2-quasiparticle states build on top of the GCV reference determinant are included into

the model space.

At this point it should also be realized, that the methods of the VAMPIR-MONSTER model family are not restricted only to the nuclear problems but could also be applied to other many-body problems if the fundamental assumptions mentioned in the beginning of the section 1.1 (now not for the nucleons but for some particles in general) are valid.

1.3.2 The Hartree-Fock-Bogoliubov Reference Determinant

The HFB-transformation [Bog58, Bog59a, Bog59b] is the most general linear quasiparticle transformation, defining a independent quasiparticle picture, with the corresponding creation- and annihilation operators in combined $2M_b$-dimensional row vector $(a_1^\dagger(F)\cdots a_{M_b}^\dagger(F)a_1(F)\cdots a_{M_b}(F)) = (a_\alpha^\dagger(F)a_\beta^\dagger(F)\cdots a_\alpha(F)a_\beta(F)\cdots) \equiv (a^\dagger(F)a(F))$ defined by

$$\begin{pmatrix} a^\dagger(F) \\ a(F) \end{pmatrix} = F \begin{pmatrix} c^\dagger \\ c \end{pmatrix} \equiv \begin{pmatrix} A^T(F) & B^T(F) \\ B^\dagger(F) & A^\dagger(F) \end{pmatrix} \begin{pmatrix} c^\dagger \\ c \end{pmatrix}. \tag{1.9}$$

The greek indices $\alpha, \beta, \ldots$ denote the quasiparticle states. The quasiparticles are also fermions, so they must obey the fermion anti-commutation relations. This leads to unitary transformation matrix F, which gives us the mathematical definition of the mean-field. The motivation for the quasiparticle transformation is to find a new and optimal quasiparticle basis, where as few configurations as possible (with respect to the mean-field) would account for as many correlations, induced by the many-body Hamiltonian into the exact eigenfunctions, as possible. The transformation F is found at the solution of the GCV variational equations. Now any operator whose representation in the particle basis is known can be casted into the quasiparticle representation using the inverse transformation $F^{-1} = F^\dagger$. The quasiparticle representation for the Hamiltonian

can be represented as

$$\hat{H}(F) = H^0(F) + \hat{H}^{11}(F) + \hat{H}^{20}(F) + \hat{H}^{22}(F) + \hat{H}^{31}(F) + \hat{H}^{40}(F) \tag{1.10}$$

The explicit expressions for these terms can be found in [Sch84a], with (unfortunately) several typos. For that reason the $\hat{H}(F)$ is given explicitly in appendix A.1.
The corresponding quasiparticle vacuum is defined by

$$a_\alpha(F)|F\rangle \equiv 0 \quad \forall\, \alpha = 1, \ldots, M_b. \tag{1.11}$$

Obviously one can choose a unique [Man75] representation via HFB quasiparticle determinant

$$|F\rangle = \left(\prod_{\alpha=1}^{M_b'} a_\alpha(F) \right) |0\rangle \quad \text{with} \quad a_\alpha(F)|0\rangle \neq 0 \quad \forall\, \alpha = 1, \ldots, M_b' \leq M_b. \tag{1.12}$$

An n-quasiparticle state with respect to the vacuum is defined by

$$|F\{a^\dagger\}_n\rangle \equiv \left(\prod_{\alpha=1}^{n} a_\alpha^\dagger(F) \right) |F\rangle \quad \text{for} \quad n = 1, \ldots, M_b. \tag{1.13}$$

Since the matrix F is unitary, the quasiparticle basis, consisting of the states (1.12) and (1.13), is orthonormal and complete for all the possible model space nuclei with $0 \leq A \leq M_b$. Its dimension $\sum_{n=0}^{M_b} \binom{M_b}{n} = 2^{M_b}$ equals the sum of the total SCM dimensions for all these nuclei. Therefore the diagonalization of the Hamiltonian in this complete basis would yield the exact solutions for all the model space nuclei simultaneously. Obviously this is numerically even more involved than a complete SCM calculation for a given particle number A. Any of the states (1.13) can be represented as a vacuum for quasiparticles, which are obtained by interchanging the n rows corresponding the operators $a_\alpha^\dagger(F)$ with those corresponding to the operators a_α in matrix F. Therefore any configuration (1.13) can be represented as a suitable chosen vacuum. In principle, for any incomplete set of quasiparticle determinants (1.11) and (1.13) one can obtain an

optimal transformation F which corresponds to an optimal mean-field. In the conventional HFB-theory a single determinant in the form of a quasiparticle vacuum is found by a variational principle for a total energy. However the quasiparticle determinant cannot be considered as a physical state because it does not have any of the symmetries (1.3) required by the many-body Hamiltonian. Since the transformation (1.9) sums over all the quantum numbers $\{nljm\tau\}$ characterizing the single nucleon basis states, the $|F\rangle$ (or any of the states (1.13)) is neither an eigenstate of the square of the total angular momentum operator I^2 nor of its 3-component I_3. Furthermore particle number and charge conservation are violated and, in general, it has no definite parity either. The only symmetry still conserved is the so-called "number-parity" [Man75], i.e. $|F\rangle$ contains either only components with even or with odd total nucleon numbers A. For a deeper insight into the contents of the transformation, as well as to the contents of the corresponding vacuum we can decompose the F into three successive transformations using the Bloch-Messiah theorem [Blo62]:

$$F \equiv C\overline{UV}D \equiv \begin{pmatrix} C^T & 0 \\ 0 & C^\dagger \end{pmatrix} \begin{pmatrix} U^T & V^T \\ V^\dagger & U^\dagger \end{pmatrix} \begin{pmatrix} D^T & 0 \\ 0 & D^\dagger \end{pmatrix}. \tag{1.14}$$

The first one D, conserves the particle number and defines a Hartree-Fock type unitary transformation among the particle operators, generating the so called canonical basis. The corresponding part of the mean-field contains all the long range particle-hole type correlations of the Hamiltonian [Rin80]. In the canonical basis with creation- and annihilation operators $(b^\dagger b)$ defined as

$$\begin{pmatrix} b^\dagger \\ b \end{pmatrix} \equiv \begin{pmatrix} D^T & 0 \\ 0 & D^\dagger \end{pmatrix} \begin{pmatrix} c^\dagger \\ c \end{pmatrix} \tag{1.15}$$

the hermitian density matrix

$$\rho_{sk}(F) \equiv \langle F|c_k^\dagger c_s|F\rangle = (B^*(F)B^T(F))_{sk} \quad k,s = 1,\ldots,M_b \tag{1.16}$$

is diagonal,

$$\tilde{\rho}_{\alpha\beta}(F) \equiv \langle F|b^{\dagger}_{\beta}b_{\alpha}|F\rangle = (D^{\dagger}\rho D)_{\alpha\beta} = (V^{*}V^{T})_{\alpha\beta} \equiv v^{2}_{\alpha}\delta_{\alpha\beta}, \tag{1.17}$$

where the eigenvalues $v^2_\alpha \geq 0$ are the occupation probabilities for the quasiparticle states α. In other words, the transformation D is used to diagonalize ρ. In this representation the skew-symmetric pairing tensor

$$\kappa_{sk}(F) \equiv \langle F|c_k c_s|F\rangle = (B^{*}(F)A^{T}(F))_{sk} \quad k,s = 1,\ldots,M_b \tag{1.18}$$

gets a canonical form

$$\tilde{\kappa}_{\alpha\beta}(F) \equiv \langle F|b_{\beta}b_{\alpha}|F\rangle = (D^{\dagger}\kappa D^{*})_{\alpha\beta} = (V^{*}U^{T})_{\alpha\beta}. \tag{1.19}$$

Unless at least 2-fold degeneracy is found for a state α i.e. a conjugate partner state $\bar{\alpha}$ with equal occupation probability $v^2_\alpha = v^2_{\bar{\alpha}}$ exists the pairing tensor vanishes and the state α is unpaired, or "blocked". The blocked states β are either fully occupied ($v^2_\beta = 1$) or empty ($v^2_\beta = 0$). It should be noted that the character of the conjugate states is not specified here. The states can have any symmetry leading to 2-fold or higher degeneracies.

The $\overline{UV}$ is a sort of BCS transformation in the canonical basis which incorporates the short range pairing correlations in the mean-field. It can be chosen to be real, because any complex phases can be shifted to the transformations C and D. The anti-commutation requirements lead again to the unitarity but as it mixes the creation and annihilation operators in the canonical basis the particle number is not anymore conserved. We obtain $U_{\alpha\beta} = u_\alpha\delta_{\alpha\beta}$ and $V_{\alpha\beta} = v_{\bar{\alpha}}\delta_{\alpha\bar{\beta}}$. An appropriate choice of the phase leads to $u_{\bar{\alpha}} = u_\alpha$ and $v_{\bar{\alpha}} = -v_\alpha$. Now one can write the pairing tensor (1.19) in the canonical form $\tilde{\kappa}_{\alpha\beta} = v_\alpha u_{\bar{\alpha}}\delta_{\bar{\alpha}\beta}$.

Since the vacuum $|F\rangle$ is defined by (1.11) the last unitary transformation C leaves it unaffected. Therefore, the structure of the HFB-quasiparticles is uniquely determined

only after fixing this last Bloch-Messiah transformation but the transformations D and $\overline{UV}$ (or the matrices ρ and κ) on the other hand uniquely determine the vacuum. Suppose we have p completely paired states α with conjugate partner $\bar{\alpha}$ while of the remaining $M_b - 2p$ states f are fully occupied and the rest are empty. The normalized vacuum can be explicitly written as

$$|F\rangle = N \left(\prod_{\beta=2p+1}^{2p+f=M_b'} a_\beta \right) \left(\prod_{\alpha=1}^{p} a_\alpha a_{\bar{\alpha}} \right) |0\rangle = \left(\prod_{\beta=2p+1}^{2p+f} b_\beta^\dagger \right) \left(\prod_{\alpha=1}^{p} (u_\alpha + v_\alpha b_\alpha^\dagger b_{\bar{\alpha}}^\dagger) \right) |0\rangle. \quad (1.20)$$

It is easy to see that the state (1.20) does not have a definite particle number, but since the paired part (which is a BCS-type vacuum) contains only components with even particle number the number parity is conserved. The high generality of the HFB-vacuum (1.12) becomes more evident when expanding it in the complete basis of SCM states (1.8). We obtain

$$|F\rangle = \sum_{SK} \sum_{\sigma=1}^{n(S)} \langle \sigma; SK|F\rangle |\sigma; SK\rangle, \quad (1.21)$$

where the first sum can cause symmetry mixing in the case of some non vanishing amplitudes $\langle \sigma; SK|F\rangle$ for different symmetries S. Only the sum over σ is wanted, because it gives an expansion in terms of the SCM configurations of type (1.8). Since the SCM configurations are itself a linear combinations of Slater determinants we end up with a reference state (1.21), which is a still more complicated combination of them. Our aim was to account for as many particle configurations (1.8) as possible via a single quasiparticle determinant (1.12). Consequently the symmetry breaking is the price we have to pay for this attempt. The physical variational wave functions can be constructed out of these intrinsic structures (1.21) by projecting to the eigenspace of the symmetry operators (1.3).

1.3.3 The Generator Wave Function

It is essential to restore the broken symmetries before determining the mean-field via variation. Otherwise the symmetry dependencies of the mean-field cannot be accounted for properly. On the other hand, if the projection were done after mean-field variation the projected wave function would not satisfy the variational equation (1.6) and hence it cannot be the optimal solution for the simultaneously conserved quantum numbers. The states with good symmetries are obtained by using projection techniques. The projection techniques for the restoration of broken rotational symmetry [Pei57, Vil66] and number (A, T_z) conservation [Bay60] from the HFB-quasiparticle determinants have been known for a long time. The combined projection operator [Sch84a, Sch87b] is defined by

$$\hat{\Theta}^S_{MK} \equiv \sum_{\sigma=1}^{n(S)} |\sigma; SM\rangle\langle\sigma; SK| \equiv \hat{P}(IM;K)\hat{P}(2T_z)\hat{P}(A)\hat{P}(\pi), \tag{1.22}$$

where the first operator from the left projects on good angular momentum I with 3-component M, the next two on good isospin z-component T_z, good mass number A and finally the last one on good parity π. The order of the projections in $\hat{\Theta}^S_{MK}$ is irrelevant, since they commute with each other. From the definition (1.22) it is clear that $[\hat{H}, \hat{\Theta}^S_{MK}] = 0$ and also

$$\begin{cases} \hat{\Theta}^{S\dagger}_{MK} = \hat{\Theta}^S_{KM} \\ \hat{\Theta}^{S\dagger}_{MK}\hat{\Theta}^S_{M'K'} = \hat{\Theta}^S_{KK'}\delta_{MM'}. \end{cases} \tag{1.23}$$

In practice it is more useful to work with the integral representation,

$$\begin{aligned} \hat{\Theta}^S_{MK} &= \frac{(2I+1)}{32\pi^4} \iiint \mathrm{d}\Omega \int_0^{2\pi} d\varphi \int_0^{2\pi} d\chi D^{I*}_{MK}(\Omega)\hat{R}(\Omega)\hat{P}(\pi)e^{2i\chi(T_z-\hat{T}_z)}e^{i\varphi(A-\hat{A})} \\ &\equiv \int \mathrm{d}\tilde{\Omega}\,\omega^{S*}_{MK}(\tilde{\Omega})\hat{\tilde{R}}(\tilde{\Omega})[1+\pi\hat{\Pi}]. \end{aligned} \tag{1.24}$$

Here $\hat{R}(\Omega) \equiv \exp[-i(\alpha I_z + \beta I_y + \gamma I_z)]$ is the usual rotation operator with the Euler angles $\Omega \equiv (\alpha, \beta, \gamma)$ and the Wigner function $D^I_{MK}(\Omega) \equiv \langle IM|\hat{R}(\Omega)|IK\rangle$ its representation in

angular momentum eigenstates [Edm57]. Good parity π is restored, if necessary, by the operator $\hat{P}(\pi) \equiv \frac{1}{2}(1 + \pi\hat{\Pi})$. In the integration α and γ go from 0 to 2π, β from 0 to π. The rotations in the coordinate space and gauge space have been combined by defining the generalized rotation operator $\hat{\tilde{R}}(\tilde{\Omega}) \equiv \hat{R}(\Omega)\exp[-i(2\chi\hat{T}_z + \varphi\hat{A})]$ with the generalized rotation angle $\tilde{\Omega} \equiv (\Omega\chi\varphi)$ and the corresponding weight function $\omega^{S*}_{MK}(\tilde{\Omega})$. The differential element $\mathrm{d}\tilde{\Omega} \equiv \mathrm{d}\Omega\,\mathrm{d}\chi\,\mathrm{d}\varphi \equiv \mathrm{d}\alpha\,\mathrm{d}\gamma\,\sin\beta\mathrm{d}\beta\,\mathrm{d}\chi\,\mathrm{d}\varphi$. An explicit derivation of the symmetry projectors can be found in [Sch84a].

Now projecting the expansion (1.21) yields configurations with good symmetry S. However, they still depend on the choice of the intrinsic frame of reference via the K-quantum number! To get rid of this very unphysical dependence, we introduce new configuration mixing coefficients f, which are to be determined in the variational process. Furthermore, these additional variation parameters guarantee that the following ansatz for the wave function of the system is orthonormalized

$$|F; SM\rangle = \sum_{K=-I}^{I} \hat{\Theta}^{S}_{MK}|F\rangle f^{S}_{K}. \tag{1.25}$$

Notice, that this is not anymore a vacuum for the quasiparticles of type (1.9), but rather a particular linear superposition of all possible even number quasiparticle states from the complete set $\{|F\rangle, |F\{a^\dagger\}_n\rangle;\ n = 1, \ldots, M_b\}$. However, in the GCV calculations one gets contributions from only up to 6 quasiparticle configurations with respect to the HFB vacuum, because the Hamiltonian contains at most 4 quasiparticle annihilation operators. Consequently, the GCV description of the states with more complicated structure is inadequate and more sophisticated methods have to be applied, see section (1.3.5). For the same reason only up to 6 quasiparticle configurations with respect to the HFB vacuum yield contributions in the GCM method, see section 1.4.1.

Consider an arbitrary intrinsic coordinate system, where the quasiparticle vacuum is defined as $\hat{R}(\Omega_0)|F\rangle$, then

$$
\begin{aligned}
|F;SM\rangle &= \sum_K \hat{\Theta}^S_{MK}\hat{R}(\Omega_0)|F\rangle f^S_K \\
&= \sum_{\sigma=1}^{n(S)} |\sigma;SM\rangle \left\{ \sum_{K'} \left[f^S D^I(\Omega_0)\right]_{K'} \langle\sigma;SK'|F\rangle \right\} \\
&= \sum_K \hat{\Theta}^S_{MK}|F\rangle \left[f^S D^I(\Omega_0)\right]_K ,
\end{aligned}
\tag{1.26}
$$

inducing an unitary transformation $f^S D^{I\dagger}(\Omega_0)$ on the variation parameters f^S without affecting the orthonormalization of the states (1.25).

In principle the ansatz (1.25) is a special case of the General Coordinate Methods generator wave function [Rin80]. Using the form (1.24) of the projection operator we have

$$
|F;SM\rangle = \int \mathrm{d}\tilde{\Omega} \left[\omega^{S*}(\tilde{\Omega})f^S\right]_M |F(\tilde{\Omega})\rangle, \tag{1.27}
$$

where the generating functions are identified as the rotated HFB-vacuums $|F(\tilde{\Omega})\rangle \equiv \hat{\tilde{R}}(\tilde{\Omega})|F\rangle$ with the corresponding weight functions $\left[\omega^{S*}(\tilde{\Omega})f^S\right]_M$. In this case the generator coordinates are the HFB-transformation (1.9) and the configuration mixing coefficients f^S_K.

1.3.4 The Variational Equations

In the GENERAL COMPLEX VAMPIR the configuration space is restricted to the test wave function of type (1.25). Actually, the symmetry projected configuration written as

$$
|F;SM\rangle = \sum_{\sigma=1}^{n(S)} |\sigma;SM\rangle \left(\sum_{K=-I}^{I} \langle\sigma;SK|F\rangle f^S_K \right) \tag{1.28}
$$

looks formally identical to the complete SCM expansion in the basis (1.8). It depends on a particular problem how complete the HFB-vacuum is with respect to the SCM-configurations. The arbitrary variations of the energy-functional

$$
\delta E[F,f^S] \equiv \delta \frac{\langle F;SM|\hat{H}|F;SM\rangle}{\langle F;SM|F;SM\rangle} = 0, \tag{1.29}
$$

with respect to the underlying HFB-transformation F as well as the configuration mixing degrees of freedom f^S yield the optimal representation of the energetically lowest, yrast, state of a given symmetry S in terms of a single symmetry projected HFB-determinant. This optimal solution, minimizing the residual interaction, corresponds to the diagonalization of the Hamiltonian (1.6) in the subspace of linear independent SCM-configurations contained in (1.28).

The variation leads to three sets of equations which have to be solved self-consistently. The first set results from the variation with respect to the configuration mixing degrees of freedom f^S. It leads to the generalized eigenvalue problem (diagonalization of the Hamiltonian)

$$\left(H^S - E^S N^S\right) f^S = 0, \tag{1.30}$$

in the non-orthogonal basis of states

$$\hat{\Theta}^S_{MK}|F\rangle \equiv |F; SMK\rangle, \tag{1.31}$$

with the orthonormalization constraint

$$\langle F; SM|F; SM\rangle = (f^S)^\dagger N^S f^S = \mathbf{1}. \tag{1.32}$$

The Hamiltonian and the overlap matrices are given by

$$\begin{aligned} \left\{ \begin{array}{c} H^S_{KK'} \\ N^S_{KK'} \end{array} \right\} &= \langle F| \left\{ \begin{array}{c} \hat{H} \\ \hat{1} \end{array} \right\} \hat{\Theta}^S_{KK'}|F\rangle \\ &= \langle F; SMK| \left\{ \begin{array}{c} \hat{H} \\ \hat{1} \end{array} \right\} |F; SMK'\rangle. \end{aligned} \tag{1.33}$$

The GCV solution corresponds to the lowest energy solution of at maximum $2I + 1$ linearly independent states $|F; SM\rangle_i$. Notice the unit matrix in (1.32), for the orthonormalization of *all* the resulting solutions.

The variation of the functional (1.29) with respect to the HFB transformation can be replaced by a variation with respect to an anti-symmetric $(M_b \times M_b)$ matrix d, which gives an unique parametrization of the transformation matrix in terms of $M_b(M_b-1)/2$ complex variables. According to the Thouless's Theorem [Tho60, Man75] any HFB-vacuum $|F^d\rangle$ can be written in terms of an arbitrary chosen vacuum $|F^0\rangle$, non-orthogonal to $|F^d\rangle$, as

$$|F^d\rangle = \langle F^0|F^d\rangle \exp\left\{\frac{1}{2}a^\dagger(F^0)d(F^d)\,a^\dagger(F^0)\right\}|F^0\rangle, \tag{1.34}$$

with the corresponding HFB-transformation

$$F^d \equiv \tilde{F}^d F^0 = \begin{pmatrix} L_d^{-1*} & -(L_d^{-1}d(F^d))^* \\ -L_d^{-1}d(F^d) & L_d^{-1} \end{pmatrix} F^0 \quad \text{with} \quad \mathbf{1} + d^T d^* = L_d L_d^\dagger. \tag{1.35}$$

The non-orthogonality of the vacuums means that in the above equation we can find the inverse ${L_d}^{-1}$, since the norm of the overlap turns out to be $|\langle F^0|F^d\rangle|^2 = |\det[L_d^{-1}]|$, see equations (C.18) and (C.10). To mention, as a special case, the reference vacuum $|F^0\rangle$ can be the particle vacuum, since we assumed only a non-vanishing normalization constant, i.e. condition $\langle F^0|F^d\rangle \neq 0$. In that case $F^0 = \mathbf{1}$, so comparing (1.35) and (1.9) one finds that $d(F) = (B(F)A^{-1}(F))^*$. The generality of the Thouless's theorem enables to apply it also when defining the rotated vacuums $\hat{\tilde{R}}(\tilde{\Omega})|F\rangle$, useful when calculating the rotated matrix elements of type (1.33) and (1.37), later in the wider context of the GCM matrix elements for the Hamiltonian and the overlap, see section 1.4.1 and appendix C. Consequently the variation with respect to the matrix elements of F can be replaced by the variation with respect to the matrix elements of d. One obtains the second set of variational equations

$$\frac{\partial E^S}{\partial d_{\alpha\beta}} = \left[(L_d^{-1})^T\,\tilde{g}\,(L_d^{-1})\right]_{\alpha\beta} = 0; \quad \alpha < \beta = 1, \ldots, M_b, \tag{1.36}$$

where the matrix element of the local gradient to the direction $\alpha\beta$ is defined by

$$\begin{aligned}\tilde{g}_{\alpha\beta} &\equiv \sum_{KK'} f^{S*}_K \langle F^d|[\hat{H} - E^S]\hat{\Theta}^S_{KK'} a^\dagger_\alpha(F^d) a^\dagger_\beta(F^d)|F^d\rangle f^S_{K'} \\ &\equiv \sum_{KK'} f^{S*}_K \langle F^d; SMK|\hat{H} - E^S|F^d_{\alpha\beta}; SMK'\rangle f^S_{K'}, \end{aligned} \tag{1.37}$$

and has to vanish at the solution. Here I have introduced a notation

$$|F^d_{\alpha\beta}; SMK\rangle \equiv \hat{\Theta}^S_{MK} a^\dagger_\alpha(F^d) a^\dagger_\beta(F^d)|F^d\rangle. \tag{1.38}$$

The equation (1.36) combined with the equation (1.37) represents a sort of generalized Brillouin theorem, which expresses the stability of the GCV solution $|F; SM\rangle$ against any arbitrary projected 2-quasiparticle states with the same symmetry S. Although the generalized Brillouin theorem holds for all GCV solutions it must be reconsidered in the case of GCM solution. In the GCM approach the configuration mixing coefficients are obtained from the new diagonalization and thus actually newly varied. For more about the Brillouin theorem in the context of the GCM approach, see section 1.4.1.

Although these two sets of equations (1.30),(1.32) and (1.36) provide a complete GCV solution they do not determine the HFB-transformation unambiguously. In general, the HFB vacuum is invariant with respect to arbitrary unitary transformations among the quasiparticle operators, see section 1.3.2. This remaining degree of freedom can be used to diagonalize any Hermitian $(M_b \times M_b)$ matrix. It is convenient to choose here the quasiparticle energy matrix $\tilde{H}^{11}(F)$, defined by

$$\tilde{H}^{11}_{\alpha\beta} \equiv \langle F|a_\alpha \left[\hat{H} - \lambda\hat{A} - \mu\hat{T}_z\right] a^\dagger_\beta|F\rangle - \langle F| \left[\hat{H} - \lambda\hat{A} - \mu\hat{T}_z\right] |F\rangle, \tag{1.39}$$

where chemical potentials λ and μ are determined in the usual way, requiring the right expectation value for the mass number and isospin projection in the HFB-quasiparticle vacuum. For more detailed discussion, see appendix B. The $\tilde{H}^{11}(F)$ is diagonalized via

the unitary transformation U,

$$U^{\dagger}\tilde{H}^{11}U = \varepsilon \mathbf{1}_{M_b}. \tag{1.40}$$

It is essential to use the operator $\hat{H} - \lambda\hat{A} - \mu\hat{T}_z$ instead of only $\hat{H}$. This ensures the right average particle number for the one-quasiparticle states. The last Bloch-Messiah transformation C (1.14) is now fixed via this particular transformation U:

$$\begin{pmatrix} \tilde{a}^{\dagger}(\tilde{F}) \\ \tilde{a}(\tilde{F}) \end{pmatrix} = \begin{pmatrix} U^T & 0 \\ 0 & U^{\dagger} \end{pmatrix} \begin{pmatrix} a^{\dagger}(F) \\ a(F) \end{pmatrix}. \tag{1.41}$$

It turns out that the resulting quasiparticle energies ε_α corresponding to the HFB transformation $\tilde{F}$ can be used later on as truncation criteria in the GCM approach.

Similar variational equations (1.30),(1.32) and (1.36) have already been proposed decades ago [Zeh65, Zeh67]. Only recently, the advent of supercomputers have made it possible to solve them also for realistic problems without any restrictions or additional approximations, see [Ham98, Hje00]. In the realistic cases studied so far, the GCV method reproduces nicely the SCM yrast spectrum, the relative deviation being typically only few tenths of a per cent, when no truncations are used. The GCV turns out to be an excellent truncation scheme, because in the problems studied so far it yields considerably more binding than the conventional SCM truncation schemes.

1.3.5 Beyond the mean-field approximation

The GCV solution does not always provide a sufficient description of the yrast state. Sometimes the complicated structure of the state due to, say high collectivity, leads to large underbinding. The most important missing correlations can be included via additional symmetry-projected quasiparticle determinants, which are achieved by chains of similar variational calculation as described above. This is a simple extension of the single

determinant GCV method to use of several determinants. Of course, the already obtained determinants must be projected out of the variation space. Since in this procedure each of the additional determinant is found via a new successive variation, some particular additional determinant cannot give more correlations than the previously added one. Usually the calculation gets numerically extremely involved after few determinants have been included. This method, where a linear combination of few states of type (1.28) is used for a description of the yrast state is known as FED (**Few** **D**eterminant) GCV [Sch89].

Up to so far only yrast states were considered. The extension for a description of excited states with the same symmetry is straightforward in the framework of the GCV of FED GCV methods. These extensions are known as EXCITED GCV [Sch87b, Zhe89] if only one determinant is used for each state or EXCITED FED GCV [Sch89, Koi89] if several of them are admitted. The orthonormality of every new state with respect to already obtained states (also yrast state) is guaranteed by Gram-Schmidt orthogonalization. Simultaneously that particular state is projected out of the variation space. The variational character of the methods ensures that the excited states are obtained successively with increasing energy. Finally, the residual interaction between all these EXCITED GCV or EXCITED FED GCV states can be diagonalized. This maneuver takes us beyond the the usual mean-field type approach. The resulting final wavefunctions are then linear combinations of the states produced by successive orthonormality-constrained variations. However, if we do not perform this diagonalization in the EXCITED GCV approach it remains as mean-field type approximation. Each of the states is then simply based on a different mean-field. The principle difference between the EXCITED GCV and EXCITED FED GCV is that in the latter method the residual interaction between the resulting states is already smaller before the diagonalization. The most correlating

determinants found in the EXCITED FED GCV can situate such high in energy that their description with the EXCITED GCV method is practically impossible.

In theory, the FED GCV, EXCITED FED GCV [Sch89, Koi89] and EXCITED VAMPIR methods converge to the exact SCM solutions when taking into account enough correlating quasiparticle determinants. In practice this is not always possible, because the numerical burden grows rapidly as the number of determinants increases. A m-determinant FED GCV calculation means at least $\frac{1}{2}m(m+1)-1$ times the computation time of a single GCV calculation due to the extra overlap and Hamiltonian matrix elements between different determinants. Consequently, one is restricted to only few determinants, and hence, to the few lowest states. Although the numerical implementation of the EXCITED GCV and the EXCITED FED GCV methods was done already years ago they have not been applied in any realistic nuclear structure calculation so far.

These methods described above are well suited for description of the few lowest states of a given symmetry with arbitrary complexity i.e. no restrictions being made on their particular structure. It is impractical to apply them for high excited states or, if for example, the complete excitation spectrum with respect to some electromagnetic one-body transition operator is required. For such task a more suitable approach must be considered. In general, the states reached by one-body operator cannot have too different structures. Intuitively, the first choice would be to expand the nuclear wavefunctions with respect to some particular GCV solution by considering only the simplest quasiparticle configurations, namely the vacuum and the all two quasiparticle excitations with respect to it, obviously combined with the symmetry restoration. Since now only one quasiparticle transformation is needed the variational calculation must be done only once for a given symmetry. This leads us to the GENERAL COMPLEX MONSTER method.

1.4 The General Complex Monster

For problems which require a complete excitation spectrum with respect to some transition operator only such specific states are relevant, which are predominantly populated in the particular transition. The GENERAL COMPLEX MONSTER (GCM) (**Mo**del for handling many **N**umber and **S**pin projected **T**wo quasi-particle **E**xcitations in **R**ealistic model spaces) approach [Sch84b, Sch87a] provides a method for producing a large spectra of states with similar structure by expanding the nuclear wave functions around a suitable GCV vacuum. The similarity ensures, that they are easily reached by simple transition operators, like one-body type. In quasiparticle picture such operator contains terms which conserve the quasiparticle number or alter it by two.

The method is especially designed for calculation of expectation values of one-body electromagnetic transition operators. Some possible applications could be the calculation of electromagnetic multipole moments and transitions, form factors, β- and double β-decay calculations.

During the years rather comprehensive calculations have been made with the symmetry restricted methods of the MONSTER model family, like the *Real* MONSTER [Sch84b, Sch87a, Ham85, Ham86a, Ham86b] and more recently with the *Complex* MONSTER [Ben95a, Ben95b, Ben96]. Also a MONSTER type model, although restricted to use fixed intrinsic mean-fields (standard HFB theory) and only separable forces have been introduced by Hara and Sun [Har91].

In the next section the theoretical basis of the most general method of the MONSTER model family, namely the GCM method is outlined. After that I consider the possibilities to solve the GCM general eigenvalue problem and discuss the dimensions of the related matrices. In subsection 1.4.4 the formulas for the general tensor operators in the GCM basis are presented with an example. In the last subsection 1.4.5 an approximate method

for elimination of the center-of-momentum (COM) excitations is presented. It becomes relevant, when the single particle basis consists more than one major oscillator shell. The new GCM code (chapter 2) is implemented with an option to make the COM-treatment.

1.4.1 The Monster on Vampir Approach

The GENERAL COMPLEX MONSTER (GCM) configuration space

$$\{|Q;SMK\rangle\} \equiv \{|F;SMK\rangle,\ |F_{\alpha\beta};SMK\rangle;\ \alpha<\beta;\ K=-I,\ldots,+I\} \tag{1.42}$$

consists out of the symmetry projected HFB-vacuum

$$|F;SMK\rangle \equiv \hat{\Theta}^{S}_{MK}|F\rangle \tag{1.43}$$

and all the possible symmetry-projected 2-quasiparticle states

$$|F_{\alpha\beta};SMK\rangle \equiv \hat{\Theta}^{S}_{MK}a^{\dagger}_{\alpha}(F)a^{\dagger}_{\beta}(F)|F\rangle \tag{1.44}$$

with respect to it in the chosen model space. Note that the transformation F is not necessarily determined for the symmetry S, but is fixed during the calculations.

Notice, that the GCM basis (1.42) is not orthonormal. Furthermore, because the Hamiltonian takes into account only 2-nucleon interactions, only particular superpositions of $0, 2, 4$ and 6 quasiparticle states have effective contributions. This was already pointed out in section 1.3.3. The consequences here are not so crucial, since we are interested only in states with structures similar to the particular yrast state. Usually the GCM configuration space (1.42) is sufficient for this purpose. Furthermore, one has the freedom of choosing the underlying mean-field F corresponding any symmetry and thus obtain states with desired structures. Hypothetically, the GCM method could be improved by including the projected $4, 6$, or even more quasiparticle states into the configuration space, but very soon one encounters the same numerical difficulties as the SCM

method. The number of projected 2-quasiparticle states is already $\frac{1}{2}M_b(M_b-1)(2I+1)$. Sometimes for large model spaces or high spins even this number has to be cut.

The diagonalization of the total Hamiltonian in the non-orthogonal basis (1.42)

$$\sum_{Q'K'}\left\{H^S_{QK;Q'K'} - E^S N^S_{QK;Q'K'}\right\} g^S_{Q'K'} = 0 \qquad \forall \quad Q,K. \tag{1.45}$$

yields the GCM wave functions

$$\begin{aligned} |\psi_i(F);SM\rangle &\equiv \sum_{QK} |Q;SMK\rangle g^S_{QK;i} \\ &= \left\{ \sum_K |F;SMK\rangle g^S_{0K;i} + \sum_{\alpha<\beta,K} |F_{\alpha\beta};SMK\rangle g^S_{\alpha\beta K;i} \right\}, \end{aligned} \tag{1.46}$$

which are orthonormalized via the constraint

$$\langle\psi(F);SM|\psi(F);SM\rangle = (g^S)^\dagger N^S g^S = \mathbf{1}. \tag{1.47}$$

The Hamiltonian and overlap matrix elements entering the above equations are given by

$$\left\{ \begin{array}{c} H^S_{QK;Q'K'} \\ N^S_{QK;Q'K'} \end{array} \right\} = \int d\tilde{\Omega}\, \omega^{S*}_{KK'}(\tilde{\Omega}) \langle Q| \left\{ \begin{array}{c} \hat{H} \\ \hat{1} \end{array} \right\} \hat{\tilde{R}}(\tilde{\Omega})[1+\pi\hat{\Pi}]|Q'\rangle \tag{1.48}$$

$$= \langle Q;SMK| \left\{ \begin{array}{c} \hat{H} \\ \hat{1} \end{array} \right\} |Q';SMK'\rangle. \tag{1.49}$$

For details of determining the rotated matrix elements in (1.48), see appendix C. The configuration mixing coefficient g^S are determined by the diagonalization (1.45). The underlying mean-field is found as a solution of the preceding GCV calculation, the transformation F being obtained from the variation of the yrast state energy functional (1.29) for some symmetry. The new GCM g^S coefficients do not necessarily have the same K-dependence than the original GCV configuration mixing coefficients f^S. That is, they can differ more than some K-independent constant and then the Brillouin theorem

(1.36) does not hold anymore for these g^S. However, the GCM calculation based on the GCV solution for $I = 0$ yrast state reproduces always the particular GCV yrast state of the same symmetry. In this case only a single normalization constant f_0^S exists and the vanishing local gradient (1.37) prevents the GCM $I = 0$ yrast state having any projected 2-quasiparticle configurations. It is easily seen, that the equation (1.45) for the vacuum configuration is then equivalent to the first GCV variational equation (1.30). In general all other GCM solutions for the yrast states being based on the GCV solution of any symmetry can get contributions from the projected 2-quasiparticle configurations.

Even so, that the GCM yrast states obtained for different symmetries than that of the underlying HFB transformation can be more bound compared to the GCV solutions for these symmetries. However, the GCM yrast description for the symmetry ($I > 0$) of the underlying mean-field is rather likely to be still lower in energy because by construction the GCV description for the particular symmetry is already the optimal one-determinant solution guaranteed by the variational principle. On contrary to the GCV approach the $I > 0$ yrast states can be correlated by the projected 2-quasiparticle configurations (1.44). That is, the GCM yrast state can be more bound than the GCV yrast of the same symmetry and the generalized Brillouin theorem holds in general only for the GCV configuration mixing coefficients f^S. In the GCM approach the coefficients f^S are varied newly by the diagonalization (1.45) resulting in the configuration mixing via the coefficients g^S.

Theoretically speaking, by varying the configuration mixing and mean-field degrees of freedom simultaneously one may obtain an even better solution than by the standard GCM approach using any of the GCV transformations.

Next I show how the GCM diagonalization (1.45) can be formulated.

1.4.2 The GCM Generalized Eigenvalue Problem

The GCM generalized eigenvalue problem (1.45) can be written in a shorter matrix form as

$$(H^S - E^S N^S) g^S = 0, \tag{1.50}$$

where the matrix elements are given in equation (1.49). The projected overlap is defined there as

$$N^S_{QK;Q'K'} = \langle Q; SMK | Q'; SMK' \rangle = \langle Q | \hat{\Theta}^S_{KK'} | Q' \rangle = (y^{S\dagger} y^S)_{QK;Q'K'}, \tag{1.51}$$

where the equation (1.22) and the notation

$$y^S_{\sigma;QK} \equiv \langle \sigma; SK | Q \rangle \tag{1.52}$$

has been used. Obviously N is Hermitian by construction and furthermore, since for an arbitrary column vector z with proper dimension

$$z^\dagger N^S z = z^\dagger (y^{S\dagger} y^S) z = (y^S z)^\dagger (y^S z) \geq 0, \tag{1.53}$$

also positive definite. This means that it can be diagonalized with orthonormalized eigenvectors $f^S_{QK;i}$ resulting real and positive eigenvalues $n_1^2, n_2^2, \ldots, n_i^2, \ldots$. That is, in matrix notation

$$f^{S\dagger} N^S f^S = \mathbf{1} n^2, \quad \text{with} \quad f^{S\dagger} f^S = \mathbf{1}. \tag{1.54}$$

Some of the eigenvalues of the overlap matrix may be zero and have to be cut out in order to be able to multiply equation (1.50) appropriately to get

$$\begin{aligned} n^{-1} f^{S\dagger} (H^S - E^S N^S) f^S n^{-1} n f^{S\dagger} g^S &= (n^{-1} f^{S\dagger} H^S f^S n^{-1} - E^S \mathbf{1})(n f^{S\dagger} g^S) \\ &\equiv (\tilde{H}^S - E^S \mathbf{1}) x^S = 0, \end{aligned} \tag{1.55}$$

which represents a standard diagonalization of the Hamiltonian $\tilde{H}^S$ yielding the eigenvalues E^S with the corresponding expansion coefficient matrices x_i^S, which are orthonormal since the constraint (1.47) must hold.

$$x^{S\dagger}x^S = g^{S\dagger}f^S n^\dagger n f^{S\dagger}g^S = g^{S\dagger}f^S \mathbf{1} n^2 f^{S\dagger}g^S = g^{S\dagger}N^S g^S = \mathbf{1}. \tag{1.56}$$

Finally, the original non-orthonormalized expansion matrices are produced via matrix multiplication

$$g^S = f^S n^{-1} x^S. \tag{1.57}$$

The orthonormalization yields

$$g_o^S \equiv \sqrt{N^S} g^S = f^S x^S. \tag{1.58}$$

For more detailed discussion of standard methods used for solving the generalized eigenvalue problem, see [Wil65].

It is interesting to notice, that this procedure is actually equivalent to the diagonalization of the Hamiltonian in the subspace of all the SCM configurations for a given symmetry existing in the GCM configuration space. This can be seen if we apply (1.22) also for the Hamiltonian and rewrite (1.50) using (1.51) as

$$y^{S\dagger}(h^S - E^S\mathbf{1})x^S = 0 \quad \Leftrightarrow \quad x^{S\dagger}(h^S - E^S\mathbf{1})x^S = 0, \tag{1.59}$$

where

$$h^S_{\sigma\sigma'} \equiv \langle \sigma; SM|\hat{H}|\sigma'; SM\rangle, \tag{1.60}$$

and the orthonormality of the eigenvectors x^S is guaranteed by equation (1.56).

An alternative way to solve a generalized eigenvalue problem is the use of so called secular equation, which is not used in the GCV or GCM code but for completeness

outlined briefly in the following. Firstly, one deduces from the equation (1.50) that the inverse of $(H^S - E^S N^S)$ cannot exist, since otherwise the g^S would be identically zero. This leads to the secular equation, $\det(H^S - E^S N^S) = 0$. The solutions are the eigenenergies, which are then substituted back to the equation (1.45) in order to get also the eigenvectors.

The numerical solutions of the GCM code support the use of equation (1.54) followed by (1.55). For more about the numerical implementation of the diagonalization, see section 2.5.

1.4.3 The Dimensions of the GCM Matrices

The projected GCM Hamiltonian and overlap (1.49) are both complex, Hermitian

$$\aleph^I \times \aleph^I \equiv \left[\left(\frac{1}{2}M_b(M_b-1)+1\right)(2I+1)\right] \times \left[\left(\frac{1}{2}M_b(M_b-1)+1\right)(2I+1)\right] \qquad (1.61)$$

matrices. Usually this dimension is not too large for the diagonalization. The first row of (1.49) consists of $2I+1$ projected vacuum energies (and overlaps), the other $\frac{1}{2}M_b(M_b-1)(2I+1)$ elements have the projected vacuum on one side and projected 2-quasiparticle state on the other. The rest of the GCM energy and overlap matrix elements are those, which have the projected 2-quasiparticle state on both sides. Since both matrices are Hermitian, only upper- or lower triangle half-matrices have to be considered. This means only those matrix elements, where $\{Q < Q'; \forall\, K, K'\}$ and $\{Q = Q';\ K \leq K'\}$. Whereas in the GCV method this amounts only two half-matrices with altogether $(2I+1)(2I+2)$ projected matrix elements for each symmetry, now in the GCM method there are altogether $\aleph^{I2} + \aleph^I$ of them.

Much larger dimensions are encountered when preparing the symmetry projection and calculating all the rotated matrix elements. The particular rotated matrix elements in

equation (1.48) have to be calculated for *every* grid point $(\tilde{\Omega}\lambda) = (\alpha\beta\gamma\varphi\chi\lambda)$. So the resulting, total number of *complex* rotated Hamiltonian and overlap matrix elements needed *before* the symmetry projections is

$$\begin{aligned}\sum_{\pi\tilde{\Omega}} \aleph^0(\aleph^0+1) &= N_\pi N_\alpha N_\beta\ N_\gamma N_\varphi N_\chi \aleph^0(\aleph^0+1) \\ &= N_\pi N_\alpha N_\beta N_\gamma N_\varphi N_\chi \big(\frac{1}{2}M_b(M_b-1)+1\big)\Big[\big(\frac{1}{2}M_b(M_b-1)+1\big)+1\Big],\end{aligned} \tag{1.62}$$

where N_π is the number of existing parities and N_α (or N_β,N_γ) represent the number of α (or β,γ) angles used in the numerical calculation of the projection integral in (1.48). Moreover, each of the matrix elements are in general complex numbers. Obviously these dimensions can easily reach the limit of available storage resources as the number of projection angles and the size of the single particle basis increases. Hence the symmetry projection must be done, at least in some extend, in parts. Notice, that although there are no dependence on the particle numbers in dimensions (1.61) the number of projection angles for an exact projection depends on the particle numbers, see subsection 2.3.1. The basic principles of the numerical solution of the GCM method will be discussed in more detail in section 2.1.

1.4.4 The General Tensor Operators

Be $\hat{T}^{L^\pi}_\Lambda$ a general tensor operator of rank L and parity π, changing the mass number and isospin 3-projection by ΔA and ΔT_z, respectively. The reduced matrix element in between two arbitrary GCM states (1.46), which may in general even belong to different HFB transformations F_i and F_f is

$$(\psi_f(F_f);S_f||\hat{T}^{L^\pi}(\Delta A,\Delta T_z)||\psi_i(F_i);S_i)=\sqrt{2I_f+1}\times$$
$$\times\sum_{\substack{Q_iQ_f\\K_iK_f}}\left\{g^{S_f^*}_{Q_fK_f;f}\,g^{S_i}_{Q_iK_i;i}\sum_{\Lambda=-L}^{L}(I_iK_f-\Lambda,L\Lambda|I_fK_f)\langle Q_f|\hat{T}^{L^\pi}_\Lambda(\Delta A,\Delta T_z)\hat{\Theta}^{S_i}_{K_f-\Lambda,K_i}|Q_i\rangle\right\}. \tag{1.63}$$

Here the index i is related to the initial state whereas the index f to the final state and $(I_iK_f-\Lambda,L\Lambda|I_fK_f)$ is the usual Clebsch-Gordan coefficient. The reduced tensor matrix element is defined via the Wigner-Eckart theorem,

$$\langle\psi_f(F_f);S_fM_f|\hat{T}^{L^\pi}_\Lambda(\Delta A,\Delta T_z)|\psi_i(F_i);S_iM_i\rangle\equiv$$
$$(-)^{I_f-M_f}\begin{pmatrix}I_f & L & I_i\\ -M_f & \Lambda & M_i\end{pmatrix}(\psi_f(F_f);S_f||\hat{T}^{L^\pi}(\Delta A,\Delta T_z)||\psi_i(F_i);S_i) \tag{1.64}$$

The associated calculation can be outlined as follows. The GCM wavefunctions (1.46) with the explicit integral form of the general projection operators $\hat{\Theta}^S_{MK}$ (1.24) are inserted into (1.64). Using the properties of the rotation operator $\hat{R}(\Omega)$ (see appendix C) and the symmetries of the corresponding Wigner D functions the expressions simplify, one finally arrives to the solution, where the reduced matrix element (1.63) is found. Obviously only states with $A_f=A_i+\Delta A$, $T_{zf}=T_{zi}+\Delta T_z$ and $\pi_f\pi\pi_i=+1$ can only yield non-zero result. Once the explicit expression for the $\hat{T}^{L^\pi}_\Lambda$ is known the same techniques applied for evaluation of the projected overlap and Hamiltonian (appendix C) become available.

As already mentioned in the preface of this section, the GCM method is especially designed for the calculation of the expectation values of some one-body transition operator. As an example I shall consider the tensor operator for spectroscopic amplitudes :

$$[c_i^\dagger c_k]_\Lambda^{L^{\pi\tau}} \equiv \sum_{m_i m_k} \delta_{\tau_i,\tau,\tau_k}\delta_{\pi_i\pi\pi_k,1}(-)^{j_k-m_k}(j_i m_i j_k - m_k|L\Lambda)c_i^\dagger c_k. \tag{1.65}$$

After transforming this operator into quasiparticle picture we are able to write the four different type of rotated matrix elements, which can be found when applying the equation (1.63). Those are the one inbetween the vacua

$$\langle F|c_i^\dagger c_k|F^\lambda(\tilde{\Omega})\rangle = \langle F|F^\lambda(\tilde{\Omega})\rangle\tilde{\rho}_{ki}^\lambda(F;\tilde{\Omega}), \tag{1.66}$$

where

$$\tilde{\rho}^\lambda(F;\tilde{\Omega}) \equiv \rho(F) + A(F)g^\lambda(F;\tilde{\Omega})B^T(F). \tag{1.67}$$

The rotated matrix elements inbetween the vacuum and 2-quasiparticle configurations

$$\begin{aligned}\langle F|c_i^\dagger c_k a_\alpha^\dagger(F(\tilde{\Omega}))a_\beta^\dagger(F(\tilde{\Omega}))|F^\lambda(\tilde{\Omega})\rangle = \langle F|F^\lambda(\tilde{\Omega})\rangle\Big\{&\tilde{\rho}_{ki}^\lambda(F;\tilde{\Omega})\tilde{g}_{\alpha\beta}^\lambda(F;\tilde{\Omega}) + \\ &[B(F)X^\lambda(F;\tilde{\Omega})]_{i\beta}[A(F)X^\lambda(F;\tilde{\Omega})]_{k\alpha} - [B(F)X^\lambda(F;\tilde{\Omega})]_{i\alpha}[A(F)X^\lambda(F;\tilde{\Omega})]_{k\beta}\Big\}\end{aligned} \tag{1.68}$$

and

$$\begin{aligned}\langle F|a_\beta(F)a_\alpha(F)c_i^\dagger c_k|F^\lambda(\tilde{\Omega})\rangle = \langle F|F^\lambda(\tilde{\Omega})\rangle\Big\{&\tilde{\rho}_{ki}^\lambda(F;\tilde{\Omega})g_{\alpha\beta}^\lambda(F;\tilde{\Omega}) + \\ &[A^*(F) + B(F)g^\lambda(F;\tilde{\Omega})]_{i\alpha}[B^*(F) + A(F)g^\lambda(F;\tilde{\Omega})]_{k\beta} - \\ &[A^*(F) + B(F)g^\lambda(F;\tilde{\Omega})]_{i\beta}[B^*(F) + A(F)g^\lambda(F;\tilde{\Omega})]_{k\alpha}\Big\}\end{aligned} \tag{1.69}$$

Finally we need the ones with 2-quasiparticle configuration on both sides,

$$
\begin{aligned}
&\langle F|a_\beta(F)a_\alpha(F)c_i^\dagger c_k a_\gamma^\dagger(F^\lambda(\tilde\Omega))a_\delta^\dagger(F^\lambda(\tilde\Omega))|F^\lambda(\tilde\Omega)\rangle = \langle F|F^\lambda(\tilde\Omega)\rangle \times \\
&\times \Big\{\tilde\rho^\lambda_{ki}(F;\tilde\Omega)\big(g^\lambda_{\alpha\beta}(F;\tilde\Omega)\tilde g^\lambda_{\gamma\delta}(F;\tilde\Omega) + X^\lambda_{\alpha\gamma}(F;\tilde\Omega)X^\lambda_{\beta\delta}(F;\tilde\Omega) - X^\lambda_{\alpha\delta}(F;\tilde\Omega)X^\lambda_{\beta\gamma}(F;\tilde\Omega)\big) \\
&+ g^\lambda_{\alpha\beta}(F;\tilde\Omega)\Big([B(F)X^\lambda(F;\tilde\Omega)]_{i\delta}[A(F)X^\lambda(F;\tilde\Omega)]_{k\gamma} - \\
&\qquad [B(F)X^\lambda(F;\tilde\Omega)]_{i\gamma}[A(F)X^\lambda(F;\tilde\Omega)]_{k\delta}\Big) \\
&+ \tilde g^\lambda_{\gamma\delta}(F;\tilde\Omega)\Big([A^*(F) + B(F)g^\lambda(F;\tilde\Omega)]_{i\alpha}[B^*(F) + A(F)g^\lambda(F;\tilde\Omega)]_{k\beta} - \\
&\qquad [A^*(F) + B(F)g^\lambda(F;\tilde\Omega)]_{i\beta}[B^*(F) + A(F)g^\lambda(F;\tilde\Omega)]_{k\alpha}\Big) \\
&+ X^\lambda_{\alpha\gamma}(F;\tilde\Omega)\Big([A^*(F) + B(F)g^\lambda(F;\tilde\Omega)]_{i\beta}[A(F)X^\lambda(F;\tilde\Omega)]_{k\delta} - \\
&\qquad [B(F)X^\lambda(F;\tilde\Omega)]_{i\delta}[B^*(F) + A(F)g^\lambda(F;\tilde\Omega)]_{k\beta}\Big) \qquad (1.70) \\
&- X^\lambda_{\alpha\delta}(F;\tilde\Omega)\Big([A^*(F) + B(F)g^\lambda(F;\tilde\Omega)]_{i\beta}[A(F)X^\lambda(F;\tilde\Omega)]_{k\gamma} - \\
&\qquad [B(F)X^\lambda(F;\tilde\Omega)]_{i\gamma}[B^*(F) + A(F)g^\lambda(F;\tilde\Omega)]_{k\beta}\Big) \\
&+ X^\lambda_{\beta\delta}(F;\tilde\Omega)\Big([A^*(F) + B(F)g^\lambda(F;\tilde\Omega)]_{i\alpha}[A(F)X^\lambda(F;\tilde\Omega)]_{k\gamma} - \\
&\qquad [B(F)X^\lambda(F;\tilde\Omega)]_{i\gamma}[B^*(F) + A(F)g^\lambda(F;\tilde\Omega)]_{k\alpha}\Big) \\
&- X^\lambda_{\beta\gamma}(F;\tilde\Omega)\Big([A^*(F) + B(F)g^\lambda(F;\tilde\Omega)]_{i\alpha}[A(F)X^\lambda(F;\tilde\Omega)]_{k\delta} - \\
&\qquad [B(F)X^\lambda(F;\tilde\Omega)]_{i\delta}[B^*(F) + A(F)g^\lambda(F;\tilde\Omega)]_{k\alpha}\Big)\Big\}
\end{aligned}
$$

What is still to be calculated is the numerical symmetry projection, which leads to the projected matrix elements $\langle Q_f|\hat T^{L^\pi}_\Lambda(\Delta A,\Delta T_z)\hat\Theta^{S_i}_{K_f-\Lambda,K_i}|Q_i\rangle$ and goes in analogy to the case of projected overlap and Hamiltonian. The rest of the calculation of the reduced matrix elements (1.63) is trivial.

1.4.5 An Approximate Treatment of Center-of-Momentum Excitations

The GCM code was equipped also with an approximate method for the elimination of the spurious center-of-momentum (COM) excitations, which was originally proposed by Giraud [Gir65]. I would like to point out, that first of all, the problem of the spurious COM-excitations exists only if the single particle basis contains more than one major oscillator shell. Otherwise the COM stays always in the ground state with a constant energy. Secondly, the method outlined in this section is not in general an exact restoration of the Galilei invariance. In the spirit of the other symmetry restorations in the GCV and GCM methods one should apply the projection techniques also for this problem. Not even the shell model type approaches are free from the spurious COM-admixtures since the complete basis of Slater- or generalized Slater determinants does not form a complete set with respect to shift operator. Thus the full Galilei invariance is achieved only if the projection to COM rest frame is done before determination of the wave function. A continuous work in this field is in progress [Sch00] and the mathematical machinery for the COM-projection is already available [Sch91, Sch95, Sch00]. Recent investigations show the importance of a proper COM-treatment. However, the supplement of $\hat{\Theta}^S$ with the COM-projection operator

$$\hat{C}(\mathbf{P}=0) = \frac{1}{(2\pi\hbar)^3}\int \mathrm{d}^3\mathbf{a}\exp\left[i\frac{\mathbf{a}\cdot\hat{\mathbf{P}}}{\hbar}\right] \tag{1.71}$$

projecting on the center-of-mass rest frame would mean an additional 3-fold integration over the complete coordinate space. This would multiply the number of matrix elements (1.62) by the number of particular discrete integration angles. It is estimated to increase the computational effort roughly by a factor of 10^3. The GCM method with the exact COM-projection offers an exact elimination of the spurious COM-excitations, but is left now as numerical challenge for the future.

The spurious COM-excitations originate from the fact that in addition to the $3A-3$ intrinsic coordinates which are sufficient to describe the A nucleon system we have 3 redundant COM-coordinates. These are unphysical degrees of freedom related to the collective motion of the nucleus as a whole. An exact elimination of the spurious COM-excitations is possible in the harmonic oscillator basis supposed that *all* oscillator many-particle determinants up to a certain energy $n\hbar\omega$ are included in the configuration space. Let us consider an example. Suppose we have A_c nucleons forming a closed major shell core and $A_v \equiv A - A_c$ nucleons in the next (open) major shell. Now the complete $1\hbar\omega$ configuration space consists out of all Slater determinants with $A_v - 1$ nucleons in the first open and an additional nucleon in the next higher major shell as well as those with $A_v + 1$ nucleons in the first open and an additional hole in the last occupied major shell of the closed core. Obviously the larger excitation quanta $(2, \ldots, n)$ involve more complicated configurations. Then the many nucleon wave function factorizes as

$$|\psi\rangle = |\phi^{cm}\rangle|\psi^{int}\rangle, \tag{1.72}$$

where the latter state $|\psi^{int}\rangle$ is the intrinsic part of the true state and the COM part, $|\phi^{cm}\rangle$ the eigenstate of COM-Hamiltonian given by

$$\hat{H}^{cm} = \frac{\hat{\mathbf{P}}^2}{2Am} + \frac{1}{2}Am\omega^2\hat{\mathbf{R}}^2, \tag{1.73}$$

with $\hat{\mathbf{P}} = \sum_{i=1}^{A}\hat{\mathbf{p}}_i$ and $\hat{\mathbf{R}} = (\sum_{1=1}^{A}\hat{\mathbf{r}}_i)/A$. Here $\hat{\mathbf{p}}_i$ are the momentum operators, $\mathbf{r}_i$ spatial coordinates, ω the harmonic oscillator constant and m the nucleon mass. In actual calculations the H^{cm} is represented in second quantization, see appendix D. In this method the spurious states are explicitly constructed by diagonalizing the $\hat{H}^{cm}$. It is evident that the GCM basis states are not oscillator-type described above, but quasiparticle determinants. So, in general, the GCM configuration space is not complete with respect to the $\hat{H}^{cm}$ and consequently the pure factorization (1.72) is not necessarily

achieved. However, in practice the diagonalization of the COM-Hamiltonian in the basis (1.42)

$$\sum_{Q'K'} \left\{ H^{cm;S}_{QK;Q'K'} - E^{cm;S} N^{S}_{QK;Q'K'} \right\} f^{S}_{Q'K'} = 0 \qquad \forall \quad Q, K. \tag{1.74}$$

yielding

$$|\phi^{cm}_i(F); SM\rangle \equiv \sum_{QK} |Q; SMK\rangle f^{S}_{QK;i}, \tag{1.75}$$

with

$$\langle \phi^{cm}(F); SM | \phi^{cm}(F); SM\rangle = (f^S)^\dagger N^S f^S = \mathbf{1}, \tag{1.76}$$

will produce energy eigenvalues $E^{cm;S}$, which are clustered around the exact COM-excitation energies [Sch82]. One can identify all the solutions $|\phi^{cm}_i(F); SM\rangle$ ($i = 1, \ldots, n_s$) with excitation energies around $1\hbar\omega, 2\hbar\omega, \ldots, n\hbar\omega$ as spurious. These solutions can be removed by performing projection on non-spurious subspace with the help of operator

$$\hat{P}_s = \mathbf{1} - \sum_{i=1}^{n_s} |\phi^{cm}_i(F); SM\rangle\langle \phi^{cm}_i(F); SM|, \tag{1.77}$$

by solving the diagonalization problem (1.45) for the modified Hamiltonian

$$\hat{\mathcal{H}} = \hat{P}_s H \hat{P}_s. \tag{1.78}$$

The spurious states occur now at energies $E^S \approx 0$ and are immediately identified. With this method at least the predominant spurious components can be eliminated.

Chapter 2

The Numerical Implementation

2.1 Introduction

The GCM program packet was implemented using FORTRAN 77 programming language. The program packet consists of three main programs, namely the number- and parity projection (GCMNUPR), angular momentum projection (GCMAMPR) and finally the diagonalization (GCMSMEQ) part. The resulting total size of the fully commented program packet is 334.8 kB including 5671 lines of code (commentlines subtracted) with 53 subroutines and 2 functions. Total number of program lines is 3746. All floating point numbers are of double precision (8 B) type. The structure of the code is illustrated in figure 2.1. First, all the input data must be gathered and read in. This is done in the first main program. The HFB transformation is the result of the preceding GCV calculation and the corresponding matrices A and B are taken, together with the Hamiltonian matrix elements in particle representation and the quasiparticle energies, as input data. Also the center-of-momentum Hamiltonian H^{cm} must be prepared and read in, if the COM-treatment is required. I will not discuss any detailed numerical solutions of the GCV code unless they are closely connected to the implementation of the GCM code. The mainlines of the GCV code are shortly outlined in Ref. [Ham98].

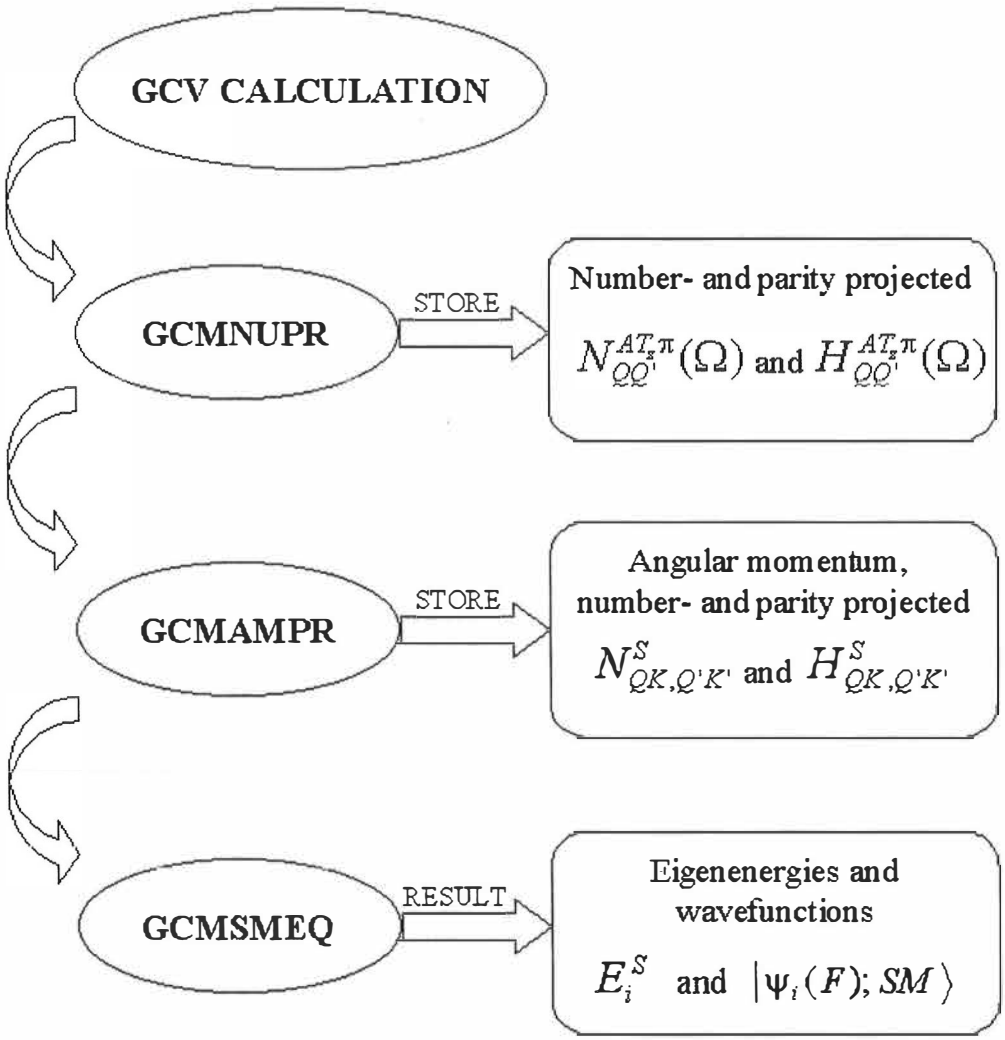

Figure 2.1: Main Structure of the GCM code

The structure of the code is designed also to make the best use of vectorization in vector platforms, i.e. all the loops perform the operations in arrays, whenever possible. Also a special attention has been paid on matrix multiplications, for example, the multiplication of three $(N \times N)$ matrices, A, B and C, is not done directly, but always forming first a matrix $D = AB$ and then multiplying with C from left. This amounts $\frac{3}{4}N$ times less floating point operations. Because, in the former method $2N^4$ multiplications and N^4 summations have to be performed, while one needs only $2N^3$ multiplications and equal number of summations in the latter. Furthermore, in the loops involving multi-dimensional arrays the consecutive index runs through the first index, whenever possible. Sometimes the symmetry properties of the involved matrices must be utilized to enable this.

It is well known that the problems involving multi-fold integration are especially well suited for parallel computing. In fact the GCV code was parallelized recently, in 1995 [Ham98], resulting almost optimal, linear speed-up. The GCM code is not yet parallelized when writing this thesis.

2.2 Order of Magnitude Estimates

The multi-fold integrations multiply the dimensions of involved matrices as the accuracy of the numerical integration i.e. number of discrete integration angles increases and as the single particle basis becomes larger, see section 1.4.3. Although the memory usage is much faster way to store, access and read data compared to the use of hard discs it is not usually possible to handle all the matrices in memory. If only memory usage was allowed the code would lose its applicability in various platforms. Thus, one has to find a satisfactory compromise in the use of memory and disc storage. In preparing the symmetry projection the largest dimensions are encountered when calculating the

rotated matrix elements.

For a concrete example let us consider a full $1p0f$-shell single particle basis, i.e. 40 nucleon orbits. Now the number of 2-quasiparticle states plus the vacuum is $\sigma \equiv 781$. The corresponding half-matrices have $\sigma(\sigma-1)/2+\sigma$ elements. Since the imaginary part of the diagonal elements in Hermitian matrix vanishes we have actually the total of $2(\sigma(\sigma-1)+\sigma)$ *real* matrix elements: $N_{QQ'}$ and $H_{QQ'}$ to be calculated. In general the eigenvalue problem $Ax = x\lambda$ for the N-dimensional complex matrix A can be always formulated as $2N$-dimensional real eigenvalue problem

$$\begin{pmatrix} \Re eA & -\Im mA \\ \Im mA & \Re eA \end{pmatrix} \begin{pmatrix} \Re ex \\ \Im mx \end{pmatrix} = \begin{pmatrix} \Re e(x\lambda) \\ \Im m(x\lambda) \end{pmatrix}, \tag{2.1}$$

where the eigenvalue-matrix is given as

$$\lambda \equiv \begin{pmatrix} \lambda_1 & & 0 \\ & \ddots & \\ 0 & & \lambda_N \end{pmatrix}. \tag{2.2}$$

Back to the example, taking into account both, the Hamiltonian and overlap, this yields 9.3 MB of data. Now supposing we calculate these in every integration point $\tilde{\Omega}$, it gives an additional factor of $N \equiv N_\alpha N_\beta N_\gamma N_\varphi N_\chi$, since we have a definite parity. For the $1p0f$-shell a sufficient projection is usually achieved with $N = 6 \times 10^5$. So, the rotated Hamiltonian and overlap alone would require over 5 TB of storage. Besides these matrices one obviously needs also the other related matrices, i.e. $\langle F|F(\tilde{\Omega})\rangle$, $g(F;\tilde{\Omega})$, $\tilde{g}(F;\tilde{\Omega})$, $X(F;\tilde{\Omega})$, $h^{02}(F;\tilde{\Omega})$, $h^{20}(F;\tilde{\Omega})$ and $h^{11}(F;\tilde{\Omega})$ for each projection angle, which amounts now over 50 TB and that number does not even contain the weights for the symmetry projection. It is obvious, that these matrices cannot be all calculated at the same time, even in this relatively small single particle basis. Therefore the numerical implementation of the GCM code turns out to be highly non-trivial.

2.3 The Number- and Parity Projection

The GCMNUPR is the first main program of the GCM code. This module consists of 39 subroutines and 2770 program lines. The first part has all the necessary input routines, where the card-input and the results of the GCV calculation are read in. These are followed with the compatibility check with maximal dimensions etc. The card-input consists of logical values for center-of-momentum treatment, odd mass number and parity projection. If the single particle basis contains states with both parities the parity projection becomes necessary, otherwise we have always definite parity and then the projection is unnecessary. Other card input is the number of projection angles $N_\alpha/2$, N_β, $N_\gamma/2$, $N_\varphi/2$, $N_\chi/2$ and the truncation limit ε_{2qp}^{max} for the quasiparticle energies in MeV. Next the integration points and gaussian weights for the number- (2.3.1) and angular momentum (2.4.1) projections are calculated and the 2-quasiparticle configurations (with quasiparticle labels α and β), for which $|\varepsilon_\alpha| + |\varepsilon_\beta| \leq \varepsilon_{2qp}^{max}$ are constructed. This part of the code is enclosed by writing a file with the following output for the later use in the next main program GCMAMPR: logical COM-treatment, logical parity projection, number of valence and core neutrons and protons, number of existing parities, the discrete projection angles α and γ, gaussian angles for β and corresponding weights $w(\beta)$, and finally the information of the chosen 2-quasiparticle configurations.

In the subsequent part the actual number- and possibly parity projections are performed with multiple loop structure. The outermost loop runs over the overlap, Hamiltonian and possibly COM-Hamiltonian. When starting the loop over Hamiltonian (and COM-Hamiltonian) the needed parts in the quasiparticle representation are calculated, these

are

$$H^0(F), \quad H^{11}_{\alpha\beta}(F)\,(\alpha \le \beta), \quad H^{20}_{\alpha\beta}\,(\alpha < \beta),$$
$$H^{22}_{\alpha\beta\gamma\delta}(F)\,(\alpha \le \beta, \gamma \le \delta), \quad H^{31}_{\alpha\beta\gamma\delta}(F)\,(\gamma < \delta) \quad \text{and} \quad H^{40}_{\alpha\beta\gamma\delta}(F)\,(\alpha < \beta < \gamma < \delta). \tag{2.3}$$

The last three matrices are stored in separate scratch discs. Next comes the loops over angles β, α, γ and χ. In the beginning of the first three loops new (corresponding) β-, α-, and γ-files are opened. All α- and γ-files have the status of scratch discs. Inside this loop structure we construct the rotated $\tilde{A}^\lambda(F;\tilde{\Omega})$ and $\tilde{B}^\lambda(F;\tilde{\Omega})$ matrices (C.11 and C.12). For odd A system one has to calculate also the $\tilde{A}^\lambda_e(F;\tilde{\Omega})$ for the even A partner. During this step one has to take into account both parities only if they exist and are projected. After that begins the possible parity projection loop over λ. First one determines the sign of the squareroot in overlap by diagonalization (C.20). For odd A nucleus this is done for even A counterpart to yield the correct sign in $\langle F_e|F^\lambda_e(\tilde{\Omega})\rangle$. This overlap is then calculated via (C.18) and finally the phase of the overlap $\langle F_o|F^\lambda_o(\tilde{\Omega})\rangle$ is modified according to (C.28). The overlap signs are calculated in this way for all points φ at particular $(\beta\alpha\gamma\chi\lambda)$-point.

This procedure is followed by the calculation of the overlaps $\langle F|F^\lambda(\tilde{\Omega})\rangle$ according to the equation (C.18) for which the sign is already known. Then one calculates the matrices

$$X^\lambda_{\alpha\beta}(F;\tilde{\Omega})\,(\forall\,\alpha,\beta), \quad g^\lambda_{\alpha\beta}(F;\tilde{\Omega})\,(\alpha < \beta), \quad \tilde{g}^\lambda_{\alpha\beta}(F;\tilde{\Omega})\,(\alpha < \beta)$$
$$h^\lambda(F;\tilde{\Omega}) \quad h^{\lambda 20}_{\alpha\beta}(F;\tilde{\Omega})\,(\alpha < \beta) \quad h^{\lambda 02}_{\alpha\beta}(F;\tilde{\Omega})\,(\alpha < \beta) \quad h^{\lambda 11}_{\alpha\beta}(F;\tilde{\Omega})\,(\forall\,\alpha,\beta), \tag{2.4}$$

which are also calculated for each angle φ in fixed $(\beta\alpha\gamma\chi\lambda)$-point.

Now that all ingredients are ready we calculate the rotated matrix elements (C.30) and (C.31) in the case of overlap, and (C.32), (C.35) and (C.41) for the Hamiltonian (or COM-Hamiltonian). We have chosen to consider the upper triangle matrices. Finally the actual number (and parity) projection subroutines are performed and the projected matrix elements are updated and stored in scratch disc after each (λ and) χ-loop until

the last (λ and) χ point, when they are stored in particular γ-disc. Notice, that the φ loops are done inside these subroutines.

After the γ-loop all the number (and parity) projected matrix elements for each γ-point are stored in the particular α-disc. The same procedure is done after the α-loop. Now all the projected matrix elements for (α, γ)-points are gathered in the particular β-disc. In this way the total number of *real* numbers (related to the number projected matrix elements) to be stored at the end is (all the β-discs)

$$2 \times N_\pi N_\beta N_\alpha N_\gamma \left[(\sigma^2 + \sigma) - \sigma\right] = 2N_\pi N_\beta N_\alpha N_\gamma \sigma^2 \tag{2.5}$$

where σ is the GCM configuration space dimension. With $N_\beta N_\alpha N_\gamma = 6144$ this amounts as much as 56 GB and 7.0 GB with all 2-quasiparticle configurations for the full $1p0f$- and $1s0d$-shells , respectively.

The number (and parity) projected Hamiltonian and overlap matrix elements are denoted as $H^{AT_z\pi}_{QQ'}(\Omega)$ and $N^{AT_z\pi}_{QQ'}(\Omega)$, see Figure 2.1.

2.3.1 The Number Projection Operator

To calculate the number projection integrals over the angles φ and χ they must be discretized. Since the states in the GCM configuration space (1.42) have always good number parity, $\mathcal{N} - \hat{\mathcal{N}}$ must be even for each component state. The abbreviation $\mathcal{N}$ refers to the mass number A or two times the isospin 3-component, $2T_z = N - Z$. Consequently the number projection integrals in (1.24) are replaced by integrals of type

$$\hat{P}(\mathcal{N}) = \frac{1}{\pi} \int_{-\pi/2}^{\pi/2} \mathrm{d}\phi \, e^{i\phi(\mathcal{N}-\hat{\mathcal{N}})}, \tag{2.6}$$

which is easily proved by applying the identity $\exp[i(\phi \pm \pi)m] = \exp[i\phi m]$ (for even m) on the above expression, where the particular m is always even. Now the integration

range covers only the half unit circle. It is well known that the integrals of type (2.6) can be discretized by using the Gauss-Chebyshev quadrature [Dav72],

$$\frac{1}{\pi}\int_{-\pi/2}^{\pi/2} \mathrm{d}\phi\, e^{i\phi(\mathcal{N}-\hat{\mathcal{N}})} \cong \frac{1}{N_\phi}\sum_{n=1}^{N_\phi} e^{i\phi_n(\mathcal{N}-\hat{\mathcal{N}})}, \tag{2.7}$$

where the angles in the first quadrant are

$$\phi_n = \frac{\pi}{2N_\phi}(2n-1) \quad n = 1, \ldots, \frac{N_\phi}{2}, \tag{2.8}$$

and in the last quadrant simply $-\phi_n$. With these angles the number projection operator takes the form

$$\hat{P}(\mathcal{N}) \cong \frac{2}{N_\phi}\sum_{n=1}^{N_\phi/2} \cos[\phi_n(\mathcal{N}-\hat{\mathcal{N}})]. \tag{2.9}$$

However, due to the special form of the generalized rotation operator $\hat{\tilde{R}}(\tilde{\Omega})$ we have to use (2.7) in the code. The quasiparticle determinants have a good number parity, i.e. they contain all even (odd) components in intervals $A' \in [0, M_b]$ and $2T_z' \in [-M_b^p, M_b^n]$ for even (odd) nucleus before the number projection. Here M_b^n (M_b^p) is the size of the single particle basis for neutrons (protons). Notice, that the order of the projections $\hat{P}(A)$ and $\hat{P}(2T_z)$ is not fixed. The freedom of choosing the integration order is useful when parallelizing the code. The operator (2.9) destroys all number impurity components $\mathcal{N}' \neq \mathcal{N}$ for which

$$\mathrm{mod}\left(\frac{\mathcal{N}-\mathcal{N}'}{2N_\phi}\right) \neq 0 \tag{2.10}$$

but fails to eliminate those with

$$A' = \mathrm{mod}\left(\frac{A}{2N_\varphi}\right), \mathrm{mod}\left(\frac{A}{2N_\varphi}\right) + 2N_\varphi, \ldots, A, \ldots, M_b + \mathrm{mod}\left(\frac{A-M_b}{2N_\varphi}\right) \tag{2.11}$$

$$2T_z' = -M_b^p + \mathrm{mod}\left(\frac{2T_z+M_b^p}{2N_\chi}\right), -M_b^p + \mathrm{mod}\left(\frac{2T_z+M_b^p}{2N_\chi}\right) + 2N_\chi, \ldots, 2T_z, \ldots, M_b^n + \mathrm{mod}\left(\frac{2T_z-M_b^n}{2N_\chi}\right) \tag{2.12}$$

The number projections are exact if only single values $A' = A$ and $T'_z = T_z$ exists, which implies that an adequate number of projection angles in the first quadrants for an exact projections are

$$N_\varphi/2 = \text{Integer}\left[\frac{1}{4}\max(A, M_b - A)\right] + 1 \tag{2.13}$$

$$N_\chi/2 = \text{Integer}\left[\frac{1}{4}\max(2T_z + M_b^p, M_b^n - 2T_z)\right] + 1 \tag{2.14}$$

Obviously these numbers depend on the size of the single particle basis for protons and neutrons, and also on proton and neutron numbers, i.e. on the nucleus in consideration. The number of projection angles $N_\varphi/2$ for an exact mass number projection in the full $1s0d$-shell is between 4 and 6, while for the full $1p0f$-shell the corresponding number is between 6 and 10. Typically, for the exact isospin 3-component projection we need 4 angels in the full $1s0d$- and $5-7$ angles in the full $1p0f$-shell. For comparison, the numbers for $1s0d + 1p0f$-shell single particle basis are $N_\varphi/2 = 9 - 16$ and $N_\chi/2 \simeq 10$.

2.4 The Angular Momentum Projection

The GCMAMPR is the second main program of the GCM code. This module is the smallest consisting out of 4 subroutines and only 277 lines of code. For input we have the results from the preceding GCMNUPR program (see section 2.3) and card-input, where limits for the angular momenta to be considered are declared.

The angular momentum projection is performed to the considered angular momenta, for overlap and Hamiltonian (and COM-Hamiltonian) by multiple loops over rotation angles β, all GCM configurations $Q \leq Q'$, all the necessary K-quantum numbers K, K' as well as the angles α and γ.

Finally, the fully projected upper-half matrices $H^S_{QK;Q'K'}$ and $N^S_{QK;Q'K'}$, where $\{Q <$

$Q'; \forall\ K, K'\}$ and $\{Q = Q';\ K \leq K'\}$ are stored in output disc right after the considered spin and information of all GCM configurations. If parity projection is done the output is written in separate discs according to the parity.

At this stage the additional disc space need in words for the fully projected upper-half matrices is

$$2N_\pi \left[\sigma(2I+1)\right]^2, \tag{2.15}$$

where N_π is the number of projected parities, σ is the GCM configuration space dimension. For example, for the full $1s0d$-shell with all 2-quasiparticle configurations this is only 1.2 MB, 140 MB, and 0.5 GB for the total angular momentum $I = 0$, 5 and 10 states, respectively. For the full $1p0f$-shell the corresponding numbers are 9.3 MB, 1.1 GB and 4.0 GB.

2.4.1 The Angular Momentum Projection Operator

The angular momentum (or spin) projection is numerically more complicated than the number projection. The angular momentum projection operator produces matrix elements of the form

$$\begin{aligned} f^I_{KK'} &= \frac{2I+1}{8\pi^2} \iiint \mathrm{d}\Omega D^{I\,*}_{KK'}(\Omega) f(\Omega) \\ &= \frac{2I+1}{8\pi^2} \int_0^{2\pi} \mathrm{d}\alpha\, e^{-i\alpha K} \int_0^{2\pi} \mathrm{d}\gamma\, e^{-i\gamma K'} \int_0^{\pi} \mathrm{d}\beta\, \sin\beta d^{I\,*}_{KK'}(\beta) f(\alpha\beta\gamma). \end{aligned} \tag{2.16}$$

Particularly in the GCM code

$$f^I_{KK'} = \begin{cases} H^S_{QK;Q'K'} \\ N^S_{QK;Q'K'} \end{cases} \quad \text{and} \quad f(\Omega) = \begin{cases} H^{AT_z\pi}_{QQ'}(\Omega) \\ N^{AT_z\pi}_{QQ'}(\Omega) \end{cases} \tag{2.17}$$

The β-integration is done using the Gauss-Legendre type finite interval formula [Dav72]

$$\int_0^\pi \sin\beta \mathrm{d}\beta f(\Omega) \approx \sum_{n=1}^{N_\beta} w(\beta)_n f(\alpha\beta_n\gamma), \tag{2.18}$$

where the discrete angles are

$$\beta_n = \frac{\pi}{2}x_n + \frac{\pi}{2} \tag{2.19}$$

and the corresponding weights are

$$w(\beta)_n = \frac{\pi}{1-x_n}[P'_{N_\beta}(x_n)]^2, \tag{2.20}$$

where x_n is the n^{th} zero of the Legendre polynomial $P_{N_\beta}(x)$. Currently the gaussian weights are tabulated up to 32 in the code, which is then the upper limit for the number of gaussian integration points N_β. For the full $1s0d$- [Ham98] and $1p0f$- [Hje00] shell calculations the sufficient number of β-points is usually $16-20$ and $20-24$, respectively.

The "left side" J_3-projection angles in the interval $(0,\pi)$ are

$$\alpha_n = \frac{\pi}{2N_\alpha}(2n-1) \quad n = 1,\ldots,\frac{N_\alpha}{2}, \tag{2.21}$$

and the rest are simply $-\alpha_n$. The integral reads

$$\frac{1}{2\pi}\int_{-\pi}^{\pi} \mathrm{d}\alpha\, e^{-i\alpha K} \cong \frac{1}{N_\alpha}\sum_{n=1}^{N_\alpha} e^{-i\alpha_n K}. \tag{2.22}$$

Similarly the "right side" J_3-projection is performed with angles

$$\gamma_n = \frac{\pi}{2N_\gamma}(2n-1) \quad n = 1,\ldots,\frac{N_\gamma}{2} \tag{2.23}$$

$$\gamma_{n+N_\gamma/2} = -\gamma_n \tag{2.24}$$

and the integral

$$\frac{1}{2\pi}\int_{-\pi}^{\pi} \mathrm{d}\gamma\, e^{-i\gamma K'} \cong \frac{1}{N_\gamma}\sum_{n=1}^{N_\gamma} e^{-i\gamma_n K'}. \tag{2.25}$$

In the integrals (2.22) and (2.25) the K-quantum numbers have all $(2I+1)$ values in the range $(-I,\ldots,I)$, so the integration is performed always in full unit circle.

2.5 The Diagonalization

The diagonalization is the third and last main program of the GCM program package. It has 699 program lines, 10 subroutines and 2 non-standard functions. The spins to be considered are read from the input file, together with the truncation limit and cut off value ϵ for the overlap eigenvalues, a logical value whether the results are written in a new file or appended to an existing one and some printing options. If the COM-treatment is done the assumed or calculated COM ground state energy and an upper limit for the considered COM-excitation energy are read in.

Next begins the loop structure. The first loop runs over the spin. In the beginning the projected overlap is read in and diagonalized according to (1.54). If the average eigenvalue $\bar{n^2}$ is less than a certain truncation limit, no solutions exist. Otherwise all the eigenvectors $\left(f^S_{QK;i};i=1,\ldots,\sigma\right)$ for which $n^2<\epsilon\bar{n^2}$, are excluded. This procedure determines the new dimension $\sigma'\leq\sigma$ for the linearly independent GCM configurations. The linear dependence arises when the number of different GCM states for a certain symmetry, which can be constructed from the GCM configuration space, is less than the actual dimension of the configuration space. Also the non-orthogonality of the projected determinants causes in general some linear dependencies between the GCM configurations. Therefore, the GCM configuration space is not necessary overcomplete, although its dimension was larger than the number of shell model states. The GCM approach gives a poor description for the states whose complicated structure is dominated by the

determinants left outside the GCM configuration space. These states have a very different configuration structure compared to the state for which the underlying mean-field is determined.

Next one calculates the squareroot of the projected overlap matrix $\sqrt{N^S} = f^S n f^{S\dagger}$ and stores it for the later use. The Hamiltonian is transformed to $\tilde{H}^S$ according to (1.55) using matrix $(f^S_{QK;i} n_i^{-1})$. The same transformation is done for the COM-Hamiltonian, if necessary. And then, in addition, the COM-Hamiltonian is diagonalized (1.74), the number of spurious COM states n_s is solved and furthermore, if $n_s > 0$ the Hamiltonian is modified according to (1.78) by projecting on the non-spurious subspace.

Finally, the transformed or transformed *and* modified Hamiltonian is diagonalized (1.55). If the COM-Hamiltonian is concerned the COM-expectation values are also calculated to check the COM-elimination. The non-orthonormal eigenvectors are contained in $(\sigma \times \sigma')$-matrix g^S, which is backtransformed using equation (1.57). The corresponding orthonormalized expansion coefficients (1.58) are obtained by constructing $\sqrt{N^S} g^S$.

Chapter 3

Application to ^{27}Al and ^{28}Si

The applications presented in this chapter represent the first GCM calculations ever made. The GCM approach is applied to two nuclei from the middle of the $1s0d$-shell, the odd $^{27}_{13}Al_{14}$ and the doubly even $^{28}_{14}Si_{14}$. The chosen nuclei have the maximal dimensions in the particular single particle basis, which consists of full $1s0d$-shell, with the basis dimension $M_b = 24$ and $^{16}_{8}O_8$ nucleus as core. The valence nucleon numbers for the considered nuclei are 11 and 12. This rather small basis was chosen in order to enable fast comparison with the complete SCM calculations and also to provide a realistic demonstration of the approach. The SCM calculations were performed with the shell model code OXBASH [Bro88b].

3.1 Force and Dimensions

As effective two-body interaction the mass-dependent Chung-Wildenthal [Wil84] force has been used as already mentioned in section 1.2. The mass dependence is given by $V(A) = V(18)(18/A)^{\alpha}$. Our choice was $\alpha = 1/3$ instead of the original value $\alpha = 0.3$. The single particle energies $t(d_{5/2}) = -4.15$ MeV, $t(s_{1/2}) = -3.28$ MeV, and $t(d_{3/2}) = +0.93$ MeV for both neutrons and protons have been taken from experiment [Ajz86]. This interaction, with a slight modification in the mass dependence, is a traditional

choice for the $1s0d$-shell VAMPIR-MONSTER calculations.

The number of shell model (SCM) and GCM configurations per angular momentum and number of linear independent GCM states obtained for the considered nuclei together with the percentual fraction of linear dependence are tabulated in table 3.1.

	^{28}Si					^{27}Al			
I^π	SCM	GCM	LI	LD%	I^π	SCM	GCM	LI	LD%
0^+	3372	277	272	1.8	$1/2^+$	5638	554	544	1.8
1^+	9216	831	816	1.8	$3/2^+$	10176	1108	1088	1.8
2^+	13562	1385	1360	1.8	$5/2^+$	12877	1662	1633	1.7
3^+	15385	1939	1905	1.8	$7/2^+$	13450	2216	2179	1.7
4^+	15089	2493	2450	1.7	$9/2^+$	12240	2770	2714	2.0
5^+	12876	3047	2981	2.2	$11/2^+$	9835	3324	3177	4.4
6^+	9900	3601	3425	4.9	$13/2^+$	7053	3878	3456	11
7^+	6691	4155	3655	12	$15/2^+$	4469	4432	2804	37
8^+	4059	4709	1848	61	$17/2^+$	2502	4986	2502	50
9^+	2121	5263	2121	60	$19/2^+$	1197	5540	1197	79
10^+	967	5817	967	83	$21/2^+$	485	6094	485	92
11^+	439	6371	439	93	$23/2^+$	152	6648	152	98
12^+	105	6925	105	98	$25/2^+$	35	7202	35	100
13^+	17	7479	17	100	$27/2^+$	3	7756	3	100
14^+	1	8033	1	100					

Table 3.1: The number of SCM and GCM configurations and linear independent GCM states (LI) per angular momentum for ^{27}Al and ^{28}Si in the full $1s0d$-shell basis. The LD% is the percentual linear dependence in the GCM approach

The GCM configuration space dimensions with respect to spin are the same for all nuclei in the $1s0d$-shell basis. The shell model dimensions for both nuclei are roughly one order of magnitude larger for the smallest spins. Up to spin 4^+ the linear dependence remains approximately constant (below 2%) and must be mainly due to the linear dependence inbetween the GCM configurations. For the states with $I \leq 6$ there are at least twice as

many SCM configurations as GCM configurations and the linear dependence is between $(2-5)\%$. The dimensions become approximately same-size around spin 7^+. From thereon the linear dependence begins to grow faster with respect to spin as the number of available GCM configurations slightly increases and, on the other hand as the number of SCM configurations decreases. At the highest spins the GCM dimensions exceed considerably the number of SCM states and the number of linear independent GCM states matches with the number of SCM states. Notice that the dimensions in table 3.1 contain all states with all possible isospins. So, for example the number of $T = 0$ states for ^{28}Si is: 839 $I^\pi = 0^+$, 2135 $I^\pi = 1^+$, 3276 $I^\pi = 2^+$, 3711 $I^\pi = 3^+$, 3793 $I^\pi = 4^+$, 3278 $I^\pi = 5^+$, 2667 $I^\pi = 6^+$, 1848 $I^\pi = 7^+$, 1205 $I^\pi = 8^+$ and 657 $I^\pi = 9^+$ states.

3.2 Results and Discussion

Let us first discuss the even mass ^{28}Si nucleus. This nucleus has 6 active protons and neutrons in the valence space. There exist altogether 93710 states for this nuclei in the full $1s0d$-shell basis. Although $T_z = 0$ for all states the total isospin is between 0 and 6. The figure 3.1 displays the energy spectra of ^{28}Si for spins $0-8$ as obtained by the GCM calculation as well as via the SCM diagonalizations. The energies are plotted up to the 17.5 MeV excitation energy with respect to the ground state. Altogether 328 SCM states with the total isospin $T = 0, 1$ and 2 can be found from the figure 3.1. In comparison, there are 260 corresponding GCM states, which have now also good isospin, because the same isospin conserving Chung-Wildenthal force was used to obtain them. All the other GCM states with, in principle, all possible isospins, lie above the considered energy range. It is important to notice that all the GCM states are build on top of the GCV solution for the 0^+ ground state. Consequently those states whose structure is

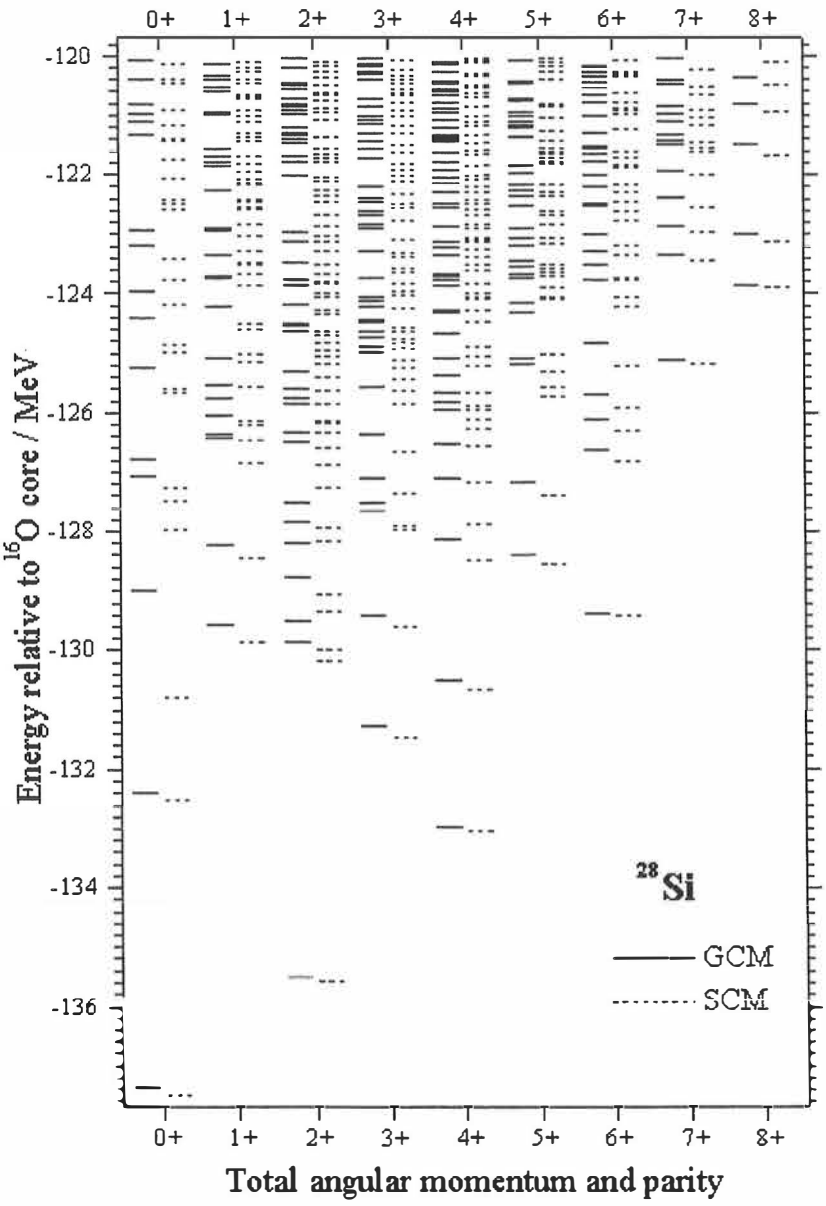

Figure 3.1: The energy spectrum of the ^{28}Si for the spins 0^+ to 8^+ obtained by full $1s0d$-shell calculations using the GENERAL COMPLEX MONSTER (GCM) and the Shell Configuration Mixing (SCM) approaches. The levels are plotted up to -120 MeV binding energy relative to the ^{16}O core.

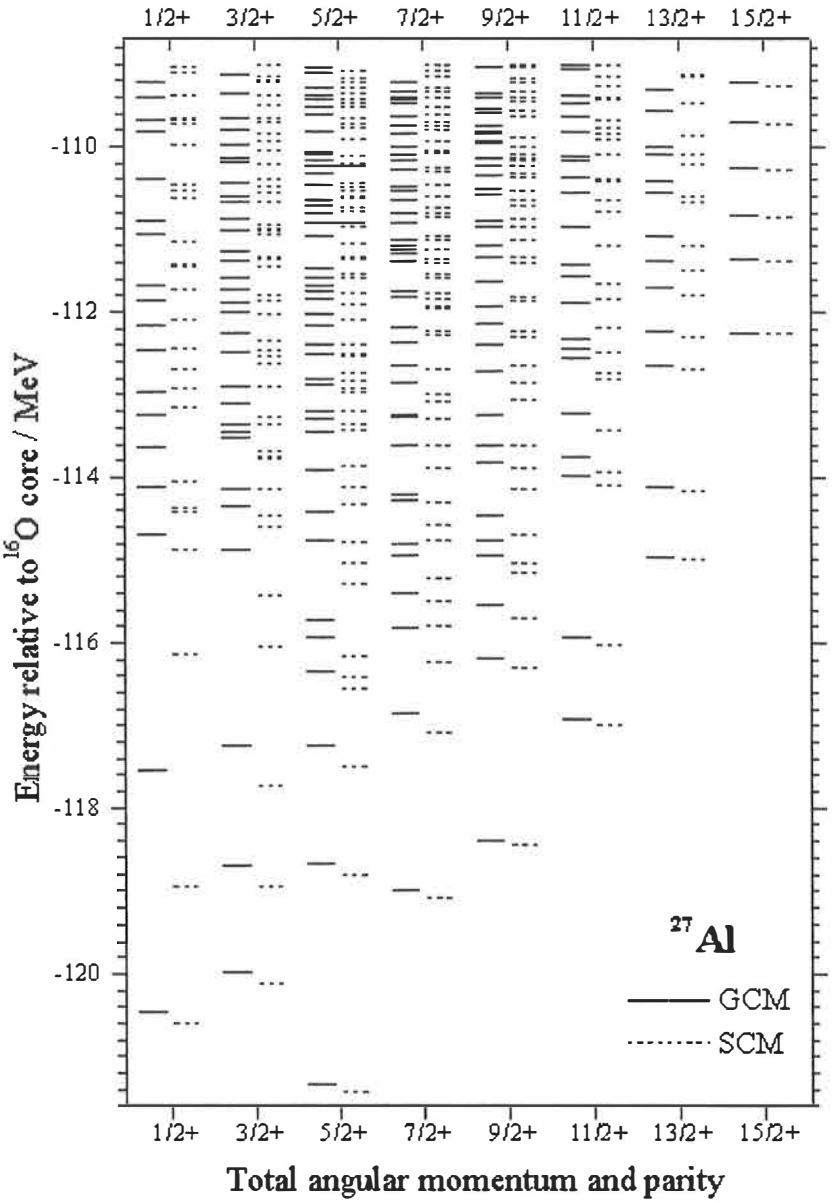

Figure 3.2: The energy spectrum of the ^{27}Al for the spins $1/2^+$ to $15/2^+$ obtained by full $1s0d$-shell calculations using the GENERAL COMPLEX MONSTER (GCM) and the Shell Configuration Mixing (SCM) approaches. The levels are plotted up to -109 MeV binding energy relative to the ^{16}O core.

similar to the particular 0^+ state are well produced while for some states the GCM description is insufficient due to their different (configuration) structure. Consequently these states cannot be described adequately in the framework of projected vacuum plus all projected 2-quasiparticle determinants. These states appear with too high energy or are completely missing. The same is true also for the odd mass ^{27}Al nucleus, which has 5 valence protons and 6 valence neutrons in the same $1s0d$-shell basis, resulting 80112 states. Now the $T_z = 1/2$ and the total isospin is between 1/2 and 11/2. In the figure 3.2 the energy spectra of ^{27}Al for spins $1/2 - 15/2$ as obtained by the GCM calculations on top of the GCV ground state $5/2^+$ solution, as well as via the SCM diagonalizations, are plotted up to the 12.0 MeV excitation energy with respect to the ground state. The number of SCM states with the total isospin $T = 1/2, 3/2$ and $5/2$ is 264 while the number of GCM states is 211 in the considered energy range.

The ground state 0^+ GCM and GCV energies are the same within the limits of the numerical accuracy. In the corresponding wavefunction the vacuum configuration obviously has the largest contribution. Although the other configurations have in general small non-zero components (because of the non-orthogonality of the projected quasiparticle determinants) they do not correlate the yrast energy according to the generalized Brillouin theorem. The underbinding compared to the SCM solution is only 120 keV, which means less than a tenth of percent relative difference. It must be regarded as a merit for the GCV approach [Ham98], where the state is produced via the variation of 552 linearly independent variables. All the other yrast states are also very well reproduced as can be seen from figure 3.3, where the yrast energies as obtained by the GCV, GCM and SCM approaches are displayed for the spins 0^+ to 6^+. The average deviation of the yrast states 0^+ to 6^+ from the exact SCM energies is only 130 keV. For comparison, the corresponding average deviation is as much as 1.7 MeV in the *Real* MONSTER, 1.1

MeV in the *Complex* MONSTER [Ben95b] and still 230 keV in the GCV. The GCM approach offers now considerably better description for these states compared to the earlier restricted MONSTER approaches and halves the deviation of even the GCV approach. The deviation from the exact SCM yrast energy does not considerably depend on the the ratio SCM per GCM dimensions, although the 3^+ state has the largest deviation in this case. The yrasts for the ^{27}Al are equally well reproduced, see figure 3.4 (notice a different scaling compared to the figure 3.3). Now the average deviation for the yrasts $1/2^+ - 9/2^+$ is 100 keV in the GCM, 330 keV in the GCV, 1.4 MeV in the *Complex* MONSTER, 1.7 MeV in the *Real* MONSTER [Ben96]. We can conclude that the GCM configuration space does contain the most important shell model configurations for the particular yrast states. The success in the description of the yrast states is mostly due to the relatively large GCM dimensions, which are at most an order of magnitude smaller than the complete SCM dimensions. In principle, the agreement of the VAMPIR type approaches can be still improved by the correlating additional projected quasiparticle determinants in the spirit of the FED GCV method described in the subsection 1.3.5. Now the GCM approach provides an easy way to obtain large number of correlating projected quasiparticle determinants for the reference GCV determinant.

I would like to emphasize once more that all the GCM states for the ^{28}Si are build on top the GCV 0^+ solution and those for the ^{27}Al on top of the GCV $5/2^+$ solution. The choice to use the mean-field of the ground-state GCV solutions is just a matter of convenience, any other solution i.e. the transformation F could have been chosen as well. Then obviously the spectra would have also changed in general. Although the yrast states (besides the 0^+) are better produced via GCM approach the use of GCV solution for the groundstate does not necessary yield the best agreement for all angular momenta compared to the SCM. Most probably the GCM description of some yrast state being

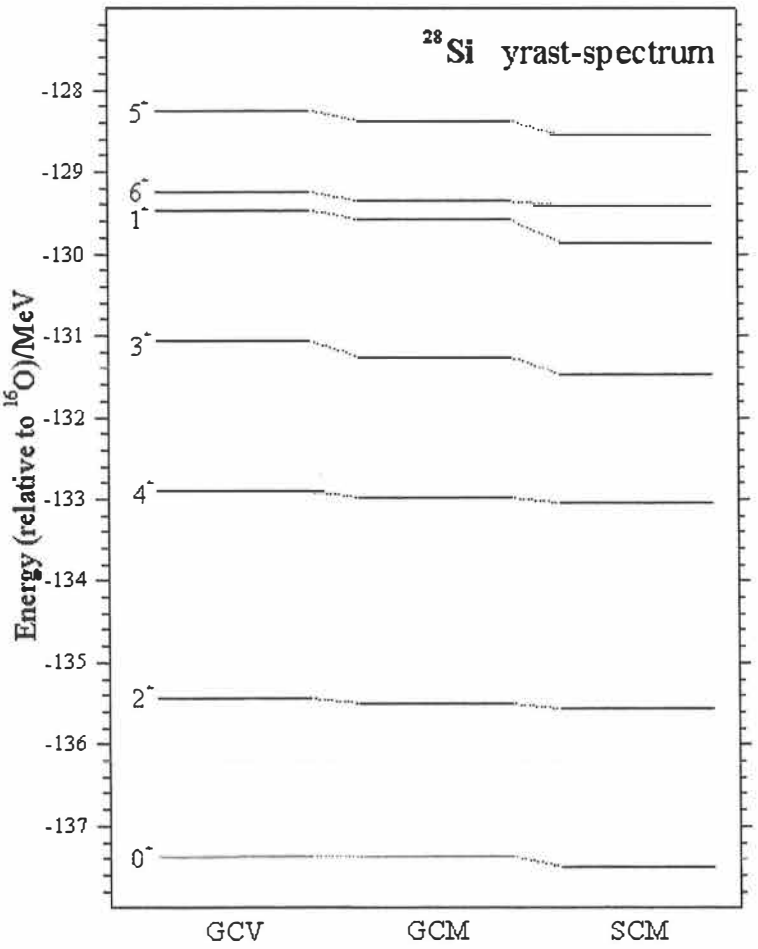

Figure 3.3: The yrast spectrum of the ^{28}Si for the spins 0^+ to 6^+ obtained by full $1s0d$-shell calculations using the GENERAL COMPLEX VAMPIR (GCV), GENERAL COMPLEX MONSTER (GCM) and the Shell Configuration Mixing (SCM) approaches.

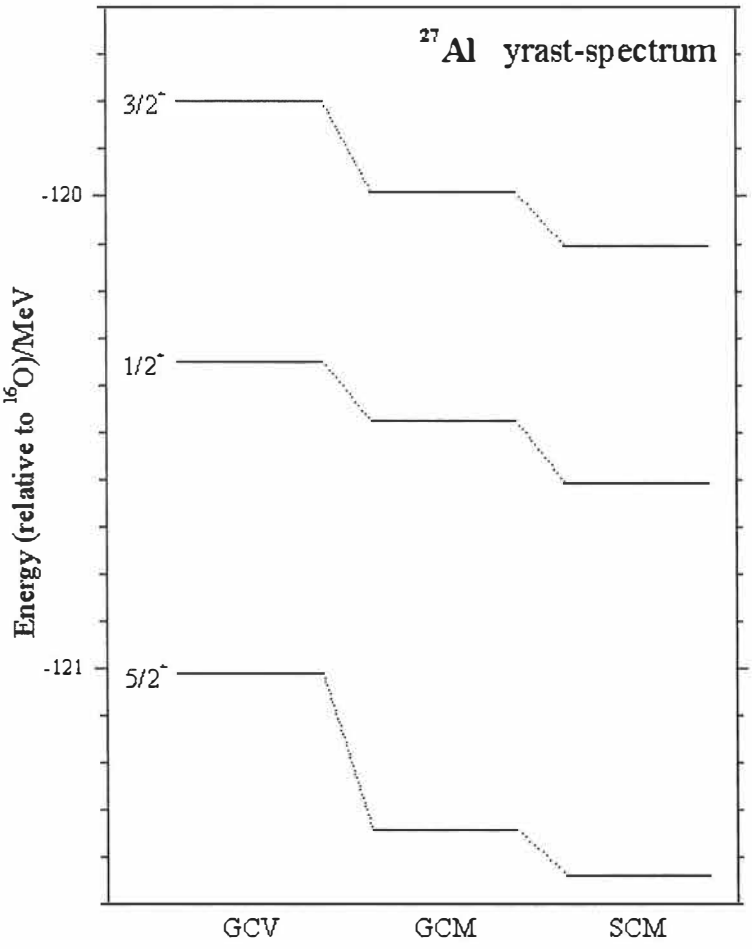

Figure 3.4: The yrast spectrum of the ^{27}Al for the spins $1/2^+$ to $5/2^+$ obtained by full $1s0d$-shell calculations using the GENERAL COMPLEX VAMPIR (GCV), GENERAL COMPLEX MONSTER (GCM) and the Shell Configuration Mixing (SCM) approaches.

based on the GCV solution for the particular spin is the most bound solution. This is because being the solution of the variational calculation the GCV description for some yrast state is already the optimal projected one-determinant solution for the particular state and hence should be the primary choice for the mean-field in that sense.

As for the excited states, they usually display various and more complicated structures than the yrast states and the agreement of the GCM with the exact solution depends strongly on the structure of the underlying mean-field. The agreement is not necessarily the best for the GCV yrast mean-field solution for the particular spin. In this case the best agreement is rather likely obtained using the mean-field with the most similar structure to the considered excited state. Although, it might be hard or sometimes even impossibly to identify the corresponding GCM and SCM states, those with similar structure are most probably very well reproduced. The above discussion holds also for the problems with larger configuration spaces, where the GCM dimension can be many orders of magnitude smaller than the SCM dimensions. This is true also here for the nuclei ^{27}Al and ^{28}Si. In figures 3.1 and 3.2 one can easily identify the lowest few excited states, since the state density is so low near the yrast states. As going up in energy the state density increases and it makes the identification much harder. However, the situation is somewhat different for the very high spins, like the largest spins $10^+ - 14^+$ for the ^{28}Si and the $21/2^+ - 23/2^+$ for the ^{27}Al, where the GCM configuration space exhausts the complete SCM spaces and the results are practically exact and depend only loosely on the symmetry of the mean-field. In fact, already the 8^+ states for the ^{28}Si and the $15/2^+$ states for the ^{27}Al are almost exactly reproduced.

In the GCM calculations 20 gaussian integration points were used in the angular momentum projection for both nuclei and all states, which turned out to be sufficient.

However, for the highest spins (> 8) this could lead to improper projection. Furthermore, 16 integration points were used for the both α and γ integration. The number projections were performed exactly with 8 integration points for the both mass number and isospin 3-component.

3.3 The Performance

The GCM calculations were performed on SGI Onyx2 computer at the Department of Physics at Jyväskylä. The disc space and memory statistics together with the percentual shares of the time consumption in each part of the program package in the $1s0d$-shell example calculations can be found in table 3.2.

GCMNUPR			GCMAMPR			GCMSMEQ		
D/MB	S/MB	T%	D/MB	S/MB	T%	D/MB	S/MB	T%
6030	12	88	340	5.2	1	260	1018	11

Table 3.2: The statistics of the GCM calculations in the full $1s0d$-shell model space for the states $I = 1/2^+ - 15/2^+$ in the nucleus ^{27}Al and the states $I = 0^+ - 8^+$ in the nucleus ^{28}Si on the SGI Onyx2 computer. The D is the maximal disc space (in megabytes) needed for the output in the particular program, the S is the maximal size of the programs for the considered states (in megabytes) and the T is the average percentual time consumption of the programs.

The GCMNUPR program requires as much as 5.9 GB disc space. Although it has to be performed only once for both considered nuclei, it takes most of the computing time (88%). The number projections were done exactly. The sufficient number of integration points were 8 for the both mass number and isospin 3-component projections. The number of α and γ points were 16 and the number β points was 20. For the even mass

nucleus ^{28}Si the code performed about 1% faster than for the odd mass ^{27}Al due to the slightly different method for determining the rotated overlaps (see appendix C).

The 20 gaussian integration points used in the angular momentum projection for both nuclei resulted in a maximum of 340 MB of output data in the GCMAMPR program for the ^{28}Si 8^+ state. In the GCMSMEQ program the diagonalization of the (4709×4709) projected overlap matrix for the same 8^+ state yields the maximum size of 1 GB. For the lower spins where the dimensions are smaller both the GCMAMPR and GCMSMEQ codes performed considerably faster. The time shares should not alter essentially if the calculations were redone on some other platform.

Chapter 4

Summary

In this thesis the numerical implementation, coding and the involved mathematical formalism of the GENERAL COMPLEX MONSTER nuclear structure approach was introduced along with an overview of the VAMPIR-MONSTER variational based model family. This approach represents an advanced stage in the continuously evolving, almost 20 years old, model family.

In the GENERAL COMPLEX MONSTER approach the nuclear wave functions are expanded around the GENERAL COMPLEX VAMPIR yrast solution. The spectrum of excited states is obtained by diagonalizing the chosen Hamiltonian in the space of the GENERAL COMPLEX VAMPIR type symmetry projected vacuum and all symmetry projected 2-quasiparticle configurations with respect to it. The approach is well suited for the problems where a complete set of excitations with respect to a particular transition operator is needed.

The first applications of the approach was presented for the ^{27}Al and ^{28}Si in the full $1s0d$-shell basis. The spectra show excellent agreement with the exact shell model results. Rather than discuss the productivity or the agreement of the calculated energies one should look for the other observables too, like the transition strengths up to high

excitation energies and analyze the wave functions. At this stage such calculations seem evident continuation for this work.

However, the full $1s0d$-shell basis is rather tiny for a GENERAL COMPLEX MONSTER calculation. It is expected that the GENERAL COMPLEX MONSTER approach will reveal its power in the applications for problems involving larger model spaces, where the exact shell model diagonalizations are impossible. However, if the model space consists of more than one major oscillator shell the exact restoration of the Galilei invariance is desired. It can be obtained by the exact center-of-momentum projection before the mean-field variation. The application of the GENERAL COMPLEX MONSTER approach in larger model spaces with the exact center-of-momentum projection is planned for the future. In order to maintain the feasibility also then the parallelization of the code is inevitable.

The results published in this thesis are the first in the series of calculations to be published in the forthcoming papers applying the GENERAL COMPLEX MONSTER and GENERAL COMPLEX VAMPIR approaches along the lines discussed above.

Appendix A

Operators in Quasiparticle Picture

A.1 The Quasiparticle Representation of the Hamiltonian

The Hamiltonian of type (1.2) can be represented in the quasiparticle formalism using the inverse transformation of F (1.9), namely $F^\dagger$. We obtain

$$\begin{aligned}\hat{H}(F) =& H^0(F) + \hat{H}^{11}(F) + \hat{H}^{20}(F) + \hat{H}^{22}(F) + \hat{H}^{31}(F) + \hat{H}^{40}(F) \\ =& H^0(F) + \sum_{\alpha\beta} H^{11}_{\alpha\beta}(F) a^\dagger_\alpha(F) a^\dagger_\beta(F) + \sum_{\alpha\beta} \left[H^{20}_{\alpha\beta}(F) a^\dagger_\alpha(F) a^\dagger_\beta(F) + \text{h.c.} \right] \\ &+ \sum_{\alpha\beta\gamma\delta} H^{22}_{\alpha\beta\gamma\delta}(F) a^\dagger_\alpha(F) a^\dagger_\beta(F) a_\delta(F) a_\gamma(F) \\ &+ \sum_{\alpha\beta\gamma\delta} \left[H^{31}_{\alpha\beta\gamma\delta}(F) a^\dagger_\delta(F) a^\dagger_\gamma(F) a^\dagger_\beta(F) a_\alpha(F) + \text{h.c.} \right] \\ &+ \sum_{\alpha\beta\gamma\delta} \left[H^{40}_{\alpha\beta\gamma\delta}(F) a^\dagger_\alpha(F) a^\dagger_\beta(F) a^\dagger_\gamma(F) a^\dagger_\delta(F) + \text{h.c.} \right].\end{aligned} \tag{A.1}$$

With the following definitions for the Γ- and pairing field

$$\begin{aligned}\Gamma_{ik}(F) &\equiv \sum_{rs} v(irks) \rho_{sr}(F) = \Gamma^*_{ki}(F) \\ \Delta_{ik}(F) &\equiv \frac{1}{2} \sum_{rs} v(ikrs) \kappa_{sr}(F) = -\Delta_{ki}(F),\end{aligned} \tag{A.2}$$

where ρ is the density matrix (1.16) and κ is the pairing tensor (1.18), we get for the HFB-vacuum energy

$$\begin{aligned} H^0(F) \equiv & \sum_{ik} \left\{ \left[t(ik) + \frac{1}{2}\Gamma_{ik}(F) \right] \rho_{ki}(F) + \frac{1}{2}\Delta_{ik}(F)\kappa^*_{ki}(F) \right\} \\ = & \mathrm{Tr}\left[(t + \frac{1}{2}\Gamma(F))\rho^*(F) - \frac{1}{2}\Delta(F)\kappa^*(F) \right] \end{aligned} \tag{A.3}$$

and also

$$\begin{aligned} H^{11}(F) \equiv & A^\dagger(F)h(F)A(F) - B^\dagger(F)h^T(F)B(F) \\ & + B^\dagger(F)\Delta^*(F)A(F) - A^\dagger(F)\Delta(F)B(F) \\ H^{20}(F) \equiv & \frac{1}{2}\Big[A^\dagger(F)h(F)B^*(F) - B^\dagger(F)h^T(F)A^*(F) \\ & + B^\dagger(F)\Delta^*(F)B^*(F) - A^\dagger(F)\Delta(F)A^*(F) \Big], \end{aligned} \tag{A.4}$$

where the matrix $h(F) \equiv t + \Gamma(F)$ is hermitian. Furthermore,

$$\begin{aligned} & H^{22}_{\alpha\beta\gamma\delta}(F) \equiv \\ & \frac{1}{4}\sum_{ikrs} v(ikrs) \Big[A^*_{i\alpha}(F)A^*_{k\beta}(F)A_{r\gamma}(F)A_{s\delta}(F) + B^*_{i\alpha}(F)B^*_{k\beta}(F)B_{r\gamma}(F)B_{s\delta}(F) \\ & - \Big(A^*_{i\alpha}(F)B_{k\delta}(F)A_{r\gamma}(F)B^*_{s\beta}(F) + B^*_{i\alpha}(F)A_{k\delta}(F)B_{r\gamma}(F)A^*_{s\beta}(F) \Big) \\ & + \Big(r \longleftrightarrow s \Big) \Big] \end{aligned} \tag{A.5}$$

$$\begin{aligned} & H^{31}_{\alpha\beta\gamma\delta}(F) \equiv \\ & \frac{1}{6}\sum_{ikrs} v(ikrs) \Big[\Big(A_{i\alpha}(F)B^*_{k\beta}(F)A^*_{r\delta}(F)A^*_{s\gamma}(F) + B_{i\alpha}(F)A^*_{k\beta}(F)B^*_{r\delta}(F)B^*_{s\gamma}(F) \Big) \\ & - \Big(\beta \longleftrightarrow \gamma \Big) \\ & + \Big(\beta \longleftrightarrow \gamma; \gamma \longleftrightarrow \delta \Big) \Big] \end{aligned} \tag{A.6}$$

$$H^{40}_{\alpha\beta\gamma\delta}(F) \equiv$$
$$-\frac{1}{24}\sum_{ikrs} v(ikrs)\Big[\Big(A^*_{i\alpha}(F)A^*_{k\gamma}(F)B^*_{r\delta}(F)B^*_{s\beta}(F) + B^*_{i\alpha}(F)B^*_{k\gamma}(F)A^*_{r\delta}(F)A^*_{s\beta}(F)\Big)$$
$$-\Big(\gamma \longleftrightarrow \delta\Big)-\Big(\gamma \longleftrightarrow \beta\Big)\Big]. \tag{A.7}$$

The symmetries of the components follow from the hermicity of the Hamiltonian and the anticommutation relations for the quasiparticle operators $a^\dagger(F)$ and $a(F)$. We have

$$\begin{aligned} &H^0(F) \in \mathbb{R}, \quad H^{11}_{\alpha\beta}(F) = H^{11\,*}_{\beta\alpha}(F) \mapsto H^{11}_{\alpha\alpha}(F) \in \mathbb{R} \\ &H^{20}_{\alpha\beta}(F) = -H^{20}_{\beta\alpha}(F) \\ &H^{22}_{\alpha\beta\gamma\delta}(F) = -H^{22}_{\beta\alpha\gamma\delta}(F) = -H^{22}_{\alpha\beta\delta\gamma}(F) = H^{22}_{\alpha\beta\gamma\delta}(F) = H^{22\,*}_{\gamma\delta\alpha\beta}(F). \end{aligned} \tag{A.8}$$

The $H^{31}_{\alpha\beta\gamma\delta}(F)$ is antisymmetric with respect to the interchange of the indices β, γ and δ:

$$H^{31}_{\alpha\beta\gamma\delta}(F) = -H^{31}_{\alpha\gamma\beta\delta}(F) = -H^{31}_{\alpha\beta\delta\gamma}(F) = -H^{31}_{\alpha\delta\gamma\beta}(F) = H^{31}_{\alpha\delta\beta\gamma}(F) = H^{31}_{\alpha\gamma\delta\beta}(F), \tag{A.9}$$

while $H^{40}_{\alpha\beta\gamma\delta}(F)$ is antisymmetric for all indices α, β, γ and δ.

A.2 The Quasiparticle Representation of the Number Operators

Next we derive the quasiparticle representation of the number operators of the form

$$_\tau\hat{\mathcal{N}} \equiv \sum_i \delta_{\tau_i\tau} c^\dagger_i c_i = \begin{cases} \hat{N} & \text{for } \tau = \frac{1}{2} \\ \hat{Z} & \text{for } \tau = -\frac{1}{2} \end{cases} \tag{A.10}$$

The mass number and isospin 3-component operators are found using these as $\hat{A} = \hat{N} + \hat{Z}$ and $2\hat{T}_z = \hat{N} - \hat{Z}$, respectively. We get

$$_\tau\hat{\mathcal{N}} = {}_\tau\mathcal{N}^0(F) + \sum_{\alpha\beta} {}_\tau\mathcal{N}^{11}_{\alpha\beta}(F) a^\dagger_\alpha a_\beta + \sum_{\alpha\beta}\Big[{}_\tau\mathcal{N}^{20}_{\alpha\beta}(F) a^\dagger_\alpha a^\dagger_\beta + \text{h.c.}\Big], \tag{A.11}$$

Using notation $(\xi_\tau)_{ik} \equiv \delta_{ik}\delta_{\tau_i\tau}$ we have

$$\begin{aligned} {}_\tau\mathcal{N}^0(F) &= \sum_i \delta_{\tau_i\tau}\rho_{ii}(F) = \mathrm{Tr}[\xi_\tau(B^*(F)B^T(F))] \\ {}_\tau\mathcal{N}^{11}(F) &= A^\dagger(F)\xi_\tau A(F) - B^\dagger(F)\xi_\tau B(F) \\ {}_\tau\mathcal{N}^{20}(F) &= \frac{1}{2}\Big[A^\dagger(F)\xi_\tau B^*(F) - B^\dagger(F)\xi_\tau A^*(F)\Big]. \end{aligned} \tag{A.12}$$

The number operator (A.10) is obviously Hermitian, and hence quite similar symmetries as in equation (A.8) follow

$$\begin{aligned} &{}_\tau\mathcal{N}^0(F) \in \mathbb{R}, \quad {}_\tau\mathcal{N}^{11}_{\alpha\beta}(F) = {}_\tau\mathcal{N}^{11*}_{\beta\alpha}(F) \mapsto {}_\tau\mathcal{N}^{11}_{\alpha\alpha}(F) \in \mathbb{R} \\ &{}_\tau\mathcal{N}^{20}_{\alpha\beta}(F) = -{}_\tau\mathcal{N}^{20}_{\beta\alpha}(F). \end{aligned} \tag{A.13}$$

Finally, one can write the mass number and isospin 3-component operator matrix components,

$$\begin{aligned} A^{11}(F) &\equiv {}_{\frac{1}{2}}\mathcal{N}^{11}(F) + {}_{-\frac{1}{2}}\mathcal{N}^{11}(F) = A^\dagger(F)\delta A(F) - B^\dagger(F)\delta B(F) \\ T_z^{11}(F) &\equiv \frac{1}{2}\Big[{}_{\frac{1}{2}}\mathcal{N}^{11}(F) - {}_{-\frac{1}{2}}\mathcal{N}^{11}(F)\Big] \\ &= \frac{1}{2}\Big[A^\dagger(F)(\xi_{\frac{1}{2}} - \xi_{-\frac{1}{2}})A(F) - B^\dagger(F)(\xi_{\frac{1}{2}} - \xi_{-\frac{1}{2}})B(F)\Big] \end{aligned} \tag{A.14}$$

and

$$\begin{aligned} A^{20}(F) &\equiv {}_{\frac{1}{2}}\mathcal{N}^{20}(F) + {}_{-\frac{1}{2}}\mathcal{N}^{20}(F) = \frac{1}{2}\Big[A^\dagger(F)\delta B^*(F) - B^\dagger(F)\delta A^*(F)\Big] \\ T_z^{20}(F) &\equiv \frac{1}{2}\Big[{}_{\frac{1}{2}}\mathcal{N}^{20}(F) - {}_{-\frac{1}{2}}\mathcal{N}^{20}(F)\Big] \\ &= \frac{1}{4}\Big[A^\dagger(F)(\xi_{\frac{1}{2}} - \xi_{-\frac{1}{2}})B^*(F) - B^\dagger(F)(\xi_{\frac{1}{2}} - \xi_{-\frac{1}{2}})A^*(F)\Big]. \end{aligned} \tag{A.15}$$

Of course, the same symmetries as in the above equation (A.13) apply also for $A(F)$ and $T_z(F)$.

Appendix B

The HFB-quasiparticle energies

In order to obtain the quasiparticle energies with respect to the Fermi level we must diagonalize the $\hat{\tilde{H}}^{11}(F)$ part of the Hermitian matrix

$$\tilde{H}(F) \equiv \hat{H} - \lambda\hat{A} - \mu\hat{T}_z, \tag{B.1}$$

using a unitary matrix U (1.40), which updates the last Bloch-Messiah transformation C (1.41). The Lagrange multiplers λ and μ are determined via the subsidiary conditions

$$\langle F|\hat{A}|F\rangle = A \quad \text{and} \quad \langle F|\hat{T}_z|F\rangle = T_z. \tag{B.2}$$

This method is well known from the standard HFB calculations with various constraints as well as from the conventional BCS-theory. Analogously to the subsection 1.3.4 the variation,

$$\delta E_0[F] \equiv \delta \frac{\langle F|\hat{H}|F\rangle}{\langle F|F\rangle} = 0 \tag{B.3}$$

can be performed by varying the anti-symmetric d matrix in the expression

$$|F^d\rangle = \langle F^0|F^d\rangle \exp\left\{\frac{1}{2}a^\dagger(F^0)da^\dagger(F^0)\right\}|F^0\rangle \tag{B.4}$$

yielding

$$\left.\frac{\partial E_0}{\partial d_{\alpha\beta}}\right|_{d=0} = \langle F^0|(\hat{H} - \lambda\hat{A} - \mu\hat{T}_z)a^\dagger_\alpha(F^0)a^\dagger_\beta(F^0)|F^0\rangle = 0 \quad \alpha \leq \beta = 1, \ldots, M_b, \tag{B.5}$$

which express the stability of the vacuum versus intrinsic 2-quasiparticle admixtures, analogously to the (1.36). The condition (B.5) is equivalent to

$$X^{20}(F) \equiv H^{20}(F) - \lambda A^{20}(F) - \mu T_z^{20}(F) = \mathbf{0}. \tag{B.6}$$

The matrices $H^{20}(F)$, $A^{20}(F)$ and $T_z^{20}(F)$ are given in equations (A.4) and (A.15). Using (B.6) we can construct relations

$$\begin{aligned} &\sum_{\alpha\beta} X^{20}_{\alpha\beta}(F) A^{20}_{\alpha\beta}(F) = \mathrm{Tr}\left[X^{20^T}(F) A^{20}(F)\right] \equiv X^{20}(F) \cdot A^{20}(F) = 0 \\ &X^{20}(F) \cdot T_z^{20}(F) = 0, \end{aligned} \tag{B.7}$$

yielding

$$\begin{aligned} \lambda &= \frac{(T_z^{20} \cdot T_z^{20})(H^{20} \cdot A^{20}) - (A^{20} \cdot T_z^{20})(H^{20} \cdot T_z^{20})}{(A^{20} \cdot A^{20})(T_z^{20} \cdot T_z^{20}) - (A^{20} \cdot T_z^{20})^2} \\ \mu &= \frac{(A^{20} \cdot A^{20})(H^{20} \cdot T_z^{20}) - (A^{20} \cdot T_z^{20})(H^{20} \cdot A^{20})}{(A^{20} \cdot A^{20})(T_z^{20} \cdot T_z^{20}) - (A^{20} \cdot T_z^{20})^2}. \end{aligned} \tag{B.8}$$

Finally we can diagonalize the $\tilde{H}^{11}(F)$ via the transformation U (1.40), the eigenvalues being the quasiparticle energies ε_α. Obviously the U transformation does not affect the HFB vacuum and thus also the GCV wavefunctions $|F; SM\rangle$ as well as the corresponding eigenenergies remain unchanged. For even A nuclei the ε_α are usually non-negative, while at least some of them are negative for odd A nuclei. This can be understood by simple reasoning. From the definition of the $\tilde{H}^{11}(F)$ (1.39), it is transparent that the ε_α is the energy of the one-quasiparticle state with respect to the HFB vacuum.

In the case of HFB vacuum for even nucleus the one-quasiparticle state has odd number parity (1.20) and is a linear superposition of states with odd nucleon number describing an odd nucleus. In general, the odd nuclei are less bound than the neighboring even A

nuclei, which means that $\varepsilon_\alpha > 0$. On the other hand, same reasoning leads to the negative quasiparticle energies for the odd A nuclei. Moreover, we find that the quasiparticle energy spectrum is always fully two-fold degenerate for even nucleus, because all the states have their conjugate partners, which is not the case for odd nuclei. The levels with the smallest absolute energy are those at the vicinity of the Fermi surface.

Appendix C

The Rotated and Parity Operated GCM Matrix Elements

In this appendix I will give an explicit expressions for the overlap and energy matrix elements needed in solving the GCV variational equations (1.30) and (1.36) as well as the GCM eigenvalue problem (1.45). Only those matrix elements which have the projected vacuum or projected 2-quasiparticle states have to be considered. Of course the extension of GCM to include higher-order projected n-quasiparticle states into the GCM basis (1.42) could be handled using the techniques presented here. In Ref. [Sch84a] similar but less general equations (without parity projection) were provided (with couple of typing errors). Since the following is an essential part of the GCM method, they will be reviewed in some extend here. I shall consider the most general case, where also the parity projection is explicitly performed.

Using the expression (1.24) we can distinguish three kind of overlap and Hamiltonian matrix elements (1.49),

$$\begin{aligned}\left\{\begin{array}{c} H^{S}_{0K;0K'} \\ N^{S}_{0K;0K'} \end{array}\right\} &= \int d\tilde{\Omega}\, \omega^{S\,*}_{KK'}(\tilde{\Omega}) \langle F| \left\{\begin{array}{c} \hat{H} \\ \hat{1} \end{array}\right\} \hat{\tilde{R}}(\tilde{\Omega}) \left[1 + \pi\hat{\Pi}\right] |F\rangle \\ &\equiv \int d\tilde{\Omega}\, \omega^{S\,*}_{KK'}(\tilde{\Omega}) \langle F| \left\{\begin{array}{c} \hat{H} \\ \hat{1} \end{array}\right\} \left[|F^1(\tilde{\Omega})\rangle + \pi |F^2(\tilde{\Omega})\rangle\right] \end{aligned} \tag{C.1}$$

$$\begin{aligned}\left\{\begin{array}{c} H^{S}_{0K;\alpha\beta K'} \\ N^{S}_{0K;\alpha\beta K'} \end{array}\right\} &= \int d\tilde{\Omega}\, \omega^{S\,*}_{KK'}(\tilde{\Omega}) \langle F| \left\{\begin{array}{c} \hat{H} \\ \hat{1} \end{array}\right\} \hat{\tilde{R}}(\tilde{\Omega}) \left[1 + \pi\hat{\Pi}\right] a^{\dagger}_{\alpha}(F) a^{\dagger}_{\beta}(F) |F\rangle \\ &\equiv \int d\tilde{\Omega}\, \omega^{S\,*}_{KK'}(\tilde{\Omega}) \langle F| \left\{\begin{array}{c} \hat{H} \\ \hat{1} \end{array}\right\} a^{\dagger}_{\alpha}(F^1(\tilde{\Omega})) a^{\dagger}_{\beta}(F^1(\tilde{\Omega})) |F^1(\tilde{\Omega})\rangle \\ &+ \pi \int d\tilde{\Omega}\, \omega^{S\,*}_{KK'}(\tilde{\Omega}) \langle F| \left\{\begin{array}{c} \hat{H} \\ \hat{1} \end{array}\right\} a^{\dagger}_{\alpha}(F^2(\tilde{\Omega})) a^{\dagger}_{\beta}(F^2(\tilde{\Omega})) |F^2(\tilde{\Omega})\rangle \\ &= \left\{\begin{array}{c} H^{S}_{\alpha\beta K;0K'} \\ N^{S}_{\alpha\beta K;0K'} \end{array}\right\}^{\dagger} \end{aligned} \tag{C.2}$$

and

$$\begin{aligned}\left\{\begin{array}{c} H^{S}_{\alpha\beta K;\gamma\delta K'} \\ N^{S}_{\alpha\beta K;\gamma\delta K'} \end{array}\right\} &= \int d\tilde{\Omega}\, \omega^{S\,*}_{KK'}(\tilde{\Omega}) \langle F| a_{\beta}(F) a_{\alpha}(F) \left\{\begin{array}{c} \hat{H} \\ \hat{1} \end{array}\right\} \hat{\tilde{R}}\left[1 + \pi\hat{\Pi}\right](\tilde{\Omega}) a^{\dagger}_{\gamma}(F) a^{\dagger}_{\delta}(F) |F\rangle \\ &\equiv \int d\tilde{\Omega}\, \omega^{S\,*}_{KK'}(\tilde{\Omega}) \langle F| a_{\beta}(F) a_{\alpha}(F) \left\{\begin{array}{c} \hat{H} \\ \hat{1} \end{array}\right\} a^{\dagger}_{\gamma}(F^1(\tilde{\Omega})) a^{\dagger}_{\delta}(F^1(\tilde{\Omega})) |F^1(\tilde{\Omega})\rangle \\ &+ \pi \int d\tilde{\Omega}\, \omega^{S\,*}_{KK'}(\tilde{\Omega}) \langle F| a_{\beta}(F) a_{\alpha}(F) \left\{\begin{array}{c} \hat{H} \\ \hat{1} \end{array}\right\} a^{\dagger}_{\gamma}(F^2(\tilde{\Omega})) a^{\dagger}_{\delta}(F^2(\tilde{\Omega})) |F^2(\tilde{\Omega})\rangle, \end{aligned} \tag{C.3}$$

In the last two equations $\alpha < \beta$ and $\gamma < \delta$. I use the abbreviations

$$|F^{\lambda}(\tilde{\Omega})\rangle \equiv \begin{cases} \hat{\tilde{R}}(\tilde{\Omega})|F\rangle & \text{for } \lambda = 1 \\ \hat{\tilde{R}}(\tilde{\Omega})\hat{\Pi}|F\rangle & \text{for } \lambda = 2 \end{cases} \tag{C.4}$$

and

$$a^{\dagger}(F^{\lambda}(\tilde{\Omega})) \equiv \begin{cases} \hat{\tilde{R}}(\tilde{\Omega})a^{\dagger}(F)\hat{\tilde{R}}^{\dagger}(\tilde{\Omega}) & \text{for } \lambda = 1 \\ \hat{\tilde{R}}(\tilde{\Omega})\hat{\Pi}\, a^{\dagger}(F)\, \hat{\Pi}^{-1}\hat{\tilde{R}}^{\dagger}(\tilde{\Omega}) & \text{for } \lambda = 2 \end{cases} \tag{C.5}$$

Whenever the first overlaps (C.1) are non-zero, the rotated HFB vacuums $|F^{\lambda}(\tilde{\Omega})\rangle$ can be written in terms of the unrotated one $|F\rangle$ using the Thouless's theorem [Tho60, Man75] (see chapter 1.3.4)

$$|F^{\lambda}(\tilde{\Omega})\rangle = \langle F|F^{\lambda}(\tilde{\Omega})\rangle \exp\left\{\frac{1}{2}a^{\dagger}(F)g^{\lambda}(F;\tilde{\Omega})\, a^{\dagger}(F)\right\}|F\rangle. \tag{C.6}$$

The antisymmetric $g^{\lambda}(F;\tilde{\Omega})$ matrix is given by

$$g^{\lambda}(F;\tilde{\Omega}) = (\tilde{B}^{\lambda}(\tilde{\Omega})[\tilde{A}^{\lambda}(\tilde{\Omega})]^{-1})^{*}, \tag{C.7}$$

where the rotated transformation matrix elements are determined via the transformation $\tilde{F}^{\lambda}(\tilde{\Omega})$ between the rotated and unrotated quasiparticle operators. It is obvious that the state (C.6), with $\lambda = 1$ is vacuum for the operators

$$\begin{aligned} \begin{pmatrix} a^{\dagger}(F(\tilde{\Omega})) \\ a(F(\tilde{\Omega})) \end{pmatrix} &\equiv F(\tilde{\Omega}) \begin{pmatrix} c^{\dagger} \\ c \end{pmatrix} \\ &\equiv \tilde{F}(\tilde{\Omega}) \begin{pmatrix} a^{\dagger}(F) \\ a(F) \end{pmatrix} = \hat{\tilde{R}}(\tilde{\Omega}) \begin{pmatrix} a^{\dagger}(F) \\ a(F) \end{pmatrix} \hat{\tilde{R}}^{\dagger}(\tilde{\Omega}) \\ &= F\hat{\tilde{R}}(\tilde{\Omega}) \begin{pmatrix} c^{\dagger} \\ c \end{pmatrix} \hat{\tilde{R}}^{\dagger}(\tilde{\Omega}) = F \begin{pmatrix} \tilde{R}^{T}(\tilde{\Omega}) & 0 \\ 0 & \tilde{R}^{\dagger}(\tilde{\Omega}) \end{pmatrix} \begin{pmatrix} c^{\dagger} \\ c \end{pmatrix}, \end{aligned} \tag{C.8}$$

because firstly, the vacuum can always be written as a quasiparticle determinant (1.12) and secondly, the generalized rotation operator $\hat{\tilde{R}}(\tilde{\Omega})$ is unitary and

$$\tilde{R}(\tilde{\Omega})_{ik} \equiv \langle i|\hat{\tilde{R}}(\tilde{\Omega})|k\rangle = \delta(n_i n_k)\delta(l_i l_k)\delta(j_i j_k)D^{j_i}_{m_i m_k}(\Omega)\delta(\tau_i \tau_k)e^{-i(2\chi\tau_i+\varphi)} \tag{C.9}$$

is its representation in the chosen spherical single particle basis. Furthermore, by applying the inverse transformation $F^\dagger$ we get

$$\tilde{F}(\tilde{\Omega}) = F \begin{pmatrix} \tilde{R}^T(\tilde{\Omega}) & 0 \\ 0 & \tilde{R}^\dagger(\tilde{\Omega}) \end{pmatrix} F^\dagger = \begin{pmatrix} \tilde{A}^T(\tilde{\Omega}) & \tilde{B}^T(\tilde{\Omega}) \\ \tilde{B}^\dagger(\tilde{\Omega}) & \tilde{A}^\dagger(\tilde{\Omega}) \end{pmatrix}, \tag{C.10}$$

where

$$\begin{aligned} \tilde{A}(\tilde{\Omega}) &\equiv A^\dagger(F)\tilde{R}(\tilde{\Omega})A(F) + B^\dagger(F)\tilde{R}^*(\tilde{\Omega})B(F) \\ \tilde{B}(\tilde{\Omega}) &\equiv B^T(F)\tilde{R}(\tilde{\Omega})A(F) + A^T(F)\tilde{R}^*(\tilde{\Omega})B(F) \end{aligned} \tag{C.11}$$

Similarly for $\lambda = 2$ we obtain

$$\begin{aligned} \tilde{A}^2(\tilde{\Omega}) &\equiv A^\dagger(F)\tilde{R}(\tilde{\Omega})\Pi A(F) + B^\dagger(F)\tilde{R}^*(\tilde{\Omega})\Pi B(F) \\ \tilde{B}^2(\tilde{\Omega}) &\equiv B^T(F)\tilde{R}(\tilde{\Omega})\Pi A(F) + A^T(F)\tilde{R}^*(\tilde{\Omega})\Pi B(F), \end{aligned} \tag{C.12}$$

where

$$\left[\tilde{R}(\tilde{\Omega})\Pi\right]_{ik} = \tilde{R}(\tilde{\Omega})_{ik}\pi_k. \tag{C.13}$$

The normalization constant $\langle F|F^\lambda(\tilde{\Omega})\rangle$ is the so called rotated overlap. It can be calculated following the Ref. [Oni66]. Be

$$\langle \zeta F|F(\tilde{\Omega})\rangle \equiv |\langle 0|F\rangle|^2\langle 0|\exp\left\{\frac{1}{2}\left[\zeta c\, d^\dagger(F)c + c^\dagger d(F(\tilde{\Omega}))c^\dagger\right]\right\}|0\rangle, \tag{C.14}$$

where

$$\begin{aligned} d(F) &= (B(F)A^{-1}(F))^* \\ d(F(\tilde{\Omega})) &= (B(F(\tilde{\Omega}))A^{-1}(F(\tilde{\Omega})))^* = \tilde{R}(\tilde{\Omega})d(F)\tilde{R}^T(\tilde{\Omega}). \end{aligned}$$

Notice, that the expression (C.14) has now the factor $\langle 0|F\rangle$, which goes to zero if $|F\rangle$ has odd number parity. So that equation cannot be used directly for problems with odd A. From the expression

$$\frac{d}{d\zeta}\left(\frac{\langle \zeta F|F(\tilde{\Omega})\rangle}{|\langle 0|F\rangle|^2}\right) \equiv \frac{de^{Q(\zeta)}}{d\zeta} = e^{Q(\zeta)}\frac{dQ}{d\zeta} \tag{C.15}$$

Q is solved by integration. The overlap $\langle 0|F\rangle$ is calculated in the same way. Instead of $\langle \zeta F|F(\tilde{\Omega})\rangle$ now $\langle \zeta F|F\rangle$ should be considered. Consequently $|\langle 0|F\rangle|^2 = |\det A(F)|$. With the help of the matrix identity

$$\exp\left[\mathrm{Tr}\ln(\mathbf{1}+M)\right] = \det(\mathbf{1}+M), \tag{C.16}$$

where M is an arbitrary square matrix, the rotated overlap reads ($\zeta = 1$):

$$\begin{aligned}\langle F|F(\tilde{\Omega})\rangle &= \left(\det A^T(F)\det\left[\mathbf{1}+d^\dagger(F)d(F(\tilde{\Omega}))\right]\det A^*(F)\right)^{1/2} \\ &= \sqrt{\det \tilde{A}^\dagger(\tilde{\Omega})}\; e^{-\frac{i}{2}\left(\chi(M_b^n-M_b^p)+\varphi M_b+2\pi n\right)} \quad \text{where} \quad n\in\mathbb{Z}. \end{aligned} \tag{C.17}$$

For both λ we obtain

$$\langle F|F^\lambda(\tilde{\Omega})\rangle = \sqrt{\det\ \tilde{A}^{\lambda^\dagger}(\tilde{\Omega})}\; e^{-\frac{i}{2}\left(\chi(M_b^n-M_b^p)+\varphi M_b+2\pi n\right)}, \quad n\in\mathbb{Z}. \tag{C.18}$$

In this equation M_b^p (M_b^n) is the total number of proton (neutron) single particle basis states, so $M_b = M_b^p + M_b^n$. Here a special caution should be exercised. The undefined sign of the rotated overlap (C.18) originates from the multivaluedness of the logarithm in (C.16). In principle the right sign is assured by requiring continuity with respect to the rotation angle $\tilde{\Omega}$ in combination with the known value $\langle F|F\rangle = +1$. In practice a finite number of integration angles is used. The mesh of chosen angles $\{\Omega,\chi,\varphi\}$ is not necessarily dense enough to yield the correct sign. Instead of calculating the square root in (C.18) one may solve the roots $\xi_i^\lambda(\tilde{\Omega})$ of the characteristic polynomial of the matrix $d^\dagger(F)d(F^\lambda(\tilde{\Omega}))$ in (C.17) and use the fact that they are pairwise degenerate. This method was first proposed by Neergård and Wüst for real transformation matrices [Nee83]. We obtain

$$\det\left(\mathbf{1}+d^\dagger(F)d(F^\lambda(\tilde{\Omega}))\right) = \prod_{i=1}^{M_b}(1+\xi_i^\lambda(\tilde{\Omega})) = \left(\prod_{i=1}^{M_b/2}(1+\xi_i^\lambda(\tilde{\Omega}))\right)^2. \tag{C.19}$$

The resulting overlap with the correct sign is

$$\langle F|F^{\lambda}(\tilde{\Omega})\rangle = |\det A(F)| \prod_{1=1}^{M_b/2} (1+\xi_i^{\lambda}(\tilde{\Omega})). \tag{C.20}$$

The case of odd number parity is actually only a continuation of the above procedure. We can write the vacuum and the rotated vacuum with odd number parity as

$$|F_o\rangle = a_{\alpha}^{\dagger}(F_e)|F_e\rangle \tag{C.21}$$

$$|F_o^{\lambda}(\tilde{\Omega})\rangle = a_{\alpha}^{\dagger}(F_e^{\lambda}(\tilde{\Omega}))|F_e^{\lambda}(\tilde{\Omega})\rangle, \tag{C.22}$$

where $|F_e\rangle$ and $|F_e^{\lambda}(\tilde{\Omega})\rangle$ have even number parity. And consequently, the problem reverts to the calculation of

$$\langle F_o|F_o^{\lambda}(\tilde{\Omega})\rangle = \langle F_e|a_{\alpha}(F_e)a_{\alpha}^{\dagger}(F_e^{\lambda}(\tilde{\Omega}))|F_e^{\lambda}(\tilde{\Omega})\rangle, \tag{C.23}$$

where $|F_e(\tilde{\Omega})\rangle$ is given by equations (C.6), (C.18) and (C.20). This type of matrix elements between two different vacua are easily calculated using the Generalized Wick's theorem [Sch84a]. Now four non-vanishing elementary contractions exists. These are, all needed later on,

$$\overbrace{a_{\alpha}(F)a_{\beta}^{\dagger}}(F) \equiv \langle F|F^{\lambda}(\tilde{\Omega})\rangle^{-1}\langle F|a_{\alpha}(F)a_{\beta}^{\dagger}(F)|F^{\lambda}(\tilde{\Omega})\rangle = \delta_{\alpha\beta} \tag{C.24}$$

$$\overbrace{a_{\beta}(F)a_{\alpha}}(F) \equiv \langle F|F^{\lambda}(\tilde{\Omega})\rangle^{-1}\langle F|a_{\beta}(F)a_{\alpha}(F)|F^{\lambda}(\tilde{\Omega})\rangle = g_{\alpha\beta}^{\lambda}(F;\tilde{\Omega}) \tag{C.25}$$

$$\begin{aligned}\overbrace{a_{\alpha}(F)a_{\beta}^{\dagger}}(F^{\lambda}(\tilde{\Omega})) &\equiv \langle F|F^{\lambda}(\tilde{\Omega})\rangle^{-1}\langle F|a_{\alpha}(F)a_{\beta}^{\dagger}(F^{\lambda}(\tilde{\Omega}))|F^{\lambda}(\tilde{\Omega})\rangle \\ &= \left[\tilde{A}^{\lambda}(\tilde{\Omega}) - g^{\lambda}(F;\tilde{\Omega})\tilde{B}^{\lambda}(\tilde{\Omega})\right]_{\alpha\beta} = \left[\ \tilde{A}^{\lambda\dagger}(\tilde{\Omega})\right]_{\alpha\beta}^{-1} \equiv X_{\alpha\beta}^{\lambda}(F;\tilde{\Omega})\end{aligned} \tag{C.26}$$

$$\begin{aligned}a_{\alpha}^{\dagger}\overbrace{(F^{\lambda}(\tilde{\Omega}))a_{\beta}^{\dagger}}(F^{\lambda}(\tilde{\Omega})) &\equiv \langle F|F^{\lambda}(\tilde{\Omega})\rangle^{-1}\langle F|a_{\alpha}^{\dagger}(F^{\lambda}(\tilde{\Omega}))a_{\beta}^{\dagger}(F^{\lambda}(\tilde{\Omega}))|F^{\lambda}(\tilde{\Omega})\rangle \\ &= \left[\ \tilde{B}^{\lambda^T}(\tilde{\Omega})X^{\lambda}(F;\tilde{\Omega})\right]_{\alpha\beta} \equiv \tilde{g}_{\alpha\beta}^{\lambda}(F;\tilde{\Omega}),\end{aligned} \tag{C.27}$$

where the last ones are obtained using the first two, which themselves follow directly from the anticommutator, $\{a_{\beta}(F), a_{\alpha}^{\dagger}(F)\} = \delta_{\alpha\beta}$. Notice that the first contraction (C.24) is

consistent with the ordinary Wick's theorem, as it should be. The resulting overlap for the vacuums with odd number parity is read directly from the contraction (C.26),

$$\langle F_o|F_o^\lambda(\tilde{\Omega})\rangle = \langle F_e|F_e^\lambda(\tilde{\Omega})\rangle X_{\alpha\alpha}^\lambda(F_e;\tilde{\Omega}). \tag{C.28}$$

Thus, the calculation of the overlaps for odd A nucleus is always slightly more involved than the one for even A counterpart.

In principle, the equation (C.20) is sufficient to determine the overlap unambiguously. However, practical calculations have shown that the equation (C.18) is numerically more accurate especially in cases with almost vanishing pairing correlations. Therefore, to ensure functionality everywhere the overlap is calculated always using both aforementioned equations. However, the (C.20) is used only to determine the correct sign for the overlap of even number parity vacuums $\langle F_e|F_e^\lambda(\tilde{\Omega})\rangle$. The overlaps in (C.2) can be read directly from equations (C.25) and (C.27).

$$\langle F|a_\beta(F)a_\alpha(F)|F^\lambda(\tilde{\Omega})\rangle = \langle F|F^\lambda(\tilde{\Omega})\rangle g_{\alpha\beta}^\lambda(F;\tilde{\Omega}) \tag{C.29}$$

$$\langle F|a_\alpha^\dagger(F^\lambda(\tilde{\Omega}))a_\beta^\dagger(F^\lambda(\tilde{\Omega}))|F^\lambda(\tilde{\Omega})\rangle = \langle F|F^\lambda(\tilde{\Omega})\rangle \tilde{g}_{\alpha\beta}^\lambda(F;\tilde{\Omega}). \tag{C.30}$$

The last missing rotated overlap (C.3) in the GCM scheme is the one between 2-quasiparticle states,

$$\begin{aligned}&\langle F|a_\beta(F)a_\alpha(F)a_\gamma^\dagger(F^\lambda(\tilde{\Omega}))a_\delta^\dagger(F^\lambda(\tilde{\Omega}))|F^\lambda(\tilde{\Omega})\rangle = \\ &\langle F|F^\lambda(\tilde{\Omega})\rangle \left(g_{\alpha\beta}^\lambda(F;\tilde{\Omega})\tilde{g}_{\gamma\delta}^\lambda(F;\tilde{\Omega}) + X_{\alpha\gamma}^\lambda(F;\tilde{\Omega})X_{\beta\delta}^\lambda(F;\tilde{\Omega}) - X_{\alpha\delta}^\lambda(F;\tilde{\Omega})X_{\beta\gamma}^\lambda(F;\tilde{\Omega})\right).\end{aligned} \tag{C.31}$$

In order to evaluate the rotated Hamiltonian matrix elements appearing in equations (C.1)-(C.3) one must find explicit expressions of them and that can be done by using the elementary contractions (C.24)-(C.27) and the quasiparticle representation of the

Hamiltonian A.1. For the rotated vacuum energy function one obtains

$$\langle F|\hat{H}|F^{\lambda}(\tilde{\Omega})\rangle \equiv h^{\lambda}(F;\tilde{\Omega}) = \langle F|F^{\lambda}(\tilde{\Omega})\rangle \left(H^{0}(F) + \tilde{H}^{\lambda 20^{*}}(F;\tilde{\Omega}) + 3\tilde{\tilde{H}}^{\lambda 40^{*}}(F;\tilde{\Omega})\right), \tag{C.32}$$

where

$$\tilde{H}^{\lambda 20^{*}}(F;\tilde{\Omega}) \equiv \mathrm{Tr}\left[H^{20}(F)g^{\lambda}(F;\tilde{\Omega})\right] \tag{C.33}$$

$$\begin{aligned}\tilde{\tilde{H}}^{\lambda 40^{*}}(F;\tilde{\Omega}) &\equiv \mathrm{Tr}\left[\tilde{H}^{\lambda 40^{\dagger}}(F;\tilde{\Omega})g^{\lambda}(F;\tilde{\Omega})\right] \\ &\equiv \sum_{\alpha\beta\gamma\delta} H^{40^{*}}_{\alpha\beta\gamma\delta}(F)g^{\lambda}_{\alpha\beta}(F;\tilde{\Omega})g^{\lambda}_{\gamma\delta}(F;\tilde{\Omega}).\end{aligned} \tag{C.34}$$

Whether one uses the upper- or lower triangle GCM matrices for overlap and Hamiltonian one needs either

$$\langle F|\tilde{H}a^{\dagger}_{\alpha}(F^{\lambda}(\tilde{\Omega}))a^{\dagger}_{\beta}(F^{\lambda}(\tilde{\Omega}))|F^{\lambda}(\tilde{\Omega})\rangle = h^{\lambda 02}_{\alpha\beta}(F;\tilde{\Omega})\langle F|F^{\lambda}(\tilde{\Omega})\rangle + h^{\lambda}(F;\tilde{\Omega})\tilde{g}^{\lambda}_{\alpha\beta}(F;\tilde{\Omega}) \tag{C.35}$$

with

$$h^{\lambda 02}(F;\tilde{\Omega}) \equiv X^{\lambda^{T}}(F;\tilde{\Omega})\left[2H^{20^{*}}(F) + 12\tilde{H}^{\lambda 40^{*}}(F;\tilde{\Omega})\right]X^{\lambda}(F;\tilde{\Omega}), \tag{C.36}$$

or

$$\langle F|a_{\beta}(F)a_{\alpha}(F)\hat{H}|F^{\lambda}(\tilde{\Omega})\rangle = h^{\lambda 20}_{\alpha\beta}(F;\tilde{\Omega})\langle F|F^{\lambda}(\tilde{\Omega})\rangle + h^{\lambda}(F;\tilde{\Omega})g^{\lambda}_{\alpha\beta}(F;\tilde{\Omega}) \tag{C.37}$$

with

$$\begin{aligned}h^{\lambda 20}(F;\tilde{\Omega}) \equiv\ & \\ & 2H^{20}(F) + 2\tilde{H}^{\lambda 22}(F;\tilde{\Omega}) + g^{\lambda}(F;\tilde{\Omega})\left[2H^{20^{*}}(F) + 12\tilde{H}^{\lambda 40^{*}}(F;\tilde{\Omega})\right]g^{\lambda}(F;\tilde{\Omega}) \\ & + \left[H^{11}(F) - 3\tilde{H}^{\lambda 31^{*}}(F;\tilde{\Omega})\right]g^{\lambda}(F;\tilde{\Omega}) + g^{\lambda}(F;\tilde{\Omega})\left[H^{11^{*}}(F) - 3\tilde{H}^{\lambda 31^{\dagger}}(F;\tilde{\Omega})\right],\end{aligned} \tag{C.38}$$

where

$$\tilde{H}^{\lambda 22}_{\alpha\beta}(F;\tilde{\Omega}) \equiv \sum_{\gamma\delta} H^{22}_{\alpha\beta\gamma\delta}(F) g^{\lambda}_{\gamma\delta}(F;\tilde{\Omega}) \tag{C.39}$$

$$\tilde{H}^{\lambda 31^*}_{\alpha\beta}(F;\tilde{\Omega}) \equiv \sum_{\gamma\delta} H^{31^*}_{\alpha\beta\gamma\delta}(F) g^{\lambda}_{\gamma\delta}(F;\tilde{\Omega}). \tag{C.40}$$

Last, for the matrix elements (C.3) one needs the rotated Hamiltonian matrix elements in between 2-quasiparticle states on both sides,

$$\begin{aligned}
&\langle F|a_\beta(F)a_\alpha(F)\hat{H}a^\dagger_\gamma(F^\lambda(\tilde{\Omega}))a^\dagger_\delta(F^\lambda(\tilde{\Omega}))|F^\lambda(\tilde{\Omega})\rangle = \\
&\quad h^\lambda(F;\tilde{\Omega})\left[g^\lambda_{\alpha\beta}(F;\tilde{\Omega})\tilde{g}^\lambda_{\gamma\delta}(F;\tilde{\Omega}) + X^\lambda_{\alpha\gamma}(F;\tilde{\Omega})X^\lambda_{\beta\delta}(F;\tilde{\Omega}) - X^\lambda_{\alpha\delta}(F;\tilde{\Omega})X^\lambda_{\beta\gamma}(F;\tilde{\Omega})\right] \\
&\quad +\langle F|F^\lambda(\tilde{\Omega})\rangle\Big(h^{\lambda 20}_{\alpha\beta}(F;\tilde{\Omega})\tilde{g}^\lambda_{\gamma\delta}(F;\tilde{\Omega}) + h^{\lambda 02}_{\gamma\delta}(F;\tilde{\Omega})g^\lambda_{\alpha\beta}(F;\tilde{\Omega}) \\
&\quad +h^{\lambda 11}_{\alpha\gamma}(F;\tilde{\Omega})X^\lambda_{\beta\delta}(F;\tilde{\Omega}) + h^{\lambda 11}_{\beta\delta}(F;\tilde{\Omega})X^\lambda_{\alpha\gamma}(F;\tilde{\Omega}) \\
&\quad -h^{\lambda 11}_{\alpha\delta}(F;\tilde{\Omega})X^\lambda_{\beta\gamma}(F;\tilde{\Omega}) - h^{\lambda 11}_{\beta\gamma}(F;\tilde{\Omega})X^\lambda_{\alpha\delta}(F;\tilde{\Omega}) \\
&\quad +v^\lambda_{\alpha\beta\gamma\delta}(F;\tilde{\Omega})\Big),
\end{aligned} \tag{C.41}$$

where

$$\begin{aligned}
h^{\lambda 11}(F;\tilde{\Omega}) \equiv &\Big\{H^{11}(F) - 3\tilde{H}^{\lambda 31^*}(F;\tilde{\Omega}) \\
&+ g^\lambda(F;\tilde{\Omega})\left[2H^{20^*}(F) + 12\tilde{H}^{\lambda 40^*}(F;\tilde{\Omega})\right]\Big\}X^\lambda(F;\tilde{\Omega}),
\end{aligned} \tag{C.42}$$

and

$$\begin{aligned}
v^\lambda_{\alpha\beta\gamma\delta}(F;\tilde{\Omega}) \equiv \sum_{\rho\sigma}\Big\{&4H^{22}_{\alpha\beta\rho\sigma}(F) - 24\sum_{\mu\nu} H^{40^*}_{\mu\nu\rho\sigma}(F) g^\lambda_{\alpha\mu}(F;\tilde{\Omega}) g^\lambda_{\beta\nu}(F;\tilde{\Omega}) \\
&+ 6\sum_\nu\Big(g^\lambda_{\beta\nu}(F;\tilde{\Omega})H^{31^*}_{\alpha\nu\rho\sigma}(F) - g^\lambda_{\alpha\nu}(F;\tilde{\Omega})H^{31^*}_{\beta\nu\rho\sigma}(F)\Big)\Big\}X^\lambda_{\rho\gamma}(F;\tilde{\Omega})X^\lambda_{\sigma\delta}(F;\tilde{\Omega}).
\end{aligned} \tag{C.43}$$

Similar expression for rotated matrix elements of general tensor operators can be obtained easily, see subsection 1.4.4.

In order to reduce the number of matrix elements to be calculated, one can make use of various symmetries displayed by the building blocks of the equations (C.29)-(C.32), (C.35),(C.37) and (C.41). For example the following skew-symmetries

$$\begin{aligned} g^{\lambda T}(F;\tilde{\Omega}) &= -g^{\lambda}(F;\tilde{\Omega}), \qquad \tilde{g}^{\lambda T}(F;\tilde{\Omega}) = -\tilde{g}^{\lambda}(F;\tilde{\Omega}) \\ h^{\lambda 02 T}(F;\tilde{\Omega}) &= -h^{\lambda 02}(F;\tilde{\Omega}) \qquad h^{\lambda 20 T}(F;\tilde{\Omega}) = -h^{\lambda 20}(F;\tilde{\Omega}), \end{aligned} \tag{C.44}$$

which follow directly from the equations (C.35) and (C.37). From the equation (C.41) one can deduce, that the $v^{\lambda}_{\alpha\beta\gamma\delta}$ must be antisymmetric with respect to the interchange of indices α and β or γ and δ. Furthermore, X^{λ}, $h^{\lambda 11}$ and v^{λ} can have in general non-zero diagonal elements and the first two must be calculated as full matrices. Since the GCM Hamiltonian and the projected overlap are Hermitian only upper- or lower triangle matrices have to be considered i.e. one needs only either (C.35) or (C.37) with the corresponding rotated overlap (C.30) or (C.29) and the corresponding parts of (C.31) and (C.41) in the numerical calculations. For more about numerical implementation of the rotated matrix elements see section 2.3.

Appendix D

The Center-of-Mass Hamiltonian in Second Quantization

In order to diagonalize the COM-Hamiltonian (1.73) we have to write it in second quantization. Using the expressions

$$\begin{aligned}\hat{\mathbf{P}}^2 &= \sum_i \hat{\mathbf{p}}_i^2 + \sum_{i\neq j} \hat{\mathbf{p}}_i \cdot \hat{\mathbf{p}}_j \\ \hat{\mathbf{R}}^2 &= \frac{1}{A^2}\left[\sum_i \hat{\mathbf{r}}_i^2 + \sum_{i\neq j} \hat{\mathbf{r}}_i \cdot \hat{\mathbf{r}}_j\right]\end{aligned} \tag{D.1}$$

and tensor identity $\hat{\mathbf{x}}_i \cdot \hat{\mathbf{x}}_j = \sum_{\mu=-1}^{1}(-)^\mu x_\mu^i x_{-\mu}^j$ the COM-Hamiltonian can be written in second quantization with antisymmetrized two-body part as

$$\begin{aligned}\hat{H}^{cm} =& \frac{\hbar\omega}{A}\Bigg\{\sum_{i=1}^{A}(N_i + 3/2)c_i^\dagger c_i \\ &+ \frac{1}{4}\sum_{ikrs}\sum_{\mu}(-)^\mu\Big[(\langle i|\hat{\varrho}_\mu|r\rangle\langle k|\hat{\varrho}_{-\mu}|s\rangle) - (s \longleftrightarrow r) + \\ &\qquad (\langle i|\hat{\xi}_\mu|s\rangle\langle k|\hat{\xi}_{-\mu}|r\rangle) - (r \longleftrightarrow s)\Big]c_i^\dagger c_k^\dagger c_s c_r\Bigg\},\end{aligned} \tag{D.2}$$

where $N_i \equiv 2n_i + l_i$ and the following dimensionless operators are used

$$\hat{\varrho} \equiv \frac{\hat{\mathbf{r}}}{b}, \quad \hat{\xi} \equiv -\frac{b\hat{\mathbf{p}}}{i\hbar} = b\hat{\nabla}, \qquad \text{where} \quad b \equiv \sqrt{\frac{\hbar}{m\omega}}. \tag{D.3}$$

Applying the Wigner-Eckart theorem we obtain

$$\langle i| \begin{Bmatrix} \hat{\varrho}_\mu \\ \hat{\xi}_\mu \end{Bmatrix} |r\rangle = (-)^{j_i - m_i} \begin{pmatrix} j_i & 1 & j_r \\ -m_i & \mu & m_r \end{pmatrix} (i|| \begin{Bmatrix} \hat{\varrho}_\mu \\ \hat{\xi}_\mu \end{Bmatrix} ||r). \tag{D.4}$$

For the reduced matrix elements we have

$$\begin{aligned} (i|| \begin{Bmatrix} \hat{\varrho}_\mu \\ \hat{\xi}_\mu \end{Bmatrix} ||r) = \delta_{\tau_i \tau_r} \delta_{l_i l_r \pm 1} (-)^{j_r + 1/2} \begin{pmatrix} j_r & j_i & 1 \\ \frac{1}{2} & -\frac{1}{2} & 0 \end{pmatrix} \times \\ \times \sqrt{(2j_i+1)(2j_r+1)} (n_i l_i| \begin{Bmatrix} \hat{\varrho}_\mu \\ \hat{\xi}_\mu \end{Bmatrix} |n_r l_r). \end{aligned} \tag{D.5}$$

A straightforward calculation of the radial matrix elements yields an analytical expressions

$$\begin{aligned} (nl+1|\hat{\varrho}|nl) &= \sqrt{(n+l+3/2)} \\ (n-1l+1|\hat{\varrho}|nl) &= -\sqrt{n} \\ (nl-1|\hat{\varrho}|nl) &= \sqrt{(n+l+1/2)} \\ (n+1l-1|\hat{\varrho}|nl) &= -\sqrt{(n+l)} \end{aligned} \tag{D.6}$$

with symmetry

$$(nl|\hat{\varrho}|n'l') = (n'l'|\hat{\varrho}|nl). \tag{D.7}$$

A slightly more complicated calculation gives

$$(nl+1|\hat{\xi}|nl) = (N_r - N_i)(n'l'|\hat{\varrho}|nl). \tag{D.8}$$

Finally, we can write

$$\begin{aligned} \hat{H}^{cm} = \frac{\hbar\omega}{A} \Big\{ \sum_{i=1}^{A} (N_i + 3/2) c_i^\dagger c_i \\ + \frac{1}{4} \sum_{ikrs} \sum_{\mu} \Big[\Big((1 + (N_r - N_i)(N_k - N_s)) \varrho_\mu(ik) \varrho_\mu(sk) \Big) - \Big(r \longleftrightarrow s \Big) \Big] c_i^\dagger c_k^\dagger c_s c_r \Big\}, \end{aligned} \tag{D.9}$$

where a notation $\varrho_\mu(ik) \equiv \langle i|\hat{\varrho}_\mu|k\rangle$ is used. The quasiparticle representation for the $\hat{H}^{cm}$ is obtained in analogy for the $\hat{H}$ in appendix A.1.

List of Figures

List of Tables

Bibliography

[Ajz86] F. Ajzenberg-Selove, Nucl. Phys. **A460**(1986)1.

[Bay60] B.F. Bayman, Nucl. Phys. **15**(1960)33.

[Ben95a] E. Bender, K.W. Schmid and A. Faessler, Nucl. Phys. **A596**(1995)1.

[Ben95b] E. Bender, K.W. Schmid and A. Faessler, Phys. Rev. **C52**(1995)3002.

[Ben96] E. Bender, PhD. Thesis, Tübingen 1996.

[Blo62] C. Bloch and A. Messiah, Nucl. Phys. **39**(1962)95.

[Bog58] N.N. Bogoliubov, Zk. Eksp. Teor. Fiz. **34**(1958)58.

[Bog59a] N.N. Bogoliubov, Usp. Fiz. Nauk. **67**(1959)541.

[Bog59b] N.N. Bogoliubov and V.G. Soloviev, Dokl. Akad. Nauk. SSSR **124**(1959)1011.

[Boh69] A. Bohr, B.R. Mottelson, *Nuclear Structure, vol.1*, Benjamin, New York Amsterdam,1969.

[Bru77] P.J. Brussard and P.W.M. Glaudemans, *Shell Model Applications in Nuclear Spectroscopy*, North-Holland, Amsterdam,1977.

[Bro88a] B.A. Brown and B.H. Wildenthal, Ann. Rev. Nucl. Part. Sci. **38**(1988)29.

[Bro88b] B.A. Brown, A. Etchegoyen, and W.D.M. Rae, *The computer code OXBASH, MSU-NSCL report* 524,1988.

[Cau94] E. Caurier, A.P. Zuker, A. Poves and G. Martinez-Pinedo, Phys. Rev. **C50**(1994)225.

[Cau95] E. Caurier, J.L. Egido, G.Martiñez-Pinedo, A. Poves, J. Retamosa, L.M. Robledo and A.P. Zuker, Phys. Rev. Lett. **75**(1995)2466.

[Cau99] E. Caurier, G. Martiñez-Pinedo, F. Nowacki, A. Poves, J. Retamosa and A.P. Zuker, Phys. Rev. **C59**(1999)2033.

[Che92] H. Cheng, D. H. Feng, C. Wu, Phys. Rev. Lett. **69**(1992)418; Phys. Rep. **242**(1994)433; Phys. Rep. **264**(1995)91.

[Coh65] S. Cohen and D. Kurath, Nucl. Phys. **73**(1965)1.

[Dav72] P.J. Davis and I. Polonsky in *Handbook of Mathematical Functions*, M. Abramowitz, I. Stegun eds.,Dover,New York,1972.

[DeS74] A. deShalit, H. Feshbach, *Theoretical Nuclear Physics, vol.1 Nuclear Structure*, Wiley, New York,1974.

[Edm57] A.R. Edmonds, *Angular Momentum in Quantum Mechanics*, Princeton University Press,Princeton,1957.

[Foc30] V. Fock,Z. Phys. **61**(1930)126.

[Fre69] J.B. French, E.C. Halbert, J.B. McGrory and S.M. Wong, Adv. Nucl. Phys. **3**(1969)193.

[Gir65] B. Giraud, Nucl. Phys. **71**(1965)373.

[Hal71] E. Halbert, J.B. McGrory, B.H. Wildenthal and S.R. Pandhya, Adv. Nucl. Phys. **1**(1971)315.

[Ham85] E. Hammarén, K.W. Schmid, F. Grümmer, A. Faessler and B. Fladt, Nucl. Phys. **A437**(1985)1.

[Ham86a] E. Hammarén, K.W. Schmid, F. Grümmer, A. Faessler and B. Fladt, Nucl. Phys. **A454**(1986)301.

[Ham86b] E. Hammarén, K.W. Schmid, A. Faessler and F. Grümmer, Phys. Lett. **B171**(1986)347.

[Ham98] E. Hammarén, K.W. Schmid and A. Faessler, Eur. Phys. J. A**2**(1998)371.

[Har91] K. Hara and Y. Sun, Nucl. Phys. **A529**(1991)445; ibid **A531**(1991)221; ibid **A537**(1992)77.

[Har28] D.R. Hartree, Proc. Cambridge Philos. Soc. **24**(1928)89.

[Hax49] O. Haxel, J.H.D. Jensen and H.E. Suess, Phys.Rev. **75**(1949)1766.

[Hey94] K.L.G Heyde, *The Nuclear shell Model, 2.ed*, Springer-Verlag, Berlin-Heidelberg,1994.

[Hje00] T. Hjelt, K.W. Schmid, E. Hammarén and A. Faessler, Eur. Phys. J. A**7**(2000)201.

[Hon96] M. Honma, T. Mizusaki, T. Otsuka, Phys. Rev. Lett. **77**(1996)3315.

[Hor94] M. Horoi, B.A. Brown and V. Zelevinsky, Phys. Rev. **C50**(1994)R2274.

[Koi89] I. Koivistoinen, PhL. Thesis, Jyväskylä 1989.

[Koo97] S.E. Koonin, D.J. Dean, K. Langanke, Phys. Rep. **278**(1997)1, and references therein.

[Law80] R.D. Lawson, *Theory of the Nuclear Shell Model*, Clarendon Press, Oxford,1980.

[Mac96] R. Machleidt, F. Sammarruca and Y. Song, Phys. Rev. **C53**(1996)R1483.

[Man75] H.J. Mang, Phys. Rep. **18**(1975)325.

[Mar97] G. Martinez-Pinedo, A.P. Zuker, A. Poves and E. Caurier, Phys. Rev. **C55**(1997)187.

[May49] M.G. Mayer, Phys. Rev. 75(1949)1969.

[Mcg80] J.B. McGrory, B.H. Wildenthal, Ann. Rev. Nucl. Part. Sci. **30**(1980)383.

[Nee83] K. Neergård and E. Wüst, Nucl. Phys. **A402**(1983)311.

[Nijmdb] Nijmegen database; A comprehensive interactive on-line database of low and intermediate energy nucleon-nucleon scattering data with compares of some exchange models, URL: http://nn-online.sci.kun.nl

[Oni66] N. Onishi and S. Yoshida, Nucl. Phys. **80**(1966)367.

[Pan96] D. Pantelica *et al*, J. Phys. G:Nucl. Part. Phys. **22**(1996)1013.

[Pei57] R.E. Peierls and I. Yoccoz, Proc. Phys. Soc. London **A70**(1957)381.

[Pet91] A. Petrovici, K.W. Schmid, F. Grümmer and A. Faessler, Z. Phys. A **339**(1991)71.

[Pet92] A. Petrovici, E. Hammarén, K.W. Schmid, F. Grümmer and A. Faessler, Nucl. Phys. **A549**(1992)352.

[Pet94] A. Petrovici, K.W. Schmid, and A. Faessler, Nucl. Phys. **A571**(1994)77.

[Pet96] A. Petrovici, K.W. Schmid, and A. Faessler, Nucl. Phys. **A605**(1996)290.

[Pet97] A. Petrovici, K.W. Schmid, and A. Faessler, Z. Phys. A**359**(1997)19.

[Pet99a] A. Petrovici, J. Phys. G:Nucl. Part. Phys. **25**(1999)803.

[Pet99b] A. Petrovici, K.W. Schmid, and A. Faessler, Nucl. Phys. **A647**(1999)197.

[Pet99c] A. Petrovici, K.W. Schmid, A. Faessler, J.H. Hamilton and A.V. Ramayya, Prog. Part. Nucl. Phys. 43(1999)485.

[Pet00] A. Petrovici, K.W. Schmid, and A. Faessler, Nucl. Phys. **A665**(2000)333.

[Rin80] P. Ring and P. Schuck, *The Nuclear Many Body Problem*, Springer,New York/Heidelberg/Berlin,1980.

[Sch82] K.W. Schmid and R. Smith, Nucl. Phys. **A381**(1982)195.

[Sch87a] K.W. Schmid and F. Grümmer, Rep. Prog. Phys. **50**(1987)731.

[Sch84a] K.W. Schmid, F. Grümmer and A. Faessler, Phys. Rev. **C29**(1984)291.

[Sch84b] K.W. Schmid, F. Grümmer and A. Faessler, Phys. Rev. **C29**(1984)308.

[Sch84c] K.W. Schmid, F. Grümmer and A. Faessler, Nucl. Phys. **A431**(1984)205.

[Sch87b] K.W. Schmid, F. Grümmer and A. Faessler, Ann. Phys. **180**(1987)1.

[Sch86] K.W. Schmid, F. Grümmer, M. Kyotoku and A. Faessler, Nucl. Phys. **A452**(1986)493.

[Sch89] K.W. Schmid, R.-R. Zheng, F. Grümmer and A. Faessler, Nucl. Phys. **A499**(1989)63.

[Sch91] K.W. Schmid and P.-G. Reinhard, Nucl. Phys. **A530**(1991)283.

[Sch92] K.W. Schmid in *Nuclear Structure Models*, R. Bengtsson, J. Drayer, W. Nazarewicz eds. World Scientific,Singapore (1992)333.

[Sch95] K.W. Schmid and G. Schmidt, Prog. Part. Nucl. Phys. **34**(1995)361.

[Sch00] K.W. Schmid in preparation.

[Son98] H.Q. Song, M. Baldo, G. Giansiracusa and U. Lombardo, Phys. Rev. Lett. **81**(1998)1584.

[Sto94] V.G.J Stoks, R.A.M. Klomp, C.P.F. Terheggen and J.J. de Swart, Phys. Rev. **C49**(1994)2950.

[Tal93] I. Talmi, *Simple Models of Complex Nuclei*, Harwood Academic, Switzerland,1993.

[Tho60] D.J. Thouless, Nucl. Phys. **21**(1960)225.

[Var94] K. Varga, R.J. Liotta, Phys. Rev. **C50**(1994)R1292.

[Vil66] F. Villars, in *Varenna Lectures* C. Bloch, Ed., Academic Press, New York (1966)1.

[Whi77] R.R. Whitehead, A. Watt, B. J. Cole and I. Morrison, Adv. Nucl. Phys. **9**(1977)123.

[Wil84] B.H. Wildenthal, Prog. Part. Nucl. Phys. **11**(1984)5.

[Wil88] B.H. Wildenthal, Ann. Phys. **182**(1988)191.

[Wil65] J.H. Wilkinson, *The Algebraic Eigenvalue Problem*,Clarence,Oxford,1965.

[Wir95] R.B. Wiringa, V.G.J. Stoks and R. Schiavilla, Phys. Rev. **C51**(1995)38.

[Wir97] R.B. Wiringa in *Comtemporary Nuclear Shell Models*, X.W. Pan, D.H. Feng and M. Vallieres eds. Springer,Berlin (1997)1.

[Zeh65] H.D. Zeh, Z .Phys. **188**(1965)361.

[Zeh67] H.D. Zeh, Z .Phys. **202**(1967)38.

[Zhe89] R-R. Zheng, K.W. Schmid, F. Grümmer and A. Faessler, Nucl. Phys. **A494**(1989)214.

Included Publications

T. Hjelt, K.W. Schmid, E. Hammaren, A. Faessler:
Unrestricted symmetry-projected
Hartree-Fock-Bogoliubov calculations for some PF-shell nuclei.
Eur. Phys. J. A 7, 201-208 (2000)

https://doi.org/10.1007/s100500050382